Structural and Mechanistic Analysis of the Regulation and Pharmacology of BRAF and MEK1

Professor Michael J. Eck Gonzalo Gonzalez del Pino

Research Advisor

Structural and mechanistic analysis of the regulation and pharmacology of BRAF and MEK1

Abstract

The Ras/RAF/MEK/ERK pathway is a nexus in growth factor signal transduction, integrating and relaying signals from membrane-bound receptors to effect growth and proliferation programs in the cell. Given this central role, it is commonly a source of oncogenic potential, as activating mutations anywhere along this axis drive different malignancies, including melanoma, pediatric low-grade gliomas, and colorectal cancers. Since specific inhibition of mutants of the small GTPase Ras eluded us until last year, the field went in search of anti-cancer drugs one step down the line, to RAF. The three isoforms of RAF (A, B, and CRAF) share high sequence similarity, but have at least some non-overlapping functions. Since the vast majority of cancer-causing BRAF mutations occur at position V600 (particularly V600E), a battery of $BRAF^{V600E}$ inhibitors made their way to the clinic. Of these, Dabrafenib, Vemurafenib, and Encorafenib were the most successful. Unfortunately, when melanoma patients were treated with these drugs, they developed secondary skin malignancies, such as squamous cell carcinomas and keratoacanthomas. In 2010, it was discovered that inhibition of $BRAF^{V600E}$ activates wildtype B and CRAF kinases by inducing membrane-localized dimerization. This phenomenon has

subsequently been termed paradoxical activation, and it leads to phosphorylation of ERK and a burst of aberrant growth and proliferation. Third- and fourth-generation RAF inhibitors, which have dual specificity for B and CRAF, and also inhibit monomeric or dimeric species of RAF kinases with roughly equal potency, show promise in the clinic.

Another approach actively being pursued is inhibition of the next step down the axis: MEK. Virtually all current MEK inhibitors (MEKis) are allosteric, and their binding sites have been determined by X-ray crystallography. Intriguingly, a number of MEKis exhibit differential potency depending on the mutational background of the upstream pathway ($KRAS^{mut}$, $BRAF^{V600E}$, KIAA:BRAF truncation/fusion). More recently, the structure of a BRAF:MEK complex with MEKi bound, as well as a new structure of full-length BRAF and MEK in complex with 14-3-3 proteins, have begun to offer clues to the mechanisms underlying the differential effect of MEKis.

In the work described here, I show how we have expanded our understanding of the basis of MEK inhibitor efficacy for shutting down MAPK signaling. Structural studies of a panel of eight clinically-relevant MEKis, coupled with corresponding inhibition and binding data, show that they work through at least one of four different mechanisms: 1) preventing MEK1 recruitment to BRAF, 2) preventing phosphorylation of MEK1, 3) preventing release of phosphorylated MEK1 from BRAF, and 4) direct inhibition of phosphorylated MEK1 activity (Graphical abstract). I also present a structure of the BRAF kinase in complex with TAK580, a new Type II inhibitor. These insights can help us develop new treatments of MAPK-driven malignancies.

Graphical Abstract

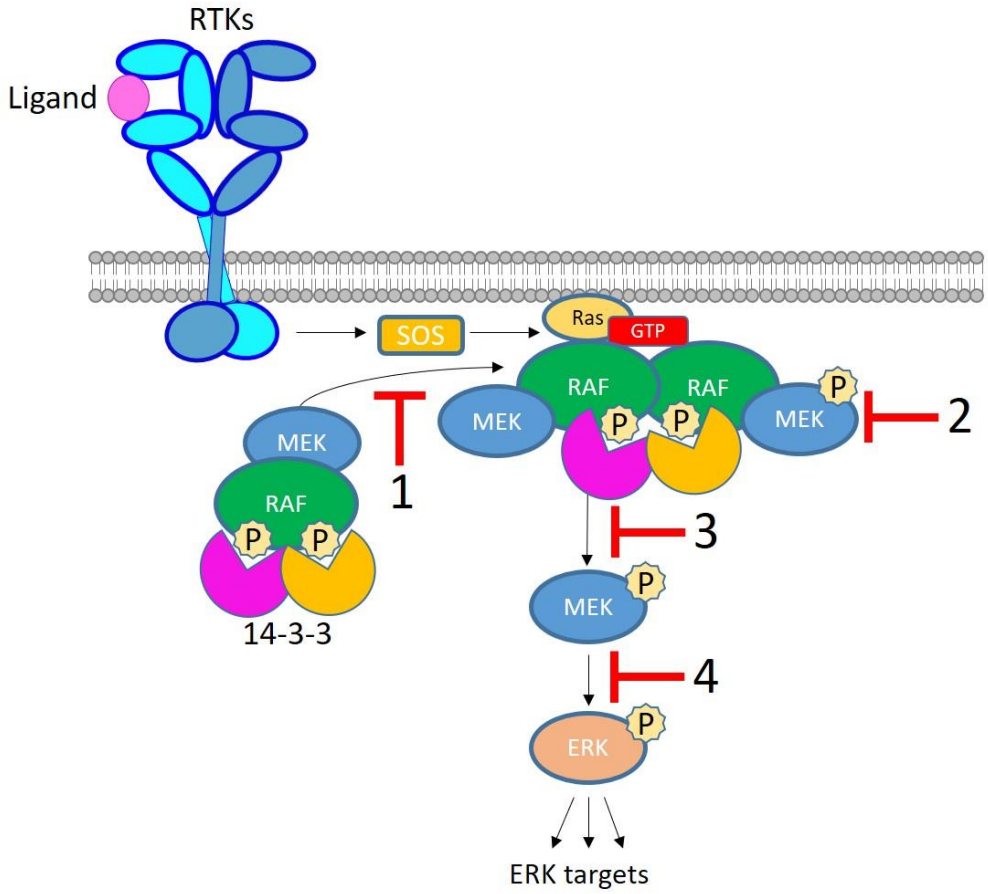

Our structural insights into the regulation of the MAP kinase cascade have revealed that MEK and RAF proteins are constitutively locked into an autoinhibited complex awaiting activation by GTP-bound Ras. MEK inhibitors can work through four possible mechanisms of action: 1) preventing recruitment of MEK to the active RAF complex, 2) preventing phosphorylation of MEK by RAF, 3) preventing release of phosphorylated MEK from the RAF complex or 4) preventing phosphorylation of ERK by active MEK.

To my family, for all their love and support. Words cannot express the gratitude I feel for the opportunities and affection they have given me.

Acknowledgments

The past seven years have been the most exciting and stimulating of my life. There are so many people I need to thank. First, I need to thank my mentor, Professor Michael Eck. Mike's patience and understanding allowed me to ask all the questions that popped into my head. I have learned so much from him – chief among them how to be a rigorous and careful biochemist.

I would like to thank Professor Victoria D'Souza, who has known me and been a mentor to me since my first year in graduate school. My time leading SROH with her showed me how caring and invested she is when it comes to diversity and the inclusion of underrepresented groups in academia. In the same vein, I would like to thank Professor Rachelle Gaudet for chairing my committee and providing me guidance and encouragement throughout even the most difficult times.

I also need to thank all the mentors I have had both in the classroom and at the bench. Teaching is important to me, and Professor Guido Guidotti has taught me so much about the joys of instilling excitement in my students. In the lab space, I have learned from each member of the Eck group. I would like to specifically acknowledge Drs. Eunyoung Park and Kunhua Li. Eunyoung is the most impressive biochemist I have ever met, and learning protein purification from the best has been a privilege. Lastly, I cannot thank Kunhua enough for his mentorship and friendship. Working with him the last two years of my PhD were fun and exciting, and led to the generation of this thesis. Thank you so much!

Table of contents

List of figures and tables

List of figures and tables (contd.)

List of figures and tables (contd.)

Chapter one: Introduction to the biology and pharmacology of the mitogen-activated protein kinase (MAPK) pathway

Overview and history of the MAPK pathway

The MAPK pathway is one of the central axes relaying extracellular growth, proliferation, and differentiation messages in the cell. It receives and transduces signals from all major types of cell surface receptors, from membrane-depolarizing ion channels[1] and G protein-coupled receptors (GPCRs)[2] to receptor tyrosine kinases (RTKs)[3]. The discovery and description of intracellular signaling pathways important in cancer occurred at roughly the same time as the initial characterization of cell surface receptors, such as the epidermal growth factor receptor (EGFR) and its cousin HER2-neu (now named ErbB2) during the late 1970s and throughout the 1980s[4]. Indeed, two of the first oncogenes identified, v-Src[5] and RAS (originally named p21)[6], were found to cause the transformation of normal cells by aberrant activation of the MAPK pathway.

Our current grasp of the events required for activation of the extracellular signal-regulated kinase (ERK) and its control of growth and proliferation programs is most easily expressed as a linear diagram connecting the cell surface receptors that activate RAS down to the terminal kinase of the pathway, ERK (Figure 1). In healthy cells, the binding of an extracellular ligand to its cognate growth factor receptor causes a change in the receptor's intracellular domains – in most cases this entails phosphorylation of tyrosine or serine/threonine residues either by intrinsic or enlisted kinases[7]. These phosphosites serve as platforms for the recruitment

of adaptor proteins that perform the first handoff to effector proteins. In RTKs, extracellular ligand-induced kinase activation leads to autophosphorylation of the intracellular portion of the molecules[8]. This enables binding of the phosphotyrosine-recognizing Src-homology 2 (SH2) domains of the adaptor protein Grb2[9].

Figure 1. Linear schematic of the mitogen-activated protein kinase (MAPK) cascade.

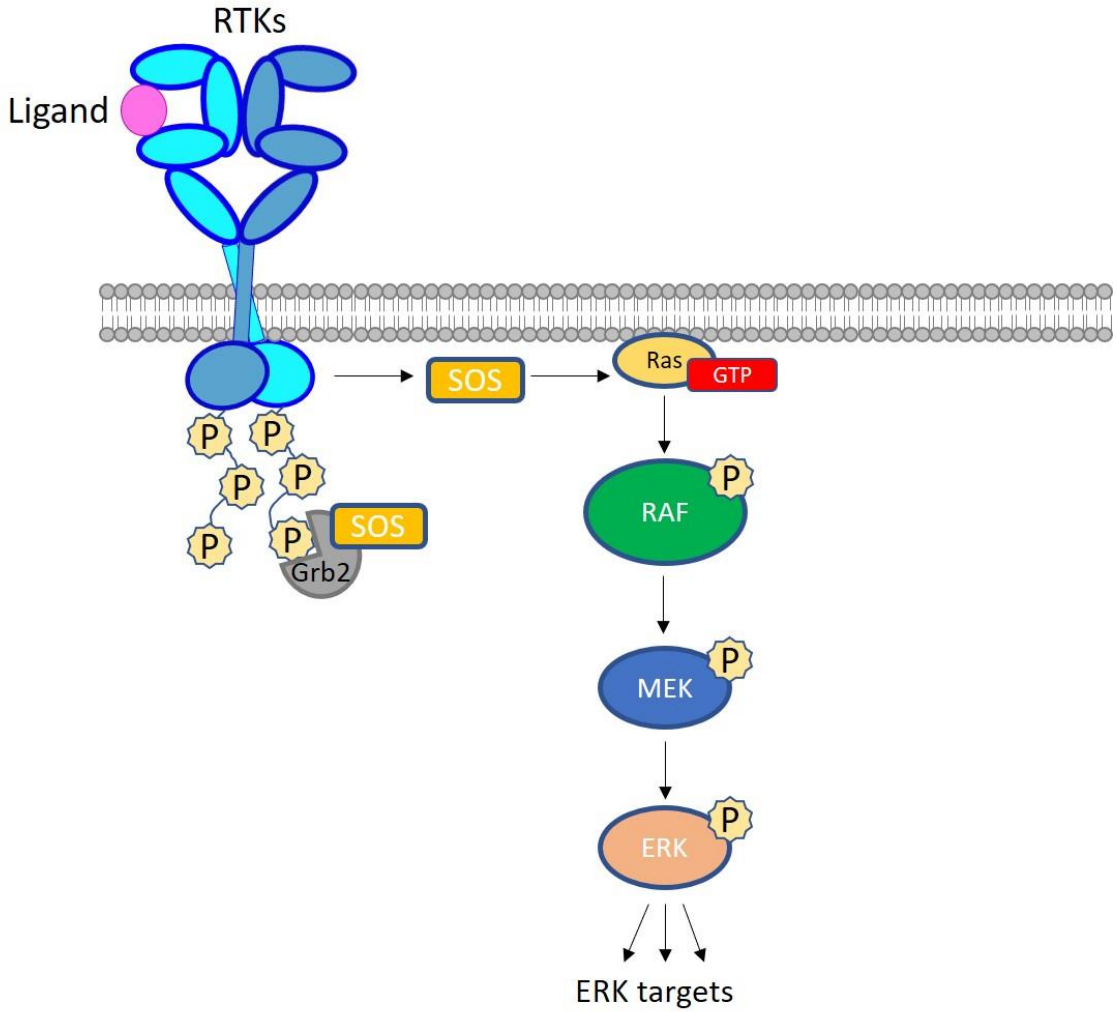

Once a cell-surface receptor binds an extracellular signaling molecule, recruitment of a nucleotide exchange factor to the receptor results in the replacement of GDP with GTP in the membrane-associated small GTPase RAS. GTP-bound RAS holds the protein kinase RAF (A, B, or CRAF isoforms) adjacent to the membrane, where it becomes active by dimerizing with another RAF. The active RAF dimer phosphorylates and activates MEK(1/2) which in turn phosphorylates and activates the terminal MAP kinase ERK. ERK then translocates to the nucleus to alter the cell's gene expression.

Binding of receptor phosphotyrosines by its SH2 domain allows the Grb2 SH3 domains to recruit Son-of-Sevenless (SOS), a guanine exchange factor, to the inner leaflet of the plasma membrane[10]. There, SOS can come into contact with the small, membrane-associated GTPase RAS and catalyze the replacement of GDP by GTP in its active site[11]. GTP-bound RAS adopts a conformation that is capable of interacting with the RAF family of serine/threonine protein kinases (ARAF, BRAF, and CRAF/RAF1 isoforms), bringing them in contact with the plasma membrane[12]. Proximity to the membrane relieves the inhibition imposed by the regulatory N-terminal region of RAFs (Figure 2). In 2009, Rajakulendran and colleagues discovered that RAF proteins are activated by homo- and heterodimerization of their kinase domains in a back-to-back configuration, where the active site clefts of both protomers are available for catalysis[13].

Figure 2. Domain architecture of BRAF.

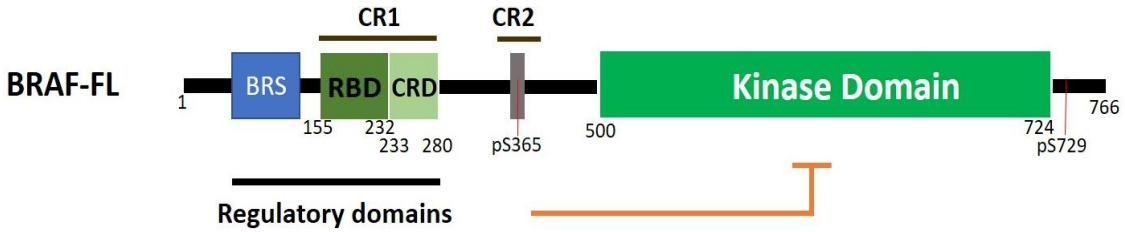

RAF proteins are made up of two distinct regions: the regulatory N-terminus and catalytic C-terminus. In BRAF, the N-terminus contains a BRAF-specific domain (BRS), Ras binding domain (RBD) that allows recruitment by the GTP-bound species of Ras, and a cysteine-rich domain (CRD) that can bind to the inner leaflet polar head groups in the membrane. The catalytic kinase domain is flanked by two phosphorylated serine residues (S365/S729) that serve as 14-3-3 binding sites.

This insight was further validated by a co-crystal structure of the BRAF and MEK1 kinase domains locked in a heterotetrameric complex bound to an allosteric MEK inhibitor solved by

Haling and colleagues in 2014[14]. In this complex, the BRAF kinases are bound back-to-back in a configuration reminiscent of the side-by-side dimer described by Rajakulendran *et al*. five years prior. Each BRAF kinase interacts face-to-face with a MEK1 protomer, whose activation segment

Figure 3. Structure of the active BRAF:MEK1 kinase complex bound to nucleotide and an allosteric MEK inhibitor.

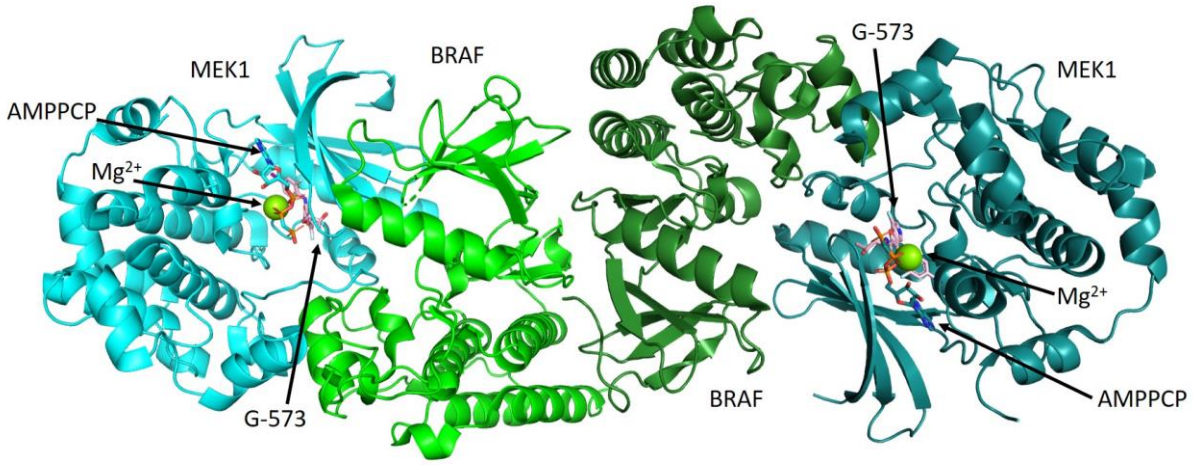

The BRAF back-to-back dimer shows hallmarks of an active kinase. Each BRAF kinase is bound face-to-face to MEK1. BRAF protomers are shown in shades of green; MEK1 protomers are in shades of cyan. G-573, an allosteric MEK inhibitor, is in pink, and the ATP analog, AMPPCP, is in the shade of cyan corresponding to its bound protomer.

(AS) serine phosphorylation sites – whose modification is required for MEK activity – are positioned near the BRAF ATP-binding cleft (Figure 3).

Comparison with other kinases and previous BRAF kinase structures indicated that the BRAF molecules in this structure were captured in an active conformation. The activation loop is extended outward from the nucleotide-binding cleft, making room for the key C-helix to swing inward toward the active site[15]. This C-helix-in state brings a glutamate residue in contact with a

catalytically essential lysine, coordinating the ATP γ-phosphate with the aspartate residue of the DFG motif, required for virtually all protein kinase-facilitated phosphotransfer reactions[16].

Phosphorylation of MEK1 AS serines 218 and 222 primes the kinase for phosphorylation of its substrate, ERK[17]. ERK is the final protein of the MAP kinase cascade, and phosphorylation on key threonine and tyrosine residues (T202/Y204) is required for enacting mitotic processes in cells[17,18]. ERK1/2 then phosphorylate a battery of proteins both in the cytoplasm and the nucleus that are involved in modulating transcription and translation, including RSK, Tau, and c-Myc[1920].

Our burgeoning understanding of the molecular mechanisms underlying the transformation of normal cells explicitly led to the development of the first targeted cancer therapeutics in the late 1990s and early 2000s. Both Glivec (imatinib)[21], a small molecule inhibitor of the BCR-Abl fusion protein, and Herceptin (trastuzumab)[22], an anti-HER2 antibody, were approved for the treatment of cancers before the start of the 21st century. These were the first steps toward a rationally designed precision medicine model that has led to significant advances in our fight against cancer.

The fact that both Glivec and Herceptin achieve their anti-cancer function by ultimately decreasing aberrant signaling through the MAPK cascade underlines the importance of this pathway. Through our accumulation and categorization of oncogenic mutations, we have found that virtually every node in this protein signaling relay is vulnerable to dysregulation[23].

The cumulative knowledge acquired over almost fifty years of research on the molecular mechanisms of signal transduction has led to a much greater awareness of how these processes work. Equally important, however, is understanding what happens when signaling networks are perturbed from their normal, tightly regulated functions. It is noteworthy that the initial discovery of most of the proteins involved in this cascade occurred in the context of virally- or otherwise exogenously transformed cells[6,24]. The early examples of Glivec and Herceptin were the beginning of a revolution in the treatment of malignancies and started our transition away from the usage of the chemotherapeutic agents that non-selectively kill rapidly dividing cells and toward genetically targeted precision medicine. The last twenty years have seen concrete advances in the prognosis and outcomes for patients suffering from virtually all types of cancer[25]. In the following sections of this introductory chapter, I will review our fight against MAPK-driven cancers, starting with our efforts at drugging RAS, continuing with the successes and challenges of targeting mutant RAF proteins, the pros and cons of MEK inhibition, and finally what are the open questions I have endeavored to answer over the course of my thesis work in the Eck group.

Pharmacological targeting of RAS mutants

The small GTPase RAS is one of the most frequently mutated genes in cancer[26]. When it comes to MAPK signaling, virtually all paths from the cell surface pass through RAS; it has been seen, therefore, as an attractive therapeutic target since it was first described as the homolog of

a viral oncogene[6,24]. Most activating RAS mutations provide oncogenic potential by impairing the protein's GTPase activity or by increasing its affinity for GTP, thereby locking it in its active, effector-binding competent form[27,28]. This issue is compounded by both its relative affinities for and the intracellular concentrations of GTP and GDP, which favor the binding of the triphosphate guanine species in the absence of tight regulation[27].

For decades, direct and specific inhibition of activating RAS mutants eluded us. In 2013, however, Ostrem and colleagues leveraged the introduction of a cysteine residue by the G12C mutation in KRAS to screen for and optimize compounds that covalently bound the oncogenic gene product. Their compounds complexed with KRAS in a conformation that favored the binding of GDP over GTP, decreasing the proportion of constitutively active RAS in transformed cells[29]. Although those compounds were not developed further than their initial characterization, the recent description of G12C-selective KRAS inhibitors represents a promising triumph and will hopefully be the first of many mutant-selective GTPase drugs to reach the clinic[30,31]. It remains to be seen how mutants that do not introduce targets for covalent modification (G12D, G12V in KRAS for example) can be specifically inhibited, given the lack of a druggable binding pocket in small GTPases such as RAS[32].

Because we are just now achieving some measure of success in the targeting of RAS itself, previous efforts at treating mutant RAS-driven cancers focused on shutting down MAPK signaling downstream of RAS, at either the RAF or MEK level. Initial trials of sorafenib, a RAF inhibitor,

showed no effect on RAS-driven tumors, and instead caused secondary skin lesions in patients[33,34]. These issues were exacerbated in clinical trials of vemurafenib, a second-generation inhibitor of mutant BRAF[35]. I will discuss the drugging of RAF proteins in more detail in the following section.

Given that inhibition of RAF to treat RAS-driven cancers has not proven as effective as had been hoped, the search began for compounds that inhibit MEK. Because MEK1/2 are the only enzymes capable of phosphorylating and activating ERK[36], they seemed like plausibly appealing drug targets. Unfortunately, this potential advantage turns out to also lead to complications. Since there are no redundant kinases capable of providing some level of ERK phosphorylation in healthy cells, there is virtually no therapeutic window to exploit: cytotoxicity of compounds that inactivate MEK is, in many cases, unacceptably high[37–40]. Compounding this is the observation that MEK inhibitors are not consistently effective at treating MAPK pathway-driven malignancies[41]. GDC0973, also known as cobimetinib, is successful at decreasing tumor size in BRAF mutant cancers, but unable to prevent the growth of KRAS mutant cell lines[41]. Similarly, Lito, Rosen and colleagues have demonstrated that PD0325901 shows promise as an inhibitor of mutant BRAF activity, but not of KRAS mutant activity[42]. The differential sensitivity of MAPK-driven malignancies to MEK inhibition is a main topic of Chapter 3 of this thesis. I will also elaborate on the history and potential of targeting MEK in a subsequent section of this introduction.

RAF-driven cancers, the development of mutant-specific inhibitors, and the specter of paradoxical activation.

RAFs are some of the main effectors of RAS signaling, and thus sit at the apex of the MAP kinase cascade[32]. As such, they have been seen as the lynchpin of signaling through ERK. Beginning in the late 1990s, pharmacologists endeavored to find compounds that selectively inactivated mutant RAF proteins to treat melanoma, glioma, and colorectal tumors[43]. BRAF is the most frequently mutated kinase in cancer, and oncogenic mutations in the gene that codes for it can be placed in three distinct classes: monomerically activating mutations, kinase-impaired transactivating mutations, and RAS-independent dimerization mutations[44]. V600E, the most prevalent point mutation in BRAF, removes the dimerization requirement for BRAF activity[45]. Most of the oncogenic point mutants in BRAF cluster in the kinase domain, and either promote constitutive activity of the kinase (V600E) or promote the activation of the mutant protein's back-to-back partner[46]. The KIAA1549:BRAF truncation/fusion mutation replaces the inhibitory N-terminal domain of the protein with a membrane-localization domain, removing its dependence on RAS activation[47]. The former mutation is responsible for the bulk of melanoma cases and the latter for a large proportion of pediatric low-grade gliomas. BRAF-specific drugs began to clear clinical trials in the early to mid-2000s: sorafenib and vemurafenib were approved for treatment of renal adenomas and melanoma, respectively[48]. The initial promise of preclinical and clinical trials of such compounds gave way to disappointment: as mentioned in the previous section,

BRAF inhibitors caused the outbreak of secondary keratoacanthomas and squamous cell carcinomas. A mechanism for this was proposed in 2010[35], but a 1999 study first coined the term that would be used to describe the phenomenon: paradoxical activation[49].

The studies referenced above present the conundrum facing researchers and drug developers: inhibitors specifically and potently shut off mutant BRAF, but in the process led to a burst of ERK phosphorylation. The discovery of RAS-mediated, dimerization-dependent activation of RAFs happened concurrently with the testing of the first- and second-generation inhibitors targeting constitutively active mutants of BRAF for the treatment of kidney, brain, and skin cancers[13]. This provided an explanation for how paradoxical activation occurred: inhibitor binding to one protomer of the active RAF dimer somehow led to activation of its dimerization partner[35]. These drugs still made it through clinical trials, and ultimately a number of them became first-line treatment options for melanoma and renal malignancies both as monotherapies and when combined with MEK inhibitors[50].

Pinning down the causes and mechanisms for paradoxical activation led to even more vigorous efforts to find compounds that circumvent inhibitor-dependent phosphorylation of ERK. Multiple groups have recently reported a suite of compounds termed “paradox breakers,” which inhibit mutant BRAFs without causing the activation of their wild-type partners. Through structural and biochemical analyses, it has been posited that inhibitors that evade paradoxical

activation of ERK2 bind mutant BRAF, but do not stabilize the back-to-back kinase dimer as do vemurafenib and dabrafenib[51].

Interestingly, new inhibitors that bind a different conformation of BRAF seem effective at inhibiting both V600E- and KIAA1546-mutant BRAF and are currently in clinical trials for the treatment of pediatric low-grade astrocytoma[52]. The structure of the BRAF kinase bound to TAK580, the compound studied by Yu Sun and colleagues, is the focus of Chapter 4 of this thesis.

Promise and peril of targeting MEK1/2 for MAPK inhibition

As mentioned in the RAS-centered section of this introduction, MEK inhibition for the treatment of MAPK pathway-dependent cancers offers new possibilities but does not come without its own obstacles. The prevailing model in the field today posits that pharmacological inhibition of ERK1/2 phosphorylation shuts down critical negative feedback loops that are required to attenuate growth factor signaling through this pathway[53]. Since MEK1/2 are the only enzymes known to phosphorylate and activate ERK1/2[54], complete abrogation of MEK activity would lead to an accumulation of upstream activity, including sustained cell surface receptor signaling, that spills over into other semi-redundant pro-growth and pro-proliferation pathways, leading to malignant transformation. In cases where negative feedback inhibition is avoided, targeting MEKs is still a precarious balancing act: MEK inhibitor monotherapy is associated with

cutaneous rashes; gastrointestinal distress, including nausea and vomiting; as well as ocular fluid pressure buildup (central serous retinopathy)[40].

Researchers and clinicians arrived at an innovative way of overcoming the obstacles of targeting RAF and MEK separately: combination therapy. By blockading MAPK signaling at the RAF level and the MEK level simultaneously, ERK phosphorylation and activation can be virtually completely abrogated. Furthermore, the synergistic effect of dual inhibition means that dosages of each inhibitor can be tuned down to decrease the onset of adverse events. Combining MEK inhibition with BRAF inhibition has thus become the gold-standard first line treatment for $BRAF^{V600E}$-driven melanoma[55]. At full monotherapy-level dosing, the dual BRAF/MEK inhibition actually decreased the prevalence of RAF inhibitor-dependent adverse effects in dabrafenib/trametinib trials. This trend continued in the two main combination therapy trials discussed by Heinzerling *et al*.[40].

Structural characterization of molecules that inhibit MEK has given us some insight into their mechanism of action, but still leave many questions unanswered. MEK has been crystalized in the presence of nucleotide and several compounds over the past decade[56,57]. All MEK inhibitors currently in the clinic or in clinical trials bind the kinase in an ATP-noncompetitive fashion, in a pocket adjacent to the nucleotide-binding cleft. Given the high similarity in binding poses among MEK inhibitors, a question naturally arises: why is inhibitor potency sensitive to the mutational background upstream of MEK? This question will be discussed at length in Chapter 3 of this thesis.

The state of the field and open questions

The continuing efforts to better understand and drug the MAPK pathway have led to tangible advances in human health. As has been made clear by the prevalence of inhibitor-dependent paradoxical activation and the effect of different mutational backgrounds on the efficacy of MEK inhibitors, however, we still lack a full picture of the complex biological and pharmacological interactions at play in such an important pillar of cellular signal transduction. Through my thesis work, I have attempted to answer some of the outstanding questions described in this introduction: what is the endogenous resting state of BRAF and MEK1? How do oncogenic mutations in BRAF activate the MAPK pathway? Why are MEK inhibitors differentially potent depending on what upstream mutations drive aberrant MAPK signaling? What is the mechanism of action of these MEK inhibitors?

In Chapter two, I describe the structure of the autoinhibited BRAF:MEK1 kinase dimer. The discovery of this complex has profound implications for how we understand regulation of the MAP kinase cascade. These findings are expanded on in Chapter three, where I report biochemical, biophysical, and structural characterization of a battery of clinically relevant MEK inhibitors. How these compounds interact with the autoinhibited BRAF:MEK1 kinase module provides insight into their mechanism of action and why they do or do not work in certain mutational backgrounds. Chapter four is a brief description of a novel mutant BRAF inhibitor, TAK580, in complex with the BRAF kinase. This structure and the results of preclinical and clinical

studies of its efficacy add to the accumulating evidence for how we can design drugs that shut down RAF activity without causing paradoxical activation of ERK.

Taken together, the experiments and analysis described here represents a concrete advance in knowledge of signal transduction, how it is dysregulated in cancer, and how we can better treat these malignancies using the structural, biochemical, and biophysical techniques currently available.

Chapter two: Crystal structure of an autoinhibited BRAF:MEK1 kinase dimer complex

Part of this work was completed in collaboration with Drs. Kunhua Li and Eunyoung Park in the Eck lab. K.L. generated the BRAF kinase baculovirus construct and guided me through structure refinement. We solved and refined structures in parallel. E.P. generated and kindly gave us access to her MEK1^{SASA} baculovirus.

Introduction

The Ras/RAF/MEK/ERK pathway is a nexus in growth factor signal transduction, integrating and relaying signals from membrane-bound receptors to effect growth and proliferation programs in the cell. Given this central role, it is commonly a source of oncogenic potential, as activating mutations anywhere along this axis drive different malignancies, including melanoma, pediatric low-grade gliomas, and colorectal cancers. Since specific inhibition of mutants of the small GTPase Ras eluded us until recently, the field went in search of anti-cancer drugs one step down the line, to RAF. The three isoforms of RAF (A, B, and CRAF) share high sequence similarity, but have at least some non-overlapping functions[58]. Since the vast majority of RAF-driven malignancies are caused by mutations in BRAF at position V600 (particularly V600E), a battery of $BRAF^{V600E}$ inhibitors made their way to the clinic. Of these, Dabrafenib, Vemurafenib, and Encorafenib were the most successful[59]. Unfortunately, when melanoma patients were treated with these drugs, they developed secondary skin malignancies, such as squamous cell carcinomas and keratoacanthomas. In 2010, Hatzivassiliou, Malek and colleagues discovered that inhibition of $BRAF^{V600E}$ activates wildtype B and CRAF kinases by inducing membrane-localized dimerization[35,60,61].

This phenomenon has subsequently been termed paradoxical activation, and it leads to phosphorylation of ERK and a burst of aberrant growth and proliferation[62]. Third- and fourth-

generation RAF inhibitors, which have dual specificity for B and CRAF, and inhibit both monomeric and dimeric species of RAF kinases with roughly equal potency, show promise in the clinic[5263].

Another approach actively being pursued is inhibition of the next step down the axis: MEK. Virtually all current MEK inhibitors (MEKis) are allosteric, and the binding sites of several of them have been determined by X-ray crystallography[5756]. Intriguingly, MEKis exhibit differential potency depending on the mutational background of the upstream pathway ($KRAS^{mut}$, $BRAF^{V600E}$, KIAA:BRAF truncation/fusion)[41,42]. More recently, the structure of a BRAF:MEK complex with MEKi bound, has offered tantalizing clues to the mechanism underlying the differential effect of MEKis[14]. This structure, coupled with corresponding inhibition and binding data[42], show that inhibitors can lock MEK in complex with RAF, or potentially destabilize the complex.

The kinase domain of BRAF has been studied extensively by X-ray crystallography, but almost always in complex with inhibitors. Of more than 50 BRAF kinase structures previously available in the Protein Data Bank, none contain ATP or a nucleotide analog and none reveal the kinase in its inactive configuration. A single structure is available for the BRAF kinase domain in complex with its substrate, MEK1[14]. This structure contains a heterotetramer in which the two BRAF kinase domain form an active-state, back-to-back dimer. Each BRAF kinase binds one MEK1 in a “face-to-face” orientation; that is with the BRAF and MEK1 active sites juxtaposed.

In a paper just published from our lab, we report the structure of full length BRAF and MEK in complex with a 14-3-3 dimer in an autoinhibited state[64]. This structure represents a paradigm shift in our understanding of the mechanism for activation of the Ras/RAF/MEK/ERK axis: we posit that RAF and MEK in the cytosol are constitutively bound to each other in a mutually inhibited complex. This complex is held together by a 14-3-3 dimer that recognizes two structurally required serine phosphorylation sites in BRAF and cradles the cysteine-rich domain between its two protomers. In this configuration, the back of the BRAF kinase is occluded, locking the kinase in an inactive state by preventing the back-to-back dimerization required for activation. BRAF binds to MEK1 in a face-to-face orientation similar to that observed in the active structure, but with a significantly smaller angle of rotation between the BRAF N- and C-lobes[14,64].

In this chapter I describe crystal structures of a complex of the BRAF kinase domain with MEK1. Together with the cryo-EM structure of a full-length autoinhibited BRAF-MEK1-14-3-3 complex, determined contemporaneously in our lab, this structure provides the first, long-sought views of the inactive state of the BRAF kinase. The structure reveals an inactive configuration of the kinase domain that closely resembles the inactive state of certain other kinases, including EGFR and Src. Extensive interactions with MEK1 and with the bound nucleotide substrate, ATP, suggest that both are required for maintenance of the BRAF kinase in its quiescent state. Comparison with the aforementioned cryo-EM structure of the full-length BRAF complex shows that the isolated kinase module in the crystal structure adopts the same conformation as the corresponding region of the intact complex, which leads us to conclude that autoinhibition is

intrinsic to the kinase module. Finally, the structure explains how V600E and other oncogenic mutations in the BRAF kinase domain disrupt key inhibitory interactions to lead to unrestrained kinase activity. Perhaps most provocatively, this work provides a compelling structural explanation for paradoxical activation of BRAF: All ATP-competitive BRAF inhibitors will be prone to conformational activation of the kinase due to displacement of ATP and consequent loss of its interactions that stabilize the inactive state.

Materials and Methods

Insect cell expression and purification of the BRAF:MEK kinase complex

For insect cell expression of the BRAF kinase domain in complex with MEK1, two recombinant baculovirus species were employed. The first was prepared using baculoviral transfer vector pFastBac Dual and encoded the BRAF kinase domain (BRAF residues 445-723, fused to an N-terminal His_6 tag and a C-terminal chitin-binding domain) and human chaperone CDC37. The second baculovirus encoded full-length human $MEK1^{SASA}$, an activation loop-phosphorylation refractory species of the MEK1 Kinase, where S218/222 in the activation segment have been mutated to alanine. For protein production, liter-scale suspension cultures of Sf9 cells were co-infected with both viruses. Cells were harvested 60-66 hours post-infection and resuspended in lysis buffer (50 mM Tris pH 8.0, 250 mM NaCl, 5% glycerol and 20mM imidazole, 1 mM tris (2-carboxyethyl)-phosphine (TCEP)) with protease inhibitor cocktail (Roche). Resuspended cells were disrupted by sonication on wet ice, and the lysate was clarified by ultracentrifugation at 40,000 rpm for two hours. Clarified lysate was batch-bound to Ni-NTA beads and washed

extensively with binding buffer before elution with elution buffer (50 mM Tris pH 8.0, 250 mM NaCl, 250 mM imidazole, 1 mM TCEP). The elution fractions were pooled and treated with 1:1000 molar ratio of TEV protease and 100 mM β-mercaptoethanesulfonic acid (MESNA) overnight to cleave N-terminal and C-terminal tags, and further purified by size-exclusion chromatography (Superdex 200 10/300, GE Healthcare) in storage buffer (50 mM HEPES pH 7.5, 150 mM NaCl, 1mM TCEP). The fractions were analyzed by SDS-PAGE, and fractions corresponding to the BRAF:MEK kinase domain complex were pooled, concentrated to 8 mg/mL, and flash frozen. Final yield of the BRAF:MEK protein complex was ~10 mg/6L preparation.

BRAF:MEK1 kinase domain crystallization and structure determination.

For crystallization, aliquots of the BRAF:MEK kinase complex were incubated with 5 mM MgCl2, 2 mM Adenosine 5'(β,γ-imido)triphosphate (AMPPNP), and with or without 0.2mM GDC-0623, in storage buffer at 4°C overnight. Rod-shaped crystals suitable for structure determination were obtained by vapor diffusion in hanging drops using two different reservoir solutions: 22% PEG3350, 0.1M Tris pH 8.5, 0.2M Lithium Sulfate (AMPPNP) and 22% PEG3350, 0.1M Bis-Tris pH 6.5, 0.2M Lithium Sulfate (GDC0623 at room temperature. Crystals were harvested and flash frozen in liquid nitrogen using additional 20-22% glycerol as a cryoprotectant. X-ray diffraction data were collected at 100 K using NE-CAT beamline ID-24-C at the Advanced Photon Source, Argonne National Laboratory, at a wavelength of 0.9786 Å. Data were integrated and merged using XDS and scaled using Aimless in the CCP4 suite, or by the Xia2 suite using the Dials mode. The initial structure of the complex containing GDC0623 was phased by molecular replacement

in PHASER using PDB entry 4MNE as an initial search model. Molecular replacement of the AMPPNP-only and all other inhibitor-bound structures was performed using the GDC0623 structure as a search model. Inhibitors were placed into positive density in an initial F_o-F_c map and included in subsequent rounds of refinement using PHENIX.REFINE. Successive manual refinement was performed using COOT. The data collection and refinement statistics are presented in Table 1.

Table 1. Data collection and refinement statistics for the BRAF:MEK1:AMPPNP and AMPPNP:GDC0623 complex structures

	AMPPNP	GDC0623
Wavelength	0.9787	0.9787
Resolution range	43.25 - 3.12 (3.232 - 3.12)	43.56 - 2.58 (2.683 - 2.58)
Space group	P 31 2 1	P 31 2 1
Unit cell	116.278 116.278 129.739 90 90 120	116.697 116.697 130.944 90 90 120
Total reflections	240226 (22157)	432523 (44314)
Unique reflections	18483 (1816)	32549 (3190)
Multiplicity	13.0 (12.2)	13.3 (13.9)
Completeness (%)	99.81 (99.62)	99.95 (100.00)
Mean I/sigma(I)	18.11 (1.66)	10.86 (2.00)
Wilson B-factor	92.09	52.17
R-merge	0.1613 (1.963)	0.215 (1.534)
R-meas	0.1679 (2.05)	0.2237 (1.593)
R-pim	0.04632 (0.5825)	0.06127(0.4253)
CC1/2	0.998 (0.628)	0.996 (0.651)
CC*	1 (0.878)	0.999 (0.888)
Reflections used in refinement	18473 (1813)	32543 (3190)
Reflections used for R-free	838 (76)	1543 (149)
R-work	0.1874 (0.3458)	0.2228 (0.2723)
R-free	0.2381 (0.3835)	0.2472 (0.3342)
CC(work)	0.964 (0.740)	0.912 (0.778)
CC(free)	0.944 (0.624)	0.900 (0.727)
Number of non-hydrogen atoms	4721	4858
macromolecules	4657	4679
ligands	64	109
Protein residues	591	590
RMS(bonds)	0.003	0.004
RMS(angles)	0.62	0.55
Ramachandran favored (%)	93.29	96.92
Ramachandran allowed (%)	5.68	3.08
Ramachandran outliers (%)	1.03	0.00
Rotamer outliers (%)	3.90	1.75
Clashscore	8.13	3.55
Average B-factor	88.26	53.12
macromolecules	88.47	
ligands	73.10	

Results

Expression and purification of the BRAF:MEK1 kinase complex.

For crystallization of the BRAF:MEK1 kinase complex, we used a truncated version of the BRAF kinase (residues 445-723). This construct removes the N-terminal BRAF-specific domain (BRS), Ras-binding domain (RBD), and cysteine-rich domain (CRD) (Figure 4a). In contrast, full-length constructs of all protomers were used in the cryo-EM reconstruction structure of the BRAF:MEK1:14-3-3 complex presented in Park *et al.* After the initial Ni-NTA affinity purification step (see Materials and Methods), a final size-exclusion chromatography step yielded a symmetric peak eluting at 13.9 mls that contained an apparently stoichiometric ratio of the BRAF:MEK1 kinase complex (Figure 4b).

Figure 4. Domain structure of BRAF and MEK1 and protein constructs purified.

4a.

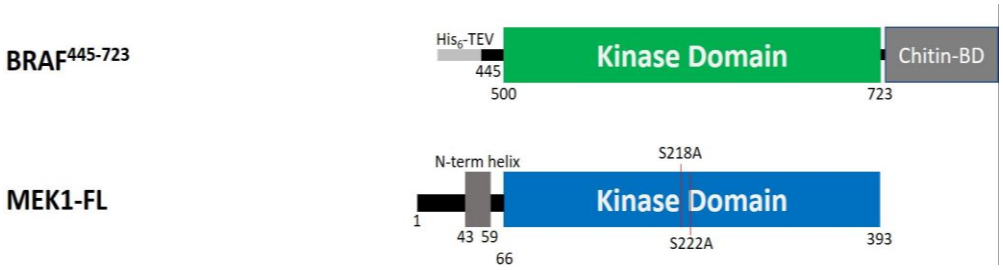

4b.

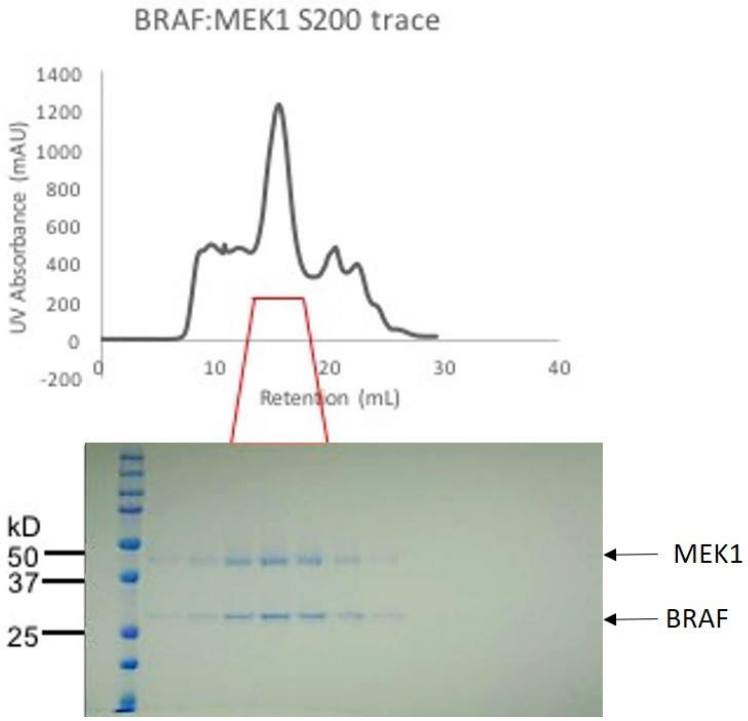

4a. The BRAF gene is made up of two main regions: the regulatory N-terminal domains and the catalytic C-terminal kinase domain. For the structure I describe here, we used the BRAF$^{445\text{-}723}$ construct, comprised of the kinase domain exclusively. This is in contrast to the full-length BRAF construct used to determine the cryo-EM structure in Park *et al.* The full-length MEK gene was used, where two active loop serines in the kinase were mutated to alanine to encourage homogeneity of phosphorylation state. 4b. S200 UV absorbance trace and corresponding SDS-PAGE analysis of fractions containing dimeric BRAF:MEK1 kinase complex.

Crystallization and structure determination

Crystals of the BRAF:MEK1:AMPPNP:MEK inhibitor mixtures initially appeared in two conditions: 22% PEG3350, 0.1M Tris pH 8.5, 0.2M Lithium Sulfate (AMPPNP) and 22% PEG3350, 0.1M Bis-Tris pH 6.5, 0.2M Lithium Sulfate (GDC0623) (Figure 5). The conditions were repeated and optimized in 2µL hanging drop format in 24-well plates. The crystals were large rods with an aqueous channel in the middle, belonging to the space group $P3_121$. Diffraction data were collected at 100K using Advanced Photon Source Beamline ID-C in Chicago through the NE-CAT browser-based system, and the structures were determined by molecular replacement using chains A and B of the active, tetrameric structure solved by Haling and colleagues (PDBID: 4MNE). The final structures were solved to 2.58 Å and 3.12 Å, for GDC0628 and AMPPNP-only containing structures, with R_{work}/R_{free} of 0.22/0.25 and 0.19/0.24, respectively.

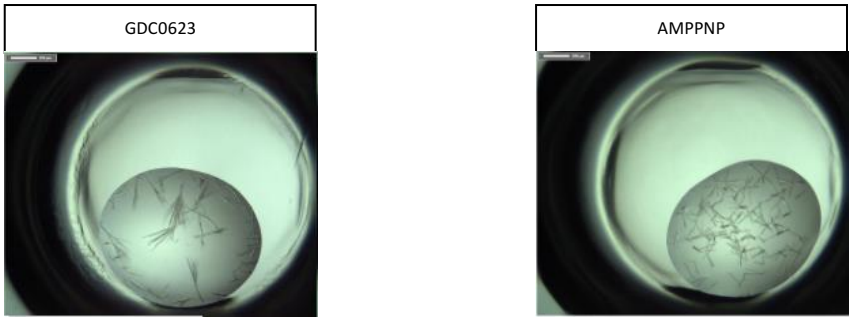

Figure 5. Crystals of the BRAF:MEK1 kinase complex. Positive conditions from 150nL 1:1 protein:precipitant sitting drop crystallization screens of the BRAF:MEK1 complex mixed GDC0623 and AMPPNP or AMPPNP only. Further rounds of optimization yielded large, rod-like crystals with an aqueous channel in the middle.

Overall architecture of the BRAF:MEK1 kinase module

In this chapter, I describe two distinct structures of the BRAF:MEK1 kinase module: an AMPPNP-only structure and a structure containing GDC0623, an allosteric MEK inhibitor. The crystal structure of the nucleotide-only kinase complex reveals a tight, face-to-face dimer with a broad interface. The N-lobes of both protomers are aligned with each other, and oriented upwards in our representation. At the bottom of the dimer are the helix-dominated C-lobes, which make extensive contacts with each other at the dimerization interface, notably where the G-helices cross. Nucleotide complexed with a magnesium ion is bound in the cleft between the two lobes; the P-loops cup the nucleotide from above in both kinases. The C-helices of either kinase are on opposite sides of the complex from each other, and an outward conformation indicative of the inactive state. Unless otherwise specified, the description below refers to the AMPNP-only structure, with MEK1 colored in blue and the BRAF kinase in forest green (Figure 6a).

The active sites of both kinases in the autoinhibited BRAF:MEK1 dimer are intimately connected. The G-helices form extensive van der Waals contacts along their inward faces as they cross each other (Figure 6b, bottom of panel). Furthermore, both BRAF and MEK1 P- and activation-loops are close to each other (~10 Å and 5 Å distance at the closest point, correspondingly). Most strikingly, the dimer is stabilized by two unexpected polar interactions that span the face-to-face interface. The BRAF arginine 662 extends its guanidinium group under

the MEK1 activation segment and is in close proximity to the activation segment S222A phosphosite. This arginine is enticingly close to the MEK1 AMPPNP γ-phosphate; however, none of our structures demonstrate evidence that would make this a *bona fide* interaction. On the MEK1 side, glutamate 102 extends across the dimerization interface and forms a polar interaction with the 3' hydroxyl of the BRAF AMPPNP (Figure 6b, center of the panel).

Figure 6. Overall architecture of the autoinhibited BRAF:MEK1 kinase module.

6a.

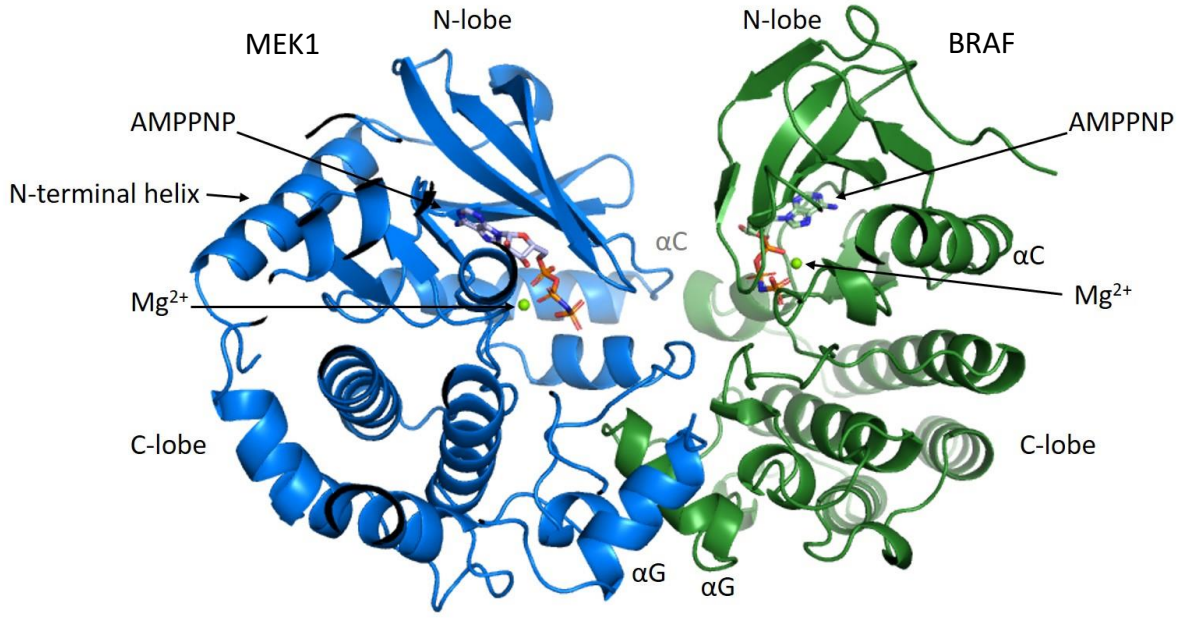

6b.

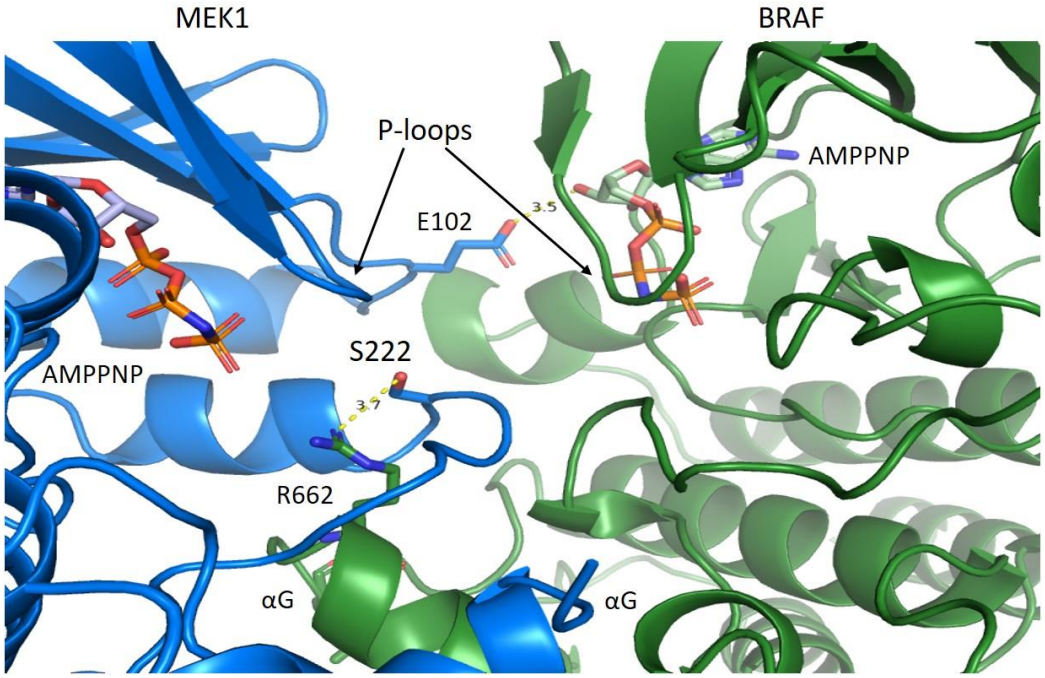

6a. Overall structure of the BRAF:MEK1 kinase module with AMPPNP bound (MEK1 in blue, BRAF in forest green) adopts an autoinhibited state in the absence of MEK inhibitors or the N-terminal BRAF domains. The MEK1 N-terminal inhibitory helix, for which there is no density in the cryo-EM map, lays along the back of the kinase, bridging across the N- and C-lobes. Both active sites bind nucleotide and are in proximity to each other. In the C-lobe, the G-helices

Figure 6 (contd.) cross each other and form extensive contacts, with the BRAF G-helix extending side chains into the MEK1 active site. 6b. The BRAF and MEK1 active sites are intrinsically linked to each other in the autoinhibited state. The BRAF R662 makes polar contacts with S222 in the MEK1 activation loop. Most strikingly, the MEK1 E102 makes direct contact with the BRAF active site AMPPNP 3' hydroxyl. MEK1 inhibitor binding brings E102 into *bona fide* hydrogen bonding range (2.9 Å, Chapter 4). Hydrophobic interactions between the G-helices of both kinases further stabilize the face-to-face dimer.

Key features of the autoinhibited BRAF kinase domain and comparison with the active state

In BRAF, the active site is disrupted by an outward rotation of the C-helix, which removes glutamate 501 from its key position in the active site. In the active state, this glutamic acid residue must form a hydrogen bond with the active site lysine 483. In BRAF, the outward position of the C-helix is enforced by a helix-like turn in the N-terminal portion of the activation loop. We term this element the "inhibitory turn" for its crucial role in stabilizing the quiescent state of the kinase. These structural differences are readily apparent in a side-by-side comparison of the inactive versus active states of the kinase (Figure 7a). For this comparison, Chain B of PDB entry 4MNE is chosen as a representative active structure. In addition to the displaced C-helix and inhibitory turn, this comparison reveals a markedly more closed relative orientation of the N- and C-lobes in the inactive state of the kinase. Superposition of the active and inactive states of the kinase using only their C-lobes shows a ~15° closure in the inactive state, as compared with the active kinase. Note also that the P-loop (for phosphate-binding loop) is well-ordered in the inactive state, due to extensive interactions with the phosphate groups of the bound nucleotide (Figure 7a). An extensive network of interactions among the C-helix, inhibitory turn, P-loop and bound nucleotide analog stabilize the inactive state. Valine 600, the most frequently mutated

single residue in BRAF-driven melanoma, is located on the inhibitory turn under the C-helix. The van der Waals contacts between valine 600 and hydrophobic residues lining the allosteric pocket prevent the C-helix from swinging inward and bringing glutamate 501 in contact with lysine 483, which is

Figure 7. Key features of the autoinhibited BRAF kinase.
7a.

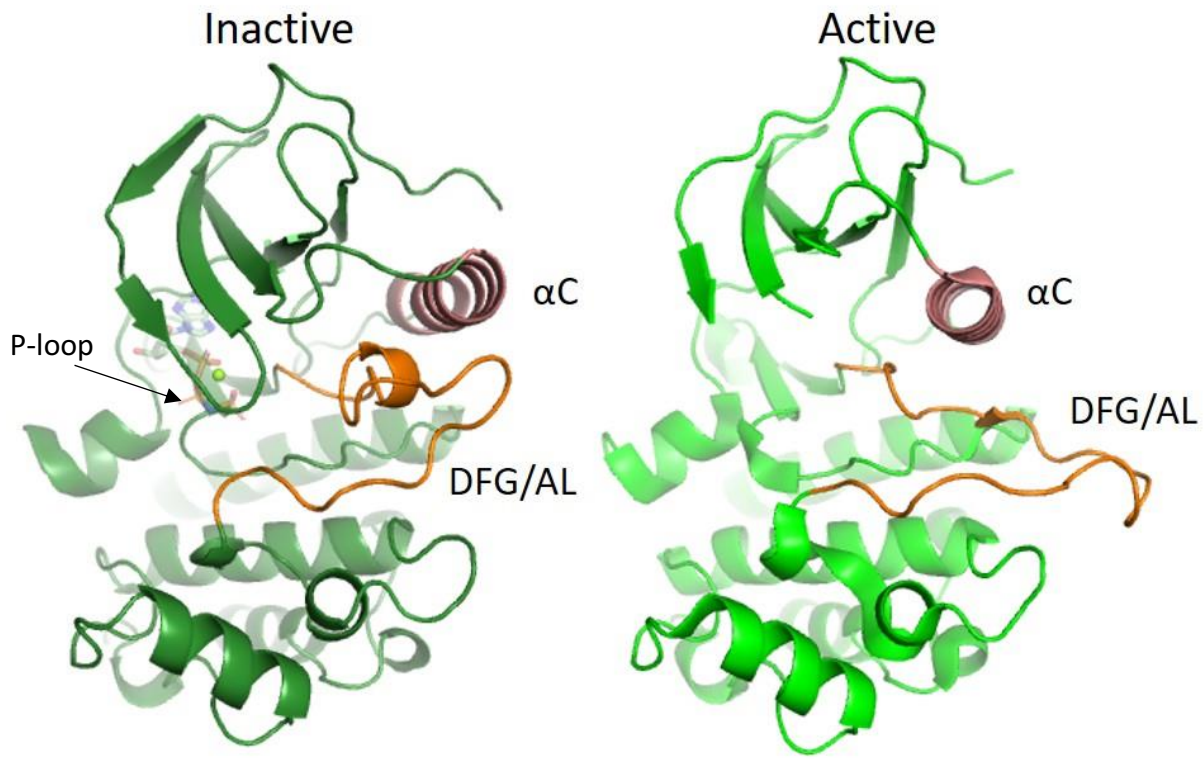

Figure 7 (contd.) 7b.

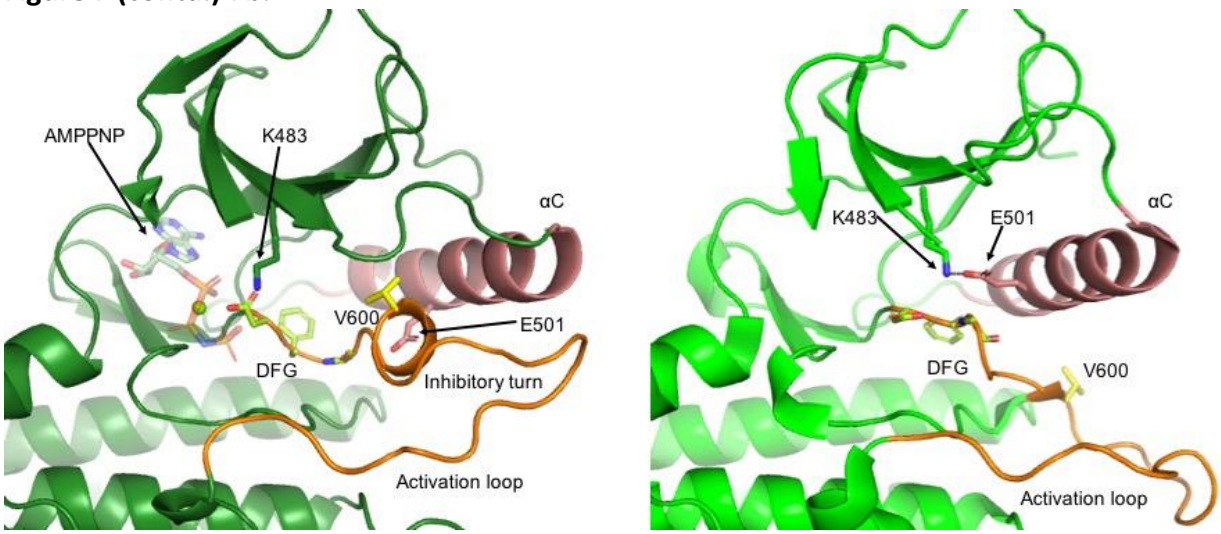

7a. The inhibitory turn prevents glutamate 501 from forming a salt bridge with lysine 483, an interaction key for phosphotransfer. Further, hydrophobic interactions between V600 (yellow) and hydrophobic residues along the inner face of the C-helix (see Figure 6b) secure the inactive state in the BRAF kinase. 7b. The inactive and active conformations of the BRAF kinase contrast in three major ways. The activation loop forms a helix-like turn under the C-helix. This sterically enforces the C-helix "out" conformation, preventing a complete active site from forming. Finally, the N- and C-lobes are closer together in the inactive conformation – most noticeable in the downward dip of the P-loop to the level of the inhibitory turn.

required to complete the catalytic site (Figures 7a, 9a). In the active state, the inhibitory turn unwinds and the activation loop extends outward, displacing V600 from the hydrophobic pocket and enabling the K483-E501 salt bridge required for catalysis.

The BRAF:MEK1 crystal structure reveals the *bona fide* inactive state of BRAF

Because the crystal structure described here contains only the kinase domain of BRAF, and the N-terminal regions are known to play a role in BRAF regulation, it is important to consider

whether the conformation present in the crystal structure fully recapitulates the inactive state. As noted above, our laboratory has also recently determined a cryo-EM structure of full-length BRAF and MEK in the active state, together with the regulatory 14-3-3 dimer (Figure 8a). In this full-length structure described in Park E *et al*., the kinase and CRD domains of BRAF are cradled by the 14-3-3 dimer. Additional BRAF:14-3-3 contacts are made between the residues surrounding pS365 and pS729. In this configuration, the BRAF back-to-back dimerization interface is occluded, providing another regulatory step for control of BRAF activation under wild-type conditions. The BRS and RBD are not resolved in this structure, suggesting they are exposed and unanchored, allowing for recruitment of the complex to the membrane by GTP-bound Ras (Figure 8b)[64].

We can directly compare the crystal structure of the BRAF:MEK kinase domain dimer with the corresponding region of the cryo-EM structure. Superposition of the two structures reveals a closely similar overall conformation, including essentially identical conformations of the inhibitory turn and outwardly displaced C-helix in BRAF (Figure 8c). Likewise, the inactive configuration of and relative orientation of MEK1 is the same in the two structures. One notable difference between the two structures is that the MEK1 N-terminal inhibitory helix is well-defined in the crystal structure, but was not-resolved in the cryo EM study (Figure 8c).

The fact that the isolated kinase domains of BRAF and MEK adopt the inactive conformation in the present crystal structure suggests that the kinase domains alone, with bound nucleotide analog, are sufficient for maintaining the inactive conformation. This interpretation is

further supported by our studies of the BRAF:MEK kinase complex in solution, where we find using size exclusion chromatography that, in the presence of ATP, it migrates as a dimer, as expected for the inactive state (as compared with a hetero-tetramer in the active state) (Figure A1)[64]. Furthermore, examination of the cryo-EM structure of the intact BRAF:MEK:14-3-3 complex suggests that the N-terminal regulatory domains of BRAF (in particular the CRD) together with the 14-3-3 dimer protect, rather that enforce, the autoinhibited conformation of the kinase module. Specifically, there are no interactions with these regulatory elements that impinge on the kinase module in a manner that is expected to affect its regulation.

Finally, it is of interest to ask why we obtained an inactive dimeric complex, rather than the active heterotetramer described by Haling et al. Indeed, our intended goal was to capture the complex in different stages of activation and inhibition by using nucleotide analogs, MEK inhibitors, and RAF inhibitors. We reasoned that the removal of the N-terminal inhibitory domains of BRAF would allow the formation of the back-to-back dimer required for activation of the wild-type kinase as observed in the Haling structure[14] (Figure 8d). In the longer term, our plan was to combine the kinase domains with synthetic, 14-3-3-binding phosphopeptides to capture what we hypothesized would be an active, 14-3-3-bound complex. After preparing the BRAF:MEK kinase complex, we sought to crystallize it with the expectation of obtaining the active heterotetramer. To our surprise, the structure revealed the inactive dimer described above. The most notable difference in our experimental approach as compared with that of Haling *et al*. is the MEK1 construct employed. Our structure included the entire MEK1 protein, whereas the

prior study truncated the first 61 residues of the protein. The truncated region removes the "negative-regulatory region" of MEK1, which in part consists of a helical segment (spanning residues 43-59) that packs against the N-lobe of the kinase. Although this helix does not interact directly with BRAF in the complex, it is thought to contribute to the stability of the inactive conformation of MEK1[56], including the displaced C-helix, which does directly contact BRAF. Thus we expect that formation of a complex with MEK1, and specifically full-length MEK1, is important for the stability of the inactive state of BRAF. In further support of this interpretation, studies of full-length BRAF and MEK in our laboratory showed that co-expression of MEK1 is required to obtain inactive-state complexes with BRAF. In the absence of overexpression of MEK1, only active BRAF:14-3-3 dimers were observed by cryo-EM.

The allosteric MEK inhibitor GDC0623 was used to determine both the cryo-EM structure of the full-length complex and the crystal structure of the kinase module (Figure 8). In both AMPPNP-GDC0623- and AMPPNP-binding structures we see a face-to-face dimer reminiscent of the tetrameric structure solved by Haling *et al*. in 2014[14], with some large-scale differences (Figures 8a, d). First, the asymmetric unit of the active structure crystal contains two heterotetramers. Each of these displays the stereotypical back-to-back BRAF dimer found in nearly all known BRAF kinase structures, and each BRAF protomer binds a MEK kinase face-to-face. In contrast, the asymmetric unit of the autoinhibited kinase module crystals contains one dimer. Upon inspection of the symmetry mates in the crystal lattice, no back-to-back BRAF dimers were observed. Indeed, most crystal contacts between adjacent dimers were MEK-mediated.

Figure 8. Both the full-length BRAF:MEK1:14-3-3 complex and the kinase module adopt an autoinhibited configuration.

Figure 8a.

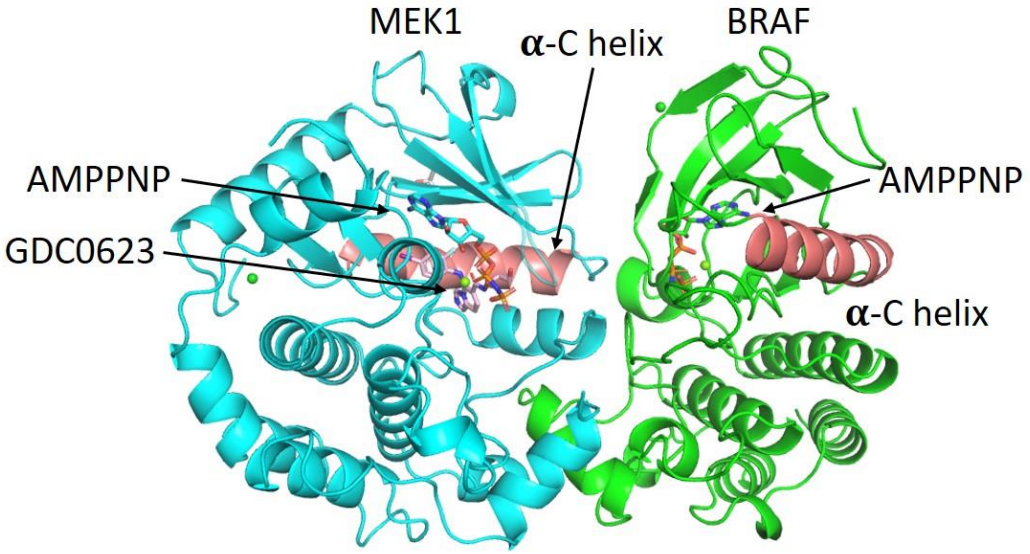

8b.

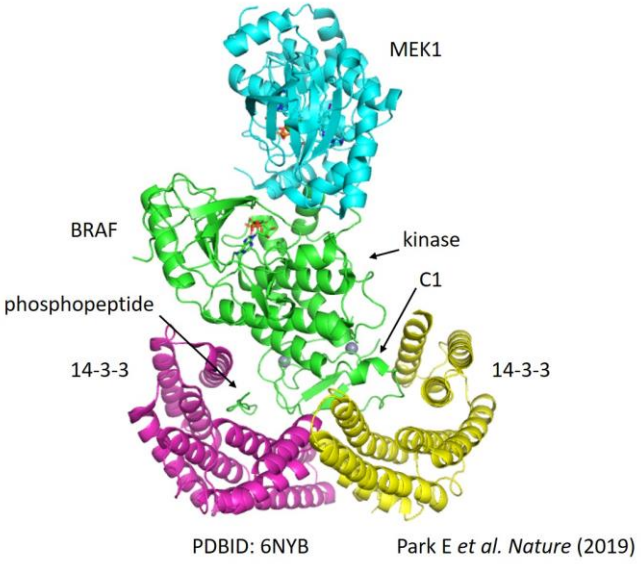

8c.

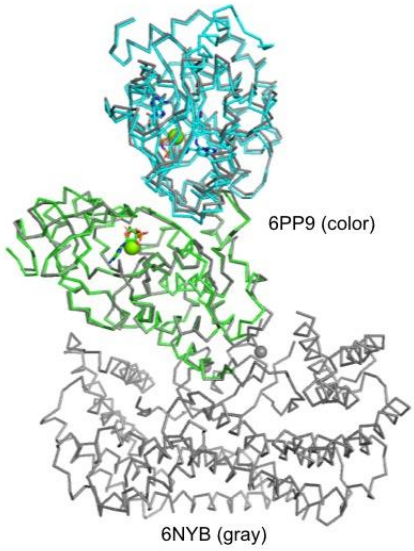

Figure 8 (contd.) 8d.

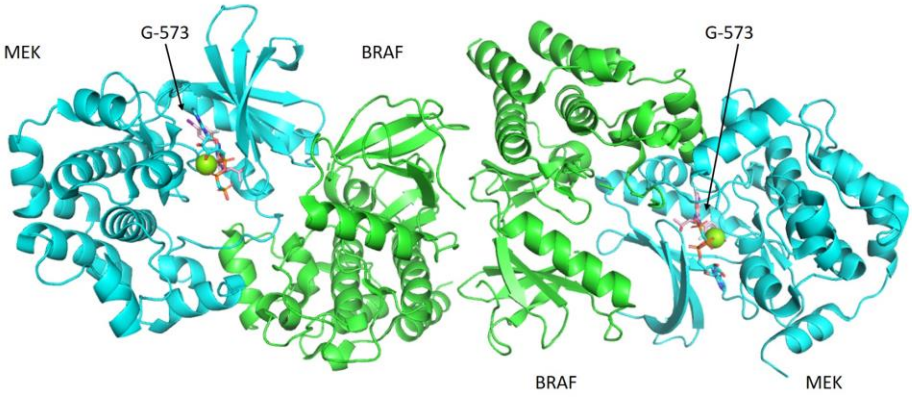

PDBID: 4MNE Haling *et al.* Cancer Cell (2014).

8a. The BRAF:MEK1:AMPPNP module bound to GDC0623 is nearly identical to the AMPNP-only structure. The MEK inhibitor binds adjacent to the nucleotide binding pocket. 8b. In the full-length autoinhibited complex, the 14-3-3 dimer envelops the BRAF CRD domain and binds the phosphoserine sites N- and C-terminal to the kinase. The BRAF back-to-back dimerization interface is occluded, and the kinase domains are bound face-to-face. 8c. A Cα alignment of the BRAF:MEK1 kinase module bound to AMPPNP and GDC-0623 (BRAF in green, MEK1 in cyan) with the full-length complex. The kinase module alone recapitulates the large-scale features of the full complex: the face-to-face BRAF:MEK1 kinase dimer is placed perfectly into the cryo-EM structure density. 8d. The active heterotetramer complex is comprised of a canonical back-to-back BRAF dimer, where each protomer binds a MEK1 kinase face-to-face. Even though G-573 is a nearly identical inhibitor to GDC0623, our two structures are vastly different both at large and small scales.

Mechanism of activation of BRAF by V600E and other oncogenic mutations

The significance of this structure extends to our understanding of how oncogenic mutations destabilize the inactive state. Point mutants at residue 600 (to glutamate or lysine) cause roughly 75% of BRAF-driven melanoma[65,66]. The introduction of a charged residue in the inhibitory helix-like turn disrupts a hydrophobic interaction network that spans β-strands 4 and 5 (Leu 485, Leu 525, and Val 487), the C-helix (Phe 498, Leu 505, and Leu 527) , and the activation loop (Gly 596, Val 600, and Lys 601) (Figure 9a, left panel). This encourages the extension of the

activation loop and allows the C-helix to swing inward. The V600E mutation further stabilizes the active conformation by introducing a salt bridge between Lys 507 on the outer face of the C-helix and Glu 600 (Figure 9a, right panel)[14]. Even more intriguingly, most oncogenic mutations of BRAF cluster around either the hydrophobic pocket between the inhibitory turn and the C-helix or the nucleotide-binding region (Figure 9b). This includes mutations that inactivate the BRAF kinase, such as D594N[46,67]. The fact that even kinase-inactivating mutations can confer oncogenic potential underscores the importance of the protein's nucleotide-binding capability for the maintenance of the autoinhibited state of the complex.

Figure 9. Structure of the inactive BRAF kinase informs mechanism by which oncogenic mutations drive aberrant signaling.

9a.

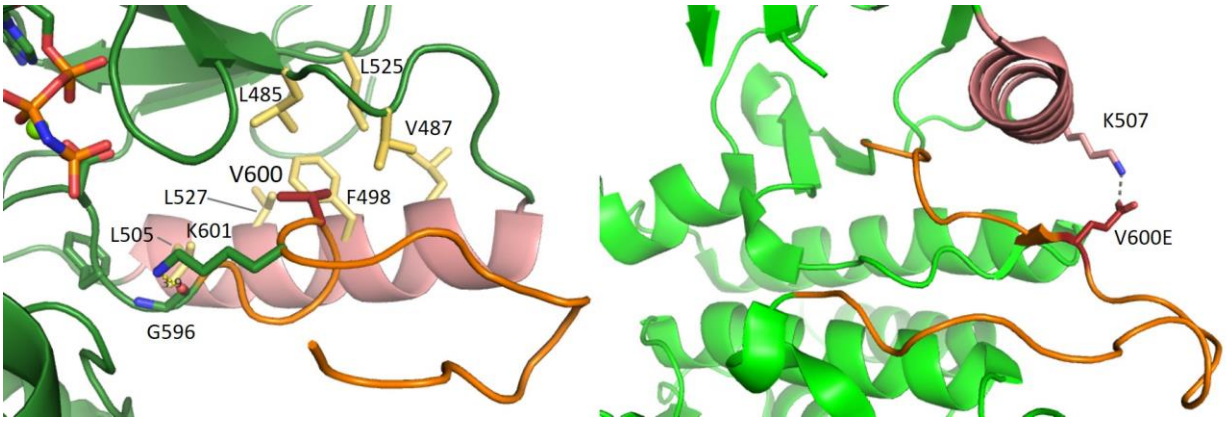

9b.

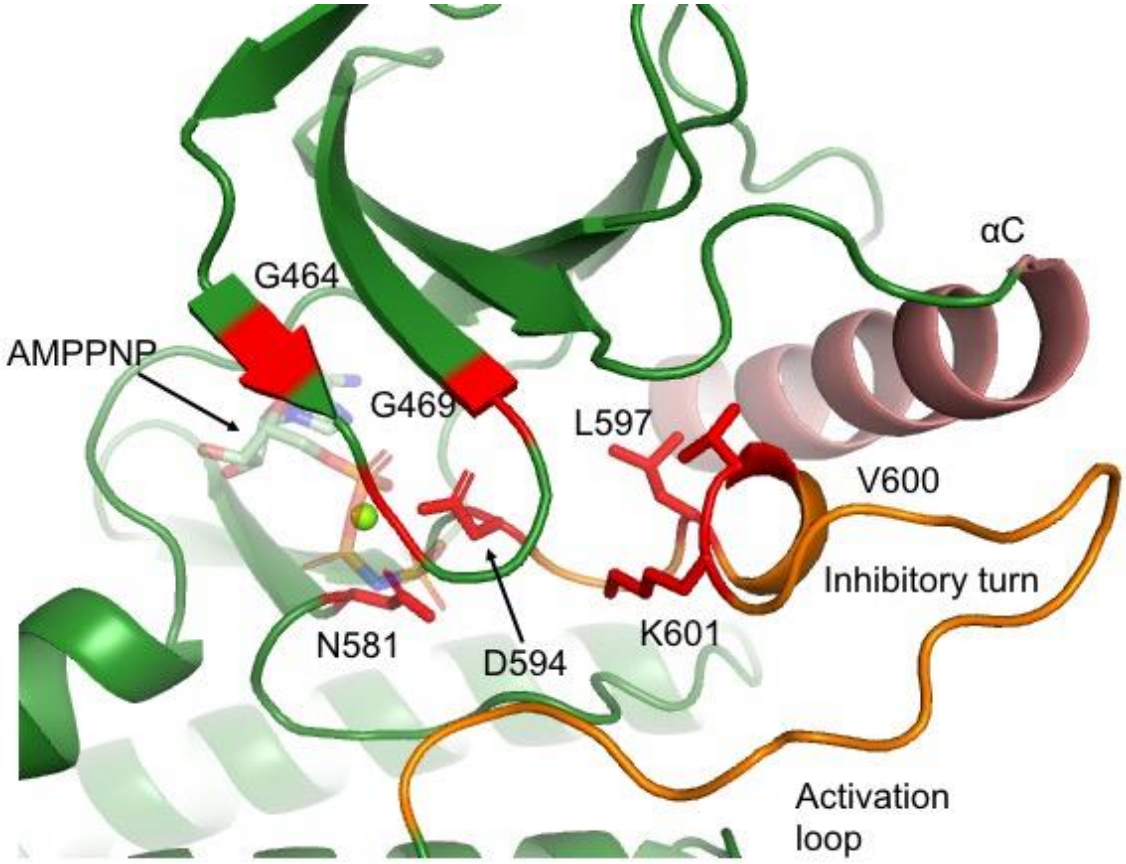

Figure 9 (contd.) 9a. Near atomic-level resolution gives us a detailed understanding of the mechanism by which the V600E mutation encourages constitutive activation of the BRAF kinase. The right panel displays the salt bridge formed by glutamate 600 with lysine 507 that stabilizes the extended activation loop conformation, conferring $BRAF^{V600E}$ its hyperactive, oncogenic character. 9b. Oncogenic mutations in BRAF cluster around the inhibitory turn:C-helix interface as well as the nucleotide-binding pocket. Our AMPPNP-bound structure (forest green) is being compared to the $BRAF^{V60E}$ structure solved by Haling *et al.* in 2013 PDBID: 4MNF.

The BRAF inactive configuration is closely similar to that of the CDK- Src- and ErbB-family kinases

The inactive configuration of BRAF described above resembles a "stereotypical" inactive conformation previously observed in other kinases, including cyclin-dependent kinases, Src- and ErbB-family kinases. In Figure 10, we compare the inactive and active conformations of BRAF with the Src and EGFR kinases. Characteristic features across kinase subfamilies include a turn or two in the activation loop which block the inward active position of C-helix. EGFR is activated by asymmetric, tail-to-head dimerization with a "donor" kinase, mechanistically similar to how cyclins allosterically activate cyclin-dependent kinases (CDKs)[68], whereas Src is activated by a shift between intra- to inter-molecular interactions involving the kinase and SH2-SH3 domains[69]. This study highlights how, under different, pathway-level activation mechanisms, the main hallmarks of the transition between states is remarkably conserved across kinases: the activation loop uncoils, allowing the C-helix to swivel inward to complete the active site.

Figure 10. Comparison of active and inactive structures of three different proteins highlights the hallmarks of kinase activation.

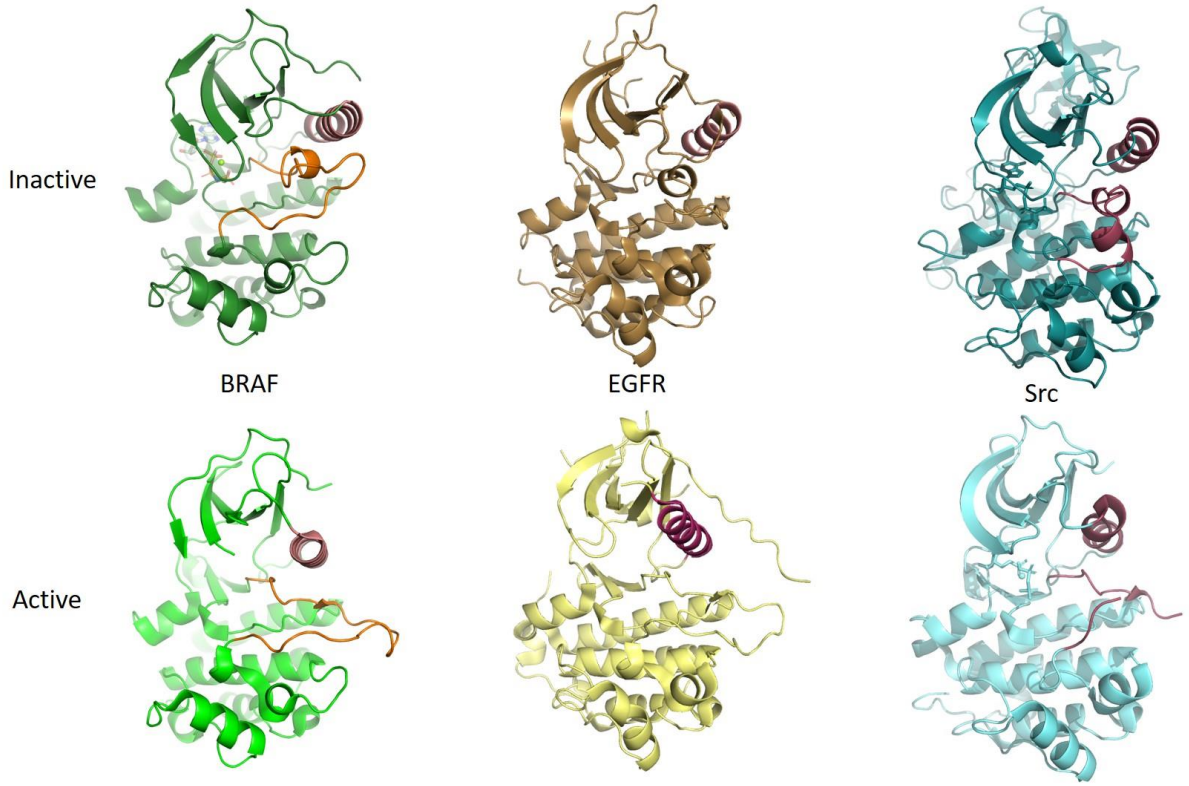

The inactive conformation of BRAF shares many defining characteristics with other kinases. The C-helix-out, activation loop-in configuration is conserved across many kinase families, including EGFR, Src, CDKs, among others. Note the transition in the activation loop required for the C-helix to swing inward: The inhibitory turn unspools, and the activation loop extends outward to make room for the C-helix "in" state that completes the kinase catalytic site.

Discussion

The structure of the autoinhibited BRAF:MEK1 kinase module described above adds further evidence that the full complex, rather than BRAF by itself, serves as the gatekeeper node for MAPK pathway activation. This is the first view of the authentic inactive state of the BRAF kinase unperturbed by inhibitor. It therefore represents our best snapshot of the "resting state"

of this molecule in cells. Our observation that the kinase module in the absence of any other regulatory domains or interactions adopts an autoinhibited state virtually identical to the full-length complex suggests that MEK1 and nucleotide are essential components of BRAF kinase regulation. The sufficiency of the kinase module for the autoinhibited state, coupled with the tight affinity of the kinase domains for each other (K_D=10-15 nM, further discussed in Chapter 3) and the relative excess of MEK in relation to RAF proteins in many human tissues[70], imply that most, if not all, the BRAF molecules in the cell are sequestered away by this complex in the absence of growth factor signaling. Biochemical and structural evidence that the other RAF proteins are also kept inactive in similar complexes would be singularly helpful in understanding MAPK biology.

In January 2020, a group at Genentech led by Jawahar Sudhamsu published an article in *Nature Structure and Molecular Biology* describing a BRAF:MEK1 kinase complex structure virtually identical to our structure (RMSD=0.386 Å)[71]. The main difference in our structures is the ATP analog cocrystallized with the kinases: we used AMPPNP and they used AMPPCP. They arrive at the same conclusion that ATP is required to form the autoinhibited complex, and provide support for this assertion by detailing the shift in retention volume on a size-exclusion column for the complex in the presence and absence of ATP, BRAF, and MEK inhibitors (Figure A1).

The elucidation of the autoinhibited state described above has two main implications for one of the thorniest problems confronting the treatment of MAPK pathway malignancies: paradoxical activation of ERK in the presence of $BRAF^{V600E}$-specific inhibitors. First, the key role that nucleotide-binding has in the maintenance of the tight inhibitory interaction between BRAF

and MEK1 poses a challenge for practically all BRAF inhibitors in the clinic today; they all displace nucleotide from the BRAF active site. Second, since BRAF inhibitors decrease the affinity of BRAF for MEK1 (Chapter 3, previous literature), they may be releasing BRAF from its autoinhibitory complex. Although these observations are preliminary and require follow up with kinase inhibition assays, as well as a better understanding of the affinities of different MEK and BRAF inhibitors to the complex versus the free kinases, they represent a considerable step toward untangling the biology and pharmacology of the MAPK pathway.

Chapter 3: Dissecting the mechanism of action of inhibitors that target the MAPK pathway

Part of this work was completed in collaboration with Dr. Kunhua Li in the Eck lab. K.L. performed the radiometric kinase activity assays and guided me through structure refinement. We solved and refined structures in parallel.

Introduction

The MAPK pathway's status as a central node in the pro-growth and pro-proliferation signaling programs in the cell makes it an obvious hotspot for oncogenic potential[67,72]. When targeting this pathway, there are many trade-offs that need to be considered. As mentioned in Chapter 2, current mutant BRAF inhibitors currently in the clinic cause an increase in ERK2 phosphorylation even though they show exquisite potency against the mutant kinases. The new mutant-specific RAS inhibitors are a welcome innovation but can only prevent MAPK signaling in mutant RAS backgrounds[24].

Given the difficulty of consistently treating BRAF mutation-driven malignancies with current mutant BRAF-specific inhibitors[57], efforts have been directed toward the discovery of MEK-inactivating molecules. MEK inhibitors alone are broadly more effective at shutting down ERK phosphorylation than are RAF inhibitors, but suffer from two main drawbacks: First, MEK inhibitors lack the therapeutic window that current RAF inhibitors exploit, since they are being used to treat tumors driven by mutations upstream of MEK; and second, they do not all inhibit ERK2 phosphorylation with equal effectiveness depending on the mutational background of the malignancy[30,31]. Combination treatments, such as dabrafenib with trametinib and vemurafenib with cobimetinib, are currently the most promising frontline treatments for V600E-driven melanoma in the clinic[58].

Insights into drugging the MAPK pathway have, until the last decade, mostly come from cell-based assays, where the redundancy of enzyme functions and multiple moving parts makes it exceedingly challenging to control enough variables to be able to unambiguously identify a compound's mechanism of action. Biochemical analyses of the mechanism of action of MEK inhibitors has traditionally focused exclusively on how potently and selectively a compound can directly inhibit the phosphorylation of ERK by MEK[43,59]. Our discovery of the BRAF:MEK1 complex bound to a suite of allosteric MEK inhibitors changes our understanding of how these compounds work in cells: inhibitors may work at the level of the RAF:MEK1 complex, not just directly on free, soluble MEK1. The recognition of the role of the RAF:MEK complex in pathway regulation, together with the allosteric binding site of MEK inhibitors, suggests many plausible mechanisms by which these agents could act: they could 1) prevent recruitment of MEK1 to BRAF, 2) prevent phosphorylation of MEK1 by BRAF, 3) prevent release of pMEK from the RAF:MEK:14-3-3 complex, and 4) inhibit pMEK activity directly (Figure 11). In order to thoroughly address this gap in our knowledge, we have reconstituted different components of the MAP kinase cascade *in vitro* for biochemical, biophysical, and structural characterization in the presence of a battery of RAF and MEK inhibitors. Our long-term goal is to develop assays that dissect out each of these specific contributions to pathway inhibition, and to understand how they relate to the differential efficacy of MEKis in various mutational contexts.

Figure 11. Model for how MEK inhibitors target the MAPK pathway. There are four possible ways a MEK inhibitor can shut down signaling through the MAPK pathway: 1) Prevent recruitment of MEK1 to BRAF, 2) Prevent phosphorylation of MEK1 by BRAF, 3) Prevent release of pMEK from the RAF:MEK:14-3-3 complex, and 4) inhibiting pMEK activity directly.

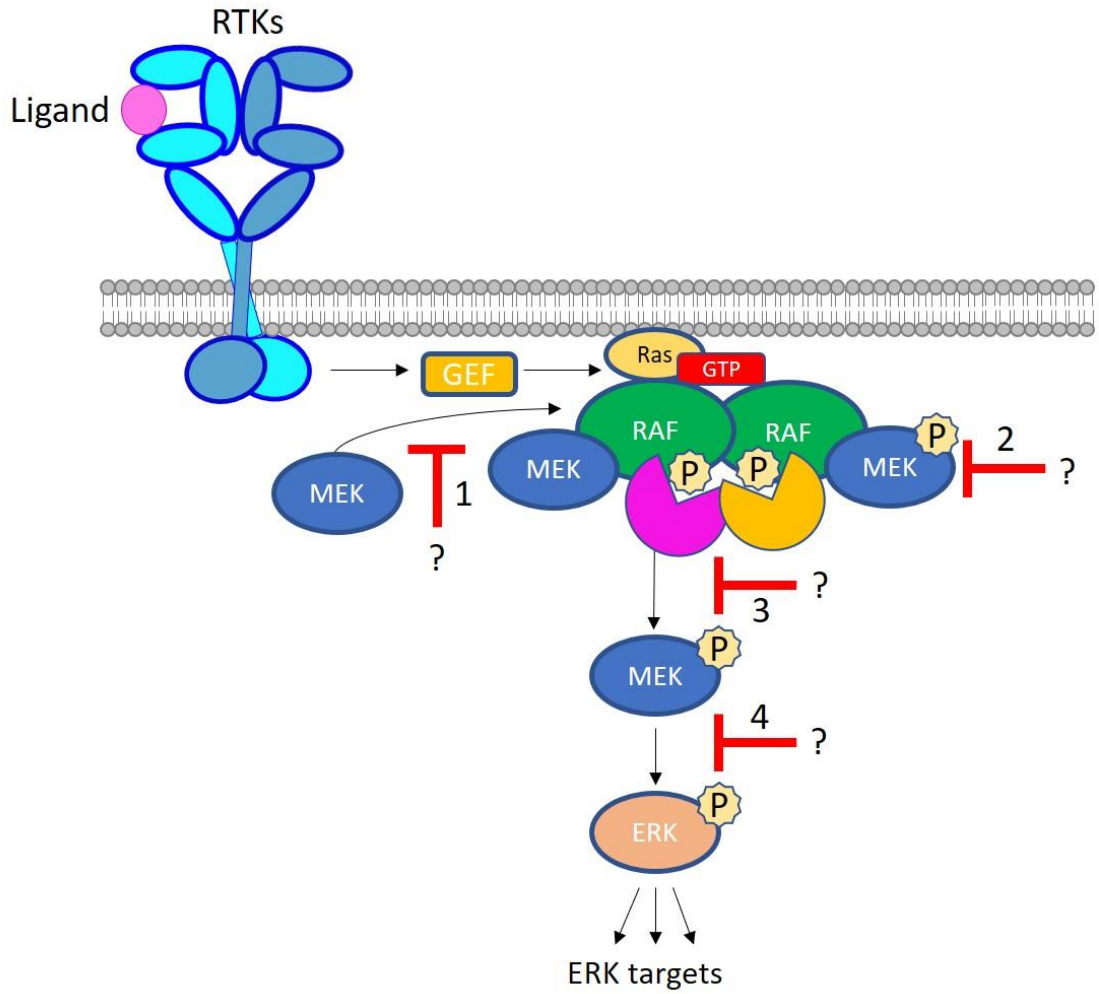

In this chapter, I report the results of MAP kinase activity assays, biolayer interferometry experiments measuring the binding affinity of the BRAF:MEK1 kinase complex, and the structures of said complex in the presence of eight clinically relevant MEK1 inhibitors. These experiments have yielded a wealth of mechanistic knowledge to help us understand how certain inhibitors work, and why they do or do not work depending on what mutations are driving the malignancy. The results of our radiometric activity assays show how all the allosteric MEK inhibitors we tested exhibit a marked decrease in potency when exposed to prephosphorylated MEK, contrasted with their effect on a coupled BRAF:MEK1:ERK2 system. The binding experiments demonstrate how MEK1 phosphorylation decreases its affinity for the BRAF kinase, and provide us with a better understanding of how certain inhibitors perturb this complex: PD0325901 increases BRAF:uMEK affinity, while cobimetinib decreases it. Most intriguingly, CH5126766 increases BRAF:pMEK affinity back to levels equivalent to that of the BRAF:uMEK interaction. Finally, the crystal structures of the BRAF:MEK1 kinase module we solved in the presence of these MEK inhibitors help explain why different compounds behave the ways they do. All MEKis, with the exception of CH5126766, interact directly with the MEK1 nucleotide in a way that stabilizes both ligands in their respective pockets. Some inhibitors interact directly with the BRAF kinase, while others change the orientation of the MEK1 activation segment phospho-serines, in a way that may encourage (or at least allow) MEK1 phosphorylation by BRAF. Taken together, these experiments start to inform a model for MAPK pharmacology where different compounds target the RAF:MEK:ERK2 axis at different stages: recruitment of MEK1 to active BRAF, phosphorylation of

MEK by BRAF, release of phosphorylated MEK from the complex, and direct inhibition of active, phosphorylated MEK1.

Materials and Methods

Insect cell expression and purification of $BRAF^{445-723}$ kinase for biophysical and kinase assays

For our binding and kinase assays, we infected Sf9 cells with the same recombinant baculovirus construct encoding the $BRAF^{445-723}$ construct used for crystallization. The expression and purification of the BRAF kinase followed the same first steps as purification of the BRAF:MEK kinase complex: briefly, cells were lysed by sonication on wet ice in the same buffer conditions, and the lysate was clarified by ultracentrifugation. After initial batch-mode Ni-NTA purification, the C-terminal chitin binding domain was cleaved by overnight incubation of the elution fractions with 100mM MESNA. The N-terminal His_6 tag was retained for use as the capture "handle" for biolayer interferometry experiments. In preparation for ion exchange chromatography, the Ni-NTA eluate was carefully diluted 1:3 into IEX buffer A (50mM HEPES pH 7.5, 1mM TCEP), and applied to a 5/50 Mono S cation exchange column. After ~50 CVs washing with 5% IEX buffer A, the BRAF kinase was eluted along a 5-50% IEX buffer B (50mM HEPES pH 7.5, 1M NaCl, 1mM TCEP) gradient for 20 CVs. Fractions were analyzed by SDS-PAGE, relevant fractions were pooled and concentrated to 16µM, and 10µL aliquots were flash-frozen in liquid nitrogen for storage at -80C. Final yield from 6L Sf9 culture was 0.8mg. Activity was assessed by ATP titration as well as BRAF kinase titration phosphorylation assays, and compared to literature and in-house standards.

Bacterial expression and purification of MEK^{62-393}

Bacteria-expressed MEK kinase (MEK^{62-393}) was engineered with an N-terminal, TEV-cleavable His_6 tag for purification purposes, We expressed these constructs in BL21 DE3 *E. coli* by growing cells at 37C at 180rpm agitation until OD 0.5-0.7, at which point the flasks were cooled by immersion in ice water for 10-15 minutes. Expression was induced by addition of 0.5mM IPTG and overnight incubation at 18C with agitation.

Cells were harvested and pelleted by centrifugation at 2500g for 20 minutes. The pellets were resuspended in roughly 20mL per L of culture of Bind/Wash buffer (50mM HEPES pH 7.5, 250mM sodium chloride, 30mM imidazole, 1mM TCEP) with 1mM phenylmethylsulfonyl fluoride to inhibit serine protease activity. Cells were disrupted in a steel beaker on wet ice using a sonicator between settings 7-8 using 2s on/8s off pulses for 1.5-2 minutes. All proceeding steps were done on ice. The lysate was clarified by centrifugation in a Sorvall floor centrifuge for 1.5-2h at 17,000rpm. After centrifugation, the cleared lysate (CL) was carefully pipetted from the centrifuge tubes, sacrificing the last 1-2 mLs of cloudy, suspended lipids and particulates. CL was then filtered using syringe-driven, 0.8um filters. Care was taken to replace the filter when resistance to pressure became significant. The cleared lysate was then applied to a pre-equilibrated 5mL bed volume HisTrap column using a P1 peristaltic pump between speed settings 2-3 in the 10x configuration. When all the lysate was passed through the column, nonspecific

impurities were removed by washing the column with 50-80mL Bind/Wash buffer on an AKTA explorer FPLC, at 2.5-3mL/min flow, or until a relatively flat UV reading was reached. $MEK1^{62-393}$ was eluted along a 100mL gradient from 0-50% Elution buffer (50mM HEPES pH 7.5, 250mM sodium chloride, 250mM imidazole, 1mM TCEP) and collected in 10mL fractions. The relevant peak eluted between 25-32% Elution buffer. Fractions were pooled (normally ~50mL for the whole peak), and the His_6 tag was then cleaved by addition of homemade TEV protease and incubation overnight at 4C in the cold room or refrigerator. The next day, the MEK/TEV mixture was concentrated using a 15mL, 30,000 NMWCO Amicon spin concentrator that had been pre-rinsed with Bind/wash buffer to no more than 15mg/mL. During the concentration step, a GE S75 10/300 size exclusion column was equilibrated with 1.5 column volumes of Sizing buffer (50mM HEPES pH 7.5, 250mM sodium chloride, 1mM TCEP). Concentrated protein was injected into the FPLC in 500µL volumes using a 1mL injection loop, and 0.5mL fractions were collected. The resulting fractions were analyzed by SDS-PAGE, and relevant fractions were pooled and concentrated to 20-25mg/mL and frozen in 20 and 50µL aliquots. Final yield of MEK^{62-393} was 10-11mg per liter of culture.

<u>$BRAF^{445-723}$ and MEK^{62-393} kinase assays</u>

Kinase activity assays for quality control and inhibition experiment optimization were performed using Kinase Buffer (100mM Hepes, pH 7.5, 150mM sodium chloride, 5mM magnesium chloride, 1 mM TCEP). Separate titrations of BRAF and ATP were used to determine the activity of my BRAF preparation. BRAF was titrated from a 1.6µM concentration by six three-

fold serial dilutions, using a fixed 100μM ATP concentration to start the reaction. ATP was titrated from 1mM concentration by six three-fold serial dilutions using a fixed 20nM concentration of BRAF. MEK^{62-393} was used as a substrate, at a final concentration of 20μM. Activity was measured by Western blot, using anti-MEKpS218/pS222 primary antibody (Cell Signaling Technologies).

In vitro reconstitution of the MAPK pathway to dissect the mechanism of action of RAF and MEK inhibitors were also performed in Kinase Buffer. Quality control and optimization was initially performed by Western blot, using phosphorylation of a kinase-dead species of ERK2 as a readout. The final ERK2 concentrations for Western Blot experiments was 20μM. For the coupled BRAF:MEK1:ERK2 assay, 20nM $BRAF^{445-723}$ and 200nM $MEK1^{62-393}$ were used, and ATP was titrated from a 1mM final concentration by six three-fold serial dilutions. For the phosphorylated MEK1 assay, I used *in vitro*-phosphorylated $MEK1^{62-393}$ (pMEK) kindly prepared by Dr. Kunhua Li. pMEK was titrated from a 1μM concentration by six three-fold serial dilutions in the presence of 100μM ATP to determine the right enzyme concentrations for inhibition experiments. Activity was measured by Western blot, using anti-phospho-p44/p42 MAPK (pT202/pY204) primary antibody (Cell Signaling Technologies).

Radiometric inhibition assays performed by Dr. Kunhua Li used the same buffer conditions described above. 1 μC of γ-^{32}P ATP (Perkin Elmer) was diluted 1:1200 into a 1mM ATP stock solution, which was further diluted ten-fold for a final ATP concentration of 100μM. MEK inhibitors were titrated from a starting concentration of 3μM using eight three-fold serial

dilutions. Kinase-dead ERK2 was used as a substrate, at a final concentration of 1μM. For the coupled enzyme assays, $BRAF^{445-723}$ was used at a final concentration of 4nM, and unphosphorylated MEK^{62-393} was used at a final concentration of 500pM. For inhibition assays of phosphorylated MEK, 500pM of pMEK was used. The reaction was started by addition of the ATP stock at room temperature (25C), and stopped by the 1:1 addition of 0.1M EDTA after one hour. SDS-PAGE was run on these samples, and the gels were dried for four hours before exposure to a detection plate overnight. Counts were measured using a phosphorimager, and relative activity was determined by densitometry using ImageJ software. IC_{50} values were determined using the PRISM software.

Biolayer interferometry binding experiments

Experiments measuring the binding affinity of MEK1 for the BRAF kinase were performed on an OCTET Red 384 Biolayer interferometer (Molecular Devices/ForteBio) at the Center for Macromolecular Interactions at Harvard Medical School. Ni-NTA-coated biosensors (ForteBio/Molecular Devices) were prewetted in Octet Soaking buffer (50mM Hepes pH 7.5, 150mM sodium chloride, 5mM magnesium chloride, 1mM TCEP, and 0.1% w/v BSA) for ten minutes before the start of the experiment. Next, the pre-loading baseline was determined by dipping the biosensors in Octet Assay buffer 1 (50mM Hepes pH 7.5, 150mM sodium chloride, 5mM magnesium chloride, 1mM TCEP, 0.1% w/v BSA, and 0.02% Tween-20) for 60 seconds. His_6-tagged BRAF kinase was diluted in Octet Assay buffer 1 to a concentration of 20μg/mL and loaded

onto the biosensors over a period of 120 seconds. The post-loading baseline was determined by dipping the biosensors in Octet Assay buffer 2 (50mM Hepes pH 7.5, 150mM sodium chloride, 5mM magnesium chloride, 1mM TCEP, 0.1% w/v BSA, 0.02% Tween-20, and either 0.5mM ATP or 0.5mM AMPPNP) for 120 seconds. Association measurements were determined by dipping the biosensors into seven three-fold serial dilutions of MEK1 (starting concentration 1µM) and one no-MEK1 well for 300 seconds, followed by a 900 second dissociation phase in the same Octet Assay buffer 2 wells. When performing experiments in the presence of MEK or RAF inhibitors, 0.5% v/v DMSO was added to all buffers, and a fixed concentration of 2µM inhibitor was used. Double subtraction was performed using the no-MEK1 condition as a sample blank, and a full dataset collected without loading BRAF onto the sensors. Kinetic and steady-state fits were determined using the Octet Data Analysis HT 11.0 Suite.

BRAF:MEK1:MEKi kinase domain crystallization and structure determination.

For crystallization, aliquots of the BRAF:MEK kinase complex were incubated with 5 mM MgCl2, 2 mM Adenosine 5'(β,γ-imido)triphosphate (AMPPNP), and 0.2 mM PD0325901 in storage buffer at 4°C overnight. Rod-shaped crystals suitable for structure determination were obtained by vapor diffusion in hanging drops using two different reservoir solutions: 22% PEG3350, 0.1M Tris pH 8.5, 0.2M Lithium Sulfate (AMPPNP) and 22% PEG3350, 0.1M Bis-Tris pH 6.5, 0.2M Ammonium Sulfate (PD0325901) at room temperature. For all other complex crystal structures, 2µL drops containing crystals of BRAF:MEK:AMPPNP were spiked with 1µL reservoir solution containing 0.2-0.5mM inhibitor (Binimetinib, trametinib, cobimetinib, pimasertib,

selumetinib, or CH5126766) for 20-30 minutes prior to harvesting. Crystals were harvested and flash frozen in liquid nitrogen using additional 20-22% glycerol as a cryoprotectant. X-ray diffraction data were collected at 100 K using NE-CAT beamline ID-24-C at the Advanced Photon Source, Argonne National Laboratory, at a wavelength of 0.9786 Å. Data were integrated and merged using XDS and scaled using Aimless in the CCP4 suite, or by the Xia2 suite using the Dials mode. The initial structure of the complex containing GDC0623 was phased by molecular replacement in PHASER using PDB entry 4MNE as an initial search model. Molecular replacement of the AMPPNP-only and all other inhibitor-bound structures was performed using the GDC0623 structure as a search model. Inhibitors were placed into positive density in an initial F_o-F_c map and included in subsequent rounds of refinement using PHENIX.REFINE. Successive manual refinement was performed using COOT. The data collection and refinement statistics are presented in Table 2.

Table 2. Data collection and refinement statistics for the BRAF:MEK1:AMPPNP:MEKi structures.

	PD0325901	Binimetinib	Trametinib	Cobimetinib	Pimasertib	Selumetinib	CH5126766
Wavelength	0.9787	0.979	0.978	0.979	0.979	0.979	0.979
Resolution range	43.57 - 2.47 (2.56 - 2.47)	43.21 - 3.09 (3.201 - 3.09)	43.35 - 3.451 (3.575 - 3.451)	43.29 - 3.16 (3.273 - 3.16)	43.55 - 3.09 (3.2 - 3.09)	43.24 - 3.19 (3.304 - 3.19)	43.33 - 3.12 (3.232 - 3.12)
Space group	P 31 2 1	P 31 2 1	P 31 2 1	P 31 2 1	P 31 2 1	P 31 2 1	P 31 2 1
Unit cell	116.53 116.53 130.71 90 90 120	115.722 115.722 129.62 90 90 120	116.716 116.716 129.483 90 90 120	116.144 116.144 129.886 90 90 120	117.334 117.334 130.004 90 90 120	116.964 116.964 129.733 90 90 120	116.784 116.784 129.256 90 90 120
Total reflections	739633 (73862)	372223 (34601)	64373 (6486)	349081 (35941)	279172 (28710)	171898(31146)	280285 (28779)
Unique reflections	37262 (3669)	18830 (1832)	13509 (1329)	17794 (1747)	19401 (1901)	17505 (1733)	18575 (1809)
Multiplicity	19.8 (20.1)	19.8 (18.9)	4.8 (4.9)	19.6 (20.6)	14.4 (15.1)	9.8 (10.0)	15.1 (15.9)
Completeness (%)	99.94 (100.00)	99.90 (99.95)	97.53 (98.37)	99.88 (100.00)	99.93 (99.89)	99.77 (100.00)	99.91 (99.89)
Mean I/sigma(I)	14.8 (2.0)	20.92 (1.65)	9.40 (2.28)	18.76 (1.63)	18.68 (1.59)	10.9 (2.0)	18.33 (1.66)
Wilson B-factor	44.52	100.21	86.04	107.26	102.34	109.82	102.01
R-merge	0.179 (2.02)	0.1424 (1.966)	0.1498 (0.6754)	0.1543 (2.097)	0.1264 (1.856)	0.138 (1.253)	0.1459 (1.833)
R-meas	0.184 (2.07)	0.1462 (2.02)	0.1685 (0.758)	0.1585 (2.15)	0.1311 (1.921)	0.153 (1.394)	0.1511 (1.893)
R-pim	0.0411 (0.459)	0.03277 (0.4624)	0.07551 (0.3383)	0.03577 (0.472)	0.03444 (0.4921)	0.066 (0.605)	0.03862 (0.4721)
CC1/2	0.998 (0.717)	0.999 (0.753)	0.992 (0.748)	0.999 (0.745)	0.999 (0.66)	0.996 (0.743)	0.999 (0.66)
CC*	1 (0.914)	1 (0.927)	0.998 (0.925)	1 (0.924)	1 (0.892)		1 (0.892)
Reflections used in refinement	37258 (3671)	18823 (1831)	13496 (1329)	17784 (1747)	19397 (1899)	17502 (1733)	18570 (1809)
Reflections used for R-free	1906 (209)	921 (67)	636 (46)	818 (92)	941 (110)	803 (84)	839 (77)
R-work	0.182 (0.234)	0.1945 (0.2925)	0.1828 (0.2671)	0.1806 (0.2698)	0.1883 (0.2855)	0.1899 (0.3014)	0.1834 (0.2679)
R-free	0.212 (0.283)	0.2174 (0.3342)	0.2089 (0.3139)	0.2253 (0.3619)	0.2280 (0.3174)	0.2309 (0.3255)	0.2230 (0.3320)
CC(work)	0.955 (0.853)	0.959 (0.831)	0.958 (0.816)	0.966 (0.861)	0.964 (0.796)		0.961 (0.807)
CC(free)	0.949 (0.760)	0.970 (0.741)	0.938 (0.790)	0.966 (0.785)	0.910 (0.738)		0.966 (0.767)
Number of non-hydrogen atoms	4970	4728	4726	4725	4735	4722	4688
macromolecules	4685	4635	4620	4631	4648	4631	4623
ligands	114	91	106	94	87	91	65
Protein residues	590	2	583	584	590	584	583
RMS(bonds)	0.004	585	0.002	0.007	0.003	0.003	0.005
RMS(angles)	0.71	0.002	0.74	0.97	0.57	0.58	0.63
Ramachandran favored (%)	97.09	0.52	93.07	93.43	93.28	92.91	93.93
Ramachandran allowed (%)	2.57	94.13	6.41	5.88	5.86	6.40	5.03
Ramachandran outliers (%)	0.34	5.18	0.52	0.69	0.86	0.69	1.04
Rotamer outliers (%)	1.74	0.69	3.54	5.70	2.15	1.38	0.98
Clashscore	4.28	2.55	12.51	8.76	4.64	6.24	6.37
Average B-factor		5.39	82.73	105.07	95.71	106.58	96.53
macromolecules	49.30	102.55	82.67	105.10	95.88	106.64	96.75
ligands		102.72	85.62	103.99	86.78	103.46	80.80

Results

Expression and purification of BRAF$^{445-723}$ and MEK1$^{62-393}$

For the biochemical characterization of the MAPK pathway, I separately purified BRAF$^{445-723}$ from insect cells and MEK1$^{62-393}$ from *E. coli* (Figure 12). MEK1$^{62-393}$ is a construct that can be expressed in *E. coli*, and is not phosphorylated, as verified by western blot and MALDI mass spectrometry. Full-length MEK1 expressed in insect cells is heterogeneously phosphorylated by endogenous kinases, and therefore not an ideal reagent for binding and activity studies.

Figure 12. Expression and purification of BRAF$^{445-723}$ and MEK$^{62-393}$.

12a.

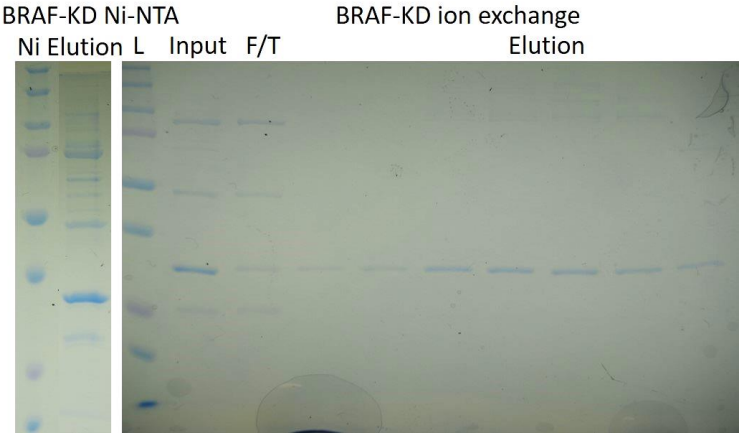

12b.

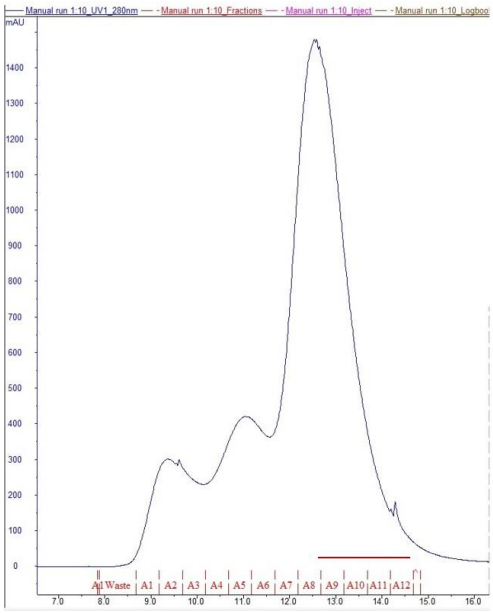

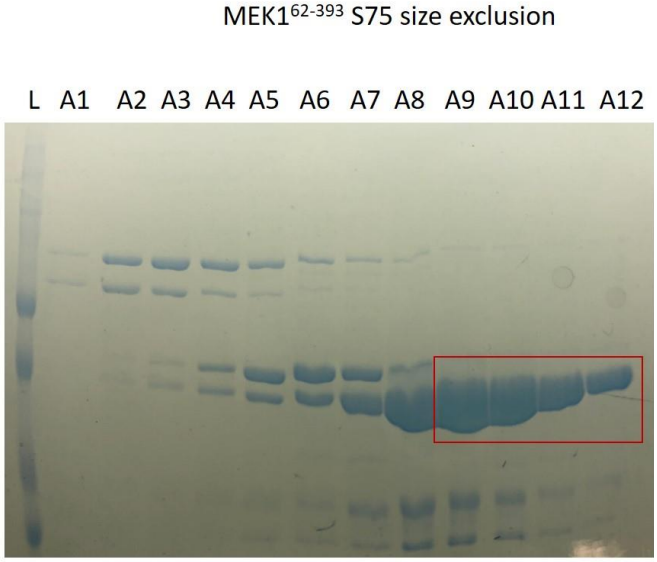

12a. Nickel NTA and cation exchange elutions of the purified BRAF kinase domain expressed in SF9 cells. Ni: Nickel, L: Molecular weight ladder, F/T: Flowthrough. 12b. S75 elution of MEK$^{62-393}$. The final four fractions of the main peak were pooled, concentrated, and aliquoted for assays.

MEK inhibitors exhibit differential potency depending on MEK1 phosphorylation status

If MEK inhibitor efficacy depended on directly binding phosphorylated MEK (pMEK), all other possible mechanisms of inhibition are moot, and there should be no dependence on the upstream mutational background driving malignancy. To address this question, we asked if MEK inhibitors exhibit different potency depending on whether MEK was previously phosphorylated (pMEK) or dependent on phosphorylation and activation by BRAF. This will allow us to identify which inhibitors work through mechanism 4 as described in Figure 11. Dr. Kunhua Li in our laboratory developed a radiometric assay reconstituting the MAP kinase cascade *in vitro* to measure the IC_{50} of eight MEK inhibitors that are in preclinical or clinical trials or are already in use in the clinic (Table 3). Inhibitor efficacy was determined under two conditions: in a coupled BRAF:MEK1:ERK2 system as well as in a pMEK:ERK2 system (Figure 13, Table 4). In the coupled assay, all eight MEK inhibitors we tested exhibited high-picomolar to low-nanomolar IC_{50} values (Figure 13, top panel). In contrast, all eight inhibitors were markedly less potent in inhibiting pMEK than in the coupled assay. ability to prevent phosphorylation of ERK (bottom panel). Three inhibitors are notable in the impact phosphorylation has on their potency: PD0325901, Pimasertib, and CHO/RO5126766. In the case of PD0325901 and Pimasertib, there is approximately a 100-fold decrease in potency. Remarkably, CHO/RO5126766 loses all potency on pre-phosphorylated MEK1. Interestingly, trametinib has roughly equal potency in the coupled assay as in the pMEK assay. We are currently in the process of validating these results using a

time-resolved Förster resonance energy transfer (TR-FRET) assay I am developing in collaboration with Dr. David Heppner in my laboratory.

Table 3. Structure of MEK inhibitors characterized in this study

Compound names	Clinical phase	Chemical Structure
Cobimetinib (GDC-0973, XL-518, RG7421); Exelixis	In clinic	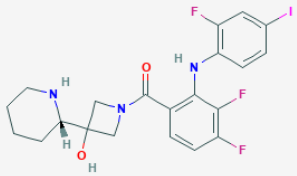
MEK162 (Binimetinib, ARRY-438162); Array Biopharma	In clinic	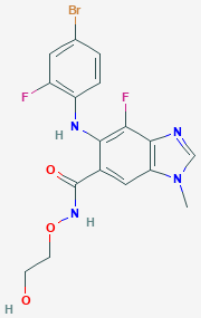
PD0325901 Pfizer, USA	Phase II	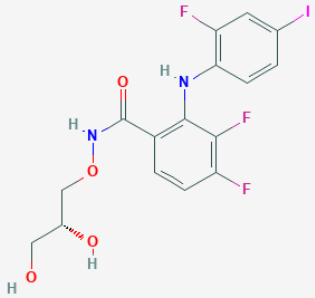
Pimasertib (AS703026, MSC1936369B)	Phase II	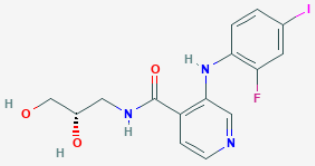

Table 3 (contd.)

RO5126766 (CH5126766); Hoffmann-La Roche	Phase I	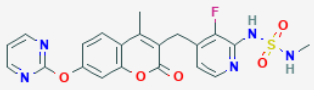	
Selumetinib (AZD6244, ARRY-142,886); AstraZeneca	In clinic	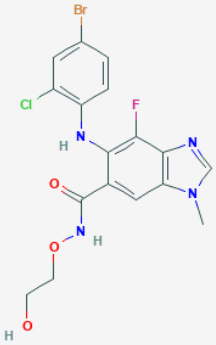	
Trametinib (GSK1120212); GlaxoSmithKline	In clinic	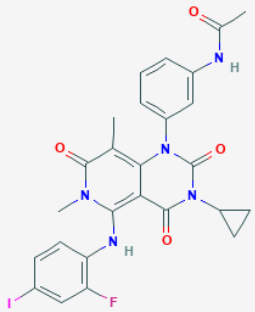	
GDC-0623; Genentech	Phase I	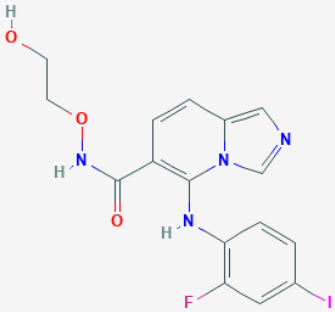	

Figure 13. MEK inhibitors have strong potency against BRAF:MEK1, but varying effectiveness against pMEK1.

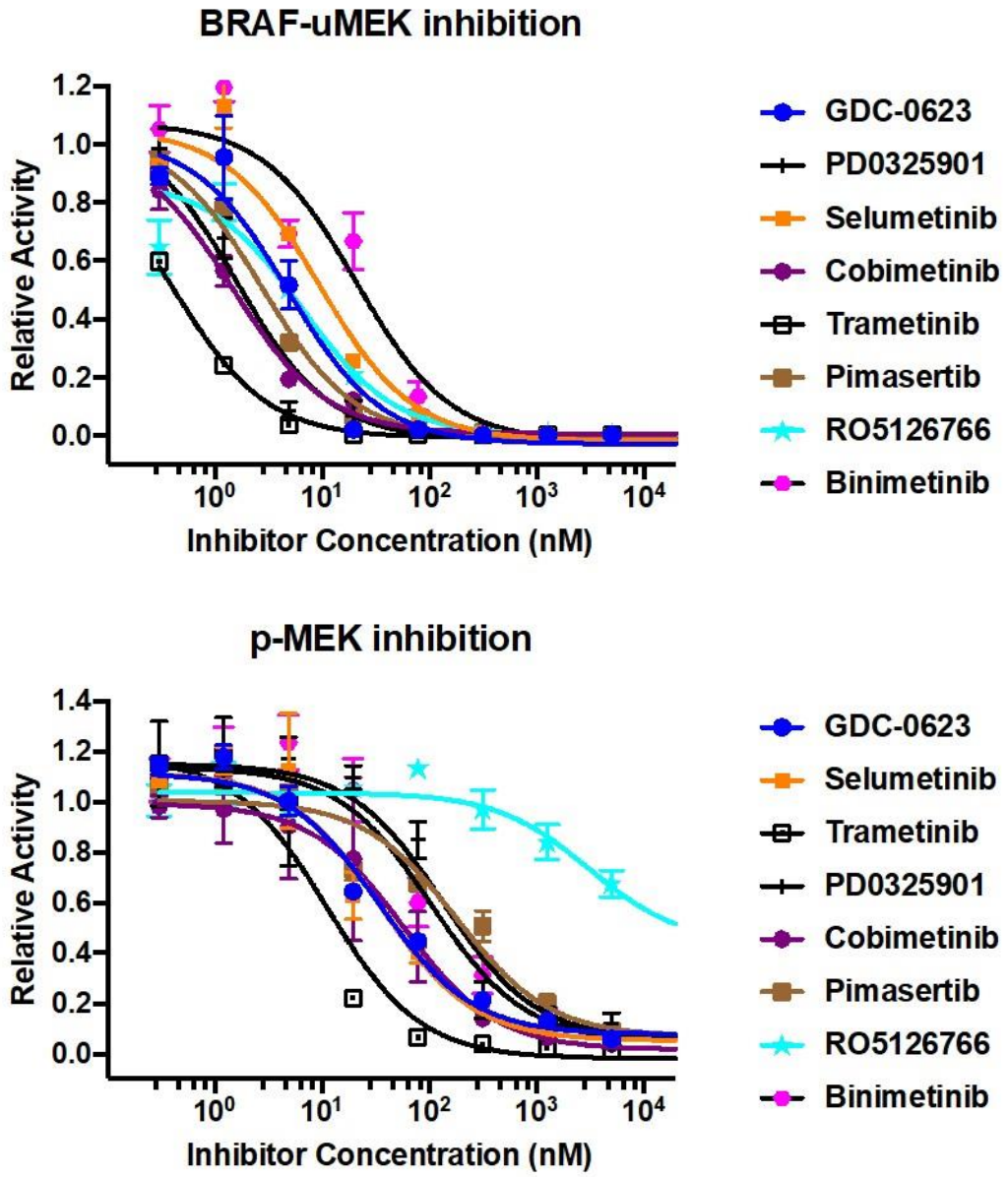

In a γ-^{32}P radiometric activity assay, all MEK inhibitors exhibit low-nanomolar potency when exposed to a coupled BRAF:MEK1:ERK2 *in vitro* system. The effectiveness of all these inhibitors decreases when MEK1 has been pre-phosphorylated (pMEK). Notably, PD0325901 and Pimasertib IC50s decrease by ~100-fold, and RO5126766 loses all potency, when testing inhibition of phospho-MEK1 as opposed to the BRAF:MEK1 complex. Credit to Dr. K. Li.

Table 4. IC_{50} measurements of eight clinically relevant MEK inhibitors on a coupled BRAF:uMEK assay vs a pMEK assay.

Inhibitor	BRAF:uMEK IC_{50} (nM)	pMEK IC_{50} (nM)
GDC0623	4.8	34
PD0325901	1.6	130
Selumetinib	9.4	35
Cobimetinib	1.4	57
Trametinib	0.42	11.2
Pimasertib	2.7	180
RO/CH5126766	6.6	3000
Binimetinib	20.8	104

Phosphorylation and exposure to MAPK inhibitors modulate the affinity of the BRAF:MEK1 interaction

To understand why certain inhibitors lose their potency once MEK1 has been phosphorylated, I developed a biolayer interferometry (BLI) assay to measure the affinity of unphosphorylated and phosphorylated MEK1 (uMEK and pMEK, respectively) for the BRAF kinase

in the presence of clinically relevant RAF and MEK inhibitors. This assay allows us to determine whether MEKis might act by inducing a conformation of MEK that is not compentent for binding to BRAF (mechanism 1 in Figure 11) or by blocking release of MEK from RAF after its phosphorylation (mechanism 3 in Figure 11). To validate the assay, we measured the affinity of unphosphorylated $MEK^{62\text{-}393}$ and MEK^{L314E}, a mutant version of $MEK^{62\text{-}393}$ incapable of binding with BRAF first characterized by Haling *et al*[15]. Unmodified $uMEK^{62\text{-}393}$ binds BRAF tightly enough to comigrate with it when applied to a size-exclusion column (Figures 14a, A1), and Lito *et al*. reported in 2014 a BRAF:MEK1 affinity of 55nM using surface plasmon resonance (SPR) in the presence of 0.5mM ATP. Our BLI experiment yielded a $K_{d\ BRAF:uMEK}$ of 19nM, and as expected, showed no binding of MEK^{L314E} to BRAF under identical conditions (Figure 14a). Performing the same experiment with pMEK1 yielded a $K_{d\ BRAF:pMEK1}$ of 334nM; a ~17-fold decrease in affinity (Figure 14a). Our BLI experiments also reveals the changes in on- and off-rates that underly the decreased affinity of pMEK1 for BRAF. The association/dissociation traces for uMEK binding to BRAF describe slow on, slow off kinetic behavior. The pMEK traces, in contrast, show fast saturation in the association phase, as well as fast decrease in signal in the dissociation phase.

Even though MEK1 phosphorylation causes the largest change in the BRAF:MEK1 K_d, MEK inhibitors modulate the affinity of RAF for unphosphorylated and phosphorylated MEK1 (Table 5). PD0325901 seems to increase the affinity of uMEK1 for BRAF by roughly one order of magnitude, which is in line with SPR results obtained by the Rosen group in 2013. Cobimetinib, also known as GDC0973, weakens the BRAF:uMEK interaction, even though it does not significantly affect BRAF:pMEK affinity. The most striking change was caused by CH5126766.

pMEK affinity for BRAF increases by more than ten-fold in the presence of CH5126766 (Figure 13b). Interestingly, the BLI traces for pMEK in the presence of CH5126766 display slower association and dissociation kinetics than pMEK alone, suggesting that this inhibitor may function at least in part by preventing the dissociation of pMEK from the BRAF:MEK1:14-3-3 complex. It has been previously shown that this compound also prevents the phosphorylation of MEK1 by BRAF, meaning that it can act by both mechanisms 2 and 3 in Figure 11.

Figure 14. Phosphorylation and exposure to inhibitors modulate MEK1's affinity for the BRAF kinase.

14a.

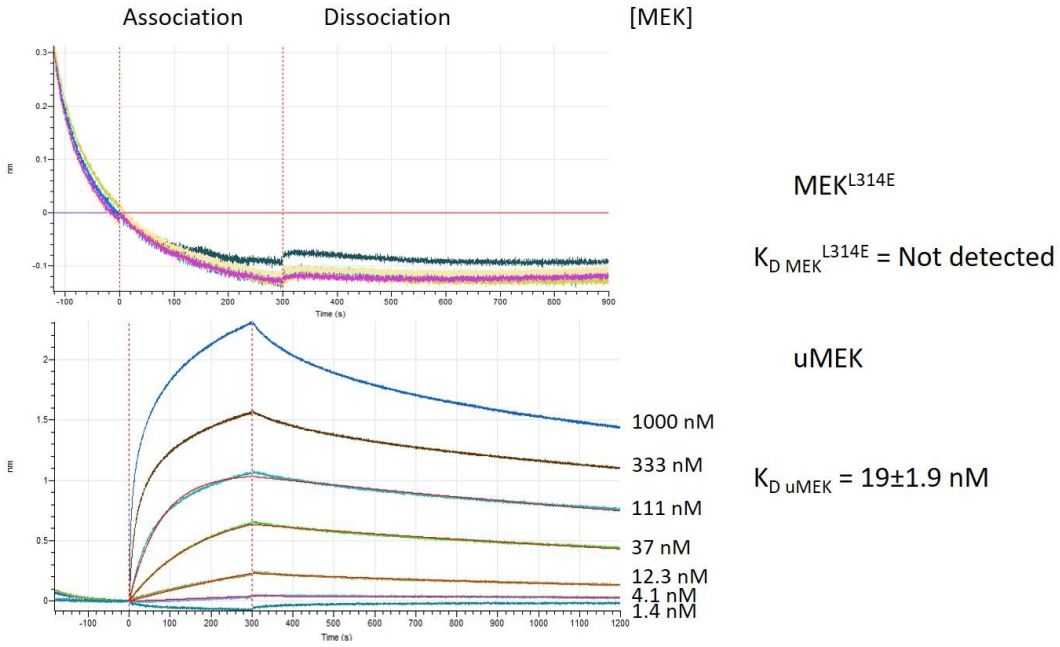

14b.

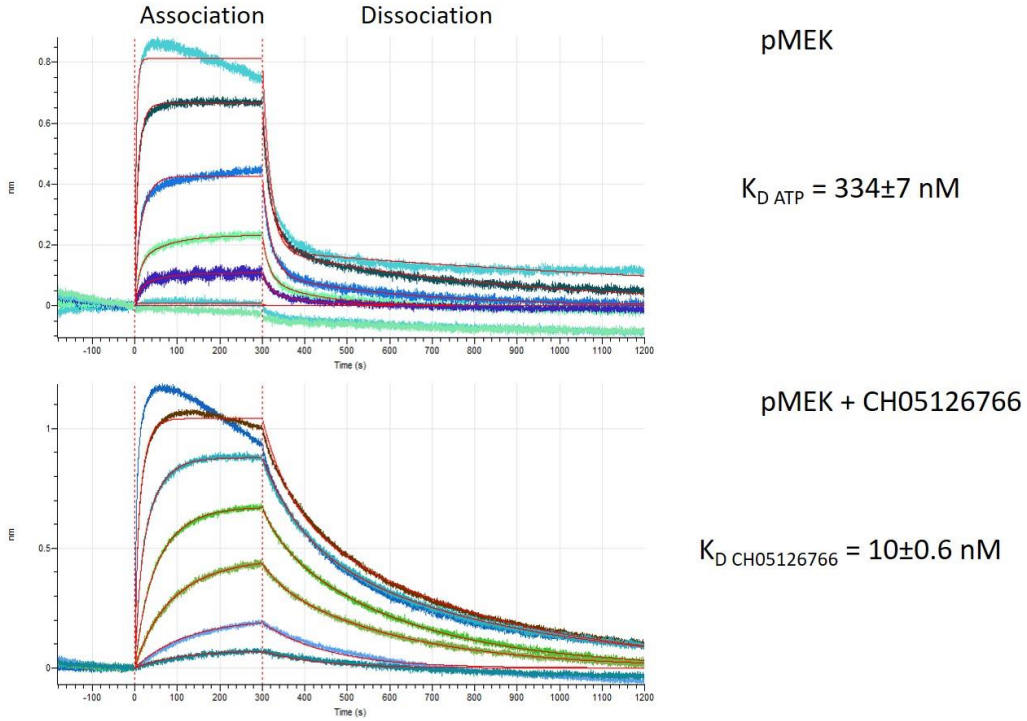

14a. MEK^{L314E} does not bind the BRAF kinase, as expected. uMEK binds BRAF tightly, with slow association and dissociation kinetics. Shown here are representative association/dissociation curves for uMEK and pMEK binding to immobilized BRAF. 14b. MEK1 phosphorylation

Figure 14 (contd.) markedly decreases BRAF:MEK1 affinity, and changes the kinetics of binding from a slow-on/slow-off to a fast-on/fast/off regime. CH5126766 increases phosphoMEK1 affinity for the BRAF kinase. Note that the kinetic behavior of BRAF:pMEK1 binding in the presence of CH5126766 resembles that of BRAF:uMEK. Both experiments show the interference response (in nm, rainbow traces), and the binding fits (thin, red lines).

Table 5. Binding affinity of BRAF for uMEK and pMEK in the presence of nucleotide and MEK inhibitors.

Condition	BRAF:uMEK K_d (nM)	BRAF:pMEK K_d (nM)	Fold-change in uMEK affinity	Fold-change in pMEK affinity
No MEKi	**11 ± 0.9**	**334 ± 7**	**-**	**-**
GDC0623	**13 ± 2.0**	**190 ± 20**	**1x**	**1.8x**
PD0325901	**3.3 ± 0.5**	**64 ± 5.2**	**-3.3x**	**-5.2x**
Selumetinib	**48 ± 5.9**	**110 ± 12**	**4.4x**	**-3x**
Cobimetinib	**96 ± 26**	**190 ± 18**	**8.7x**	**1.8x**
Trametinib	**68 ± 16**	**120 ± 6.6**	**6.2x**	**2.8x**
Pimasertib	**77 ± 9.6**	**65 ± 9.4**	**7x**	**-5.2x**
RO/CH5126766	**26 ± 5.5**	**10 ± 0.6**	**2.4x**	**33x**
Binimetinib	**20 ± 2.3**	**220 ± 11**	**1.8x**	**1.5x**

Allosteric MEK inhibitors bind the BRAF:MEK1 kinase in a preformed, ATP-adjacent pocket

We determined the structure of all eight MEK inhibitors characterized here bound to the BRAF:MEK1 kinase complex. With some subtle differences, the inhibitor-bound structures closely resemble the GDC0623 and AMPPNP-only structures described in Figures 4 and 6 of Chapter 2. As seen in Figure 15, all allosteric MEK inhibitors we examined bind the same preformed site in MEK1: An ATP-adjacent pocket circumscribed by the C-helix from above, the hinge region from behind, and the activation segment (AS) from the front of the kinase. Our structures revealed clear density in this allosteric binding site for each of these structures (Figure 16). All eight MEK inhibitors insert a ring system into the hydrophobic cleft between the DFG motif of the activation segment, C-helix, and β-strands 4 and 5 (Figure 17a). The most noticeable large-scale difference among the structures is a ~4 Å inward swing of the end of the activation segment helix in the complexes containing GDC0623, CH5126766, cobimetinib, and PD0325901 when compared with the AMPPNP-only structure. Of these, GDC0623, cobimetinib, and PD0325901 also cause an upward rotation by ~56^{o} of the end of the MEK1 activation segment helix (Figure 17b).

Figure 15. Overall structures of MEK1 bound to MEK inhibitors.

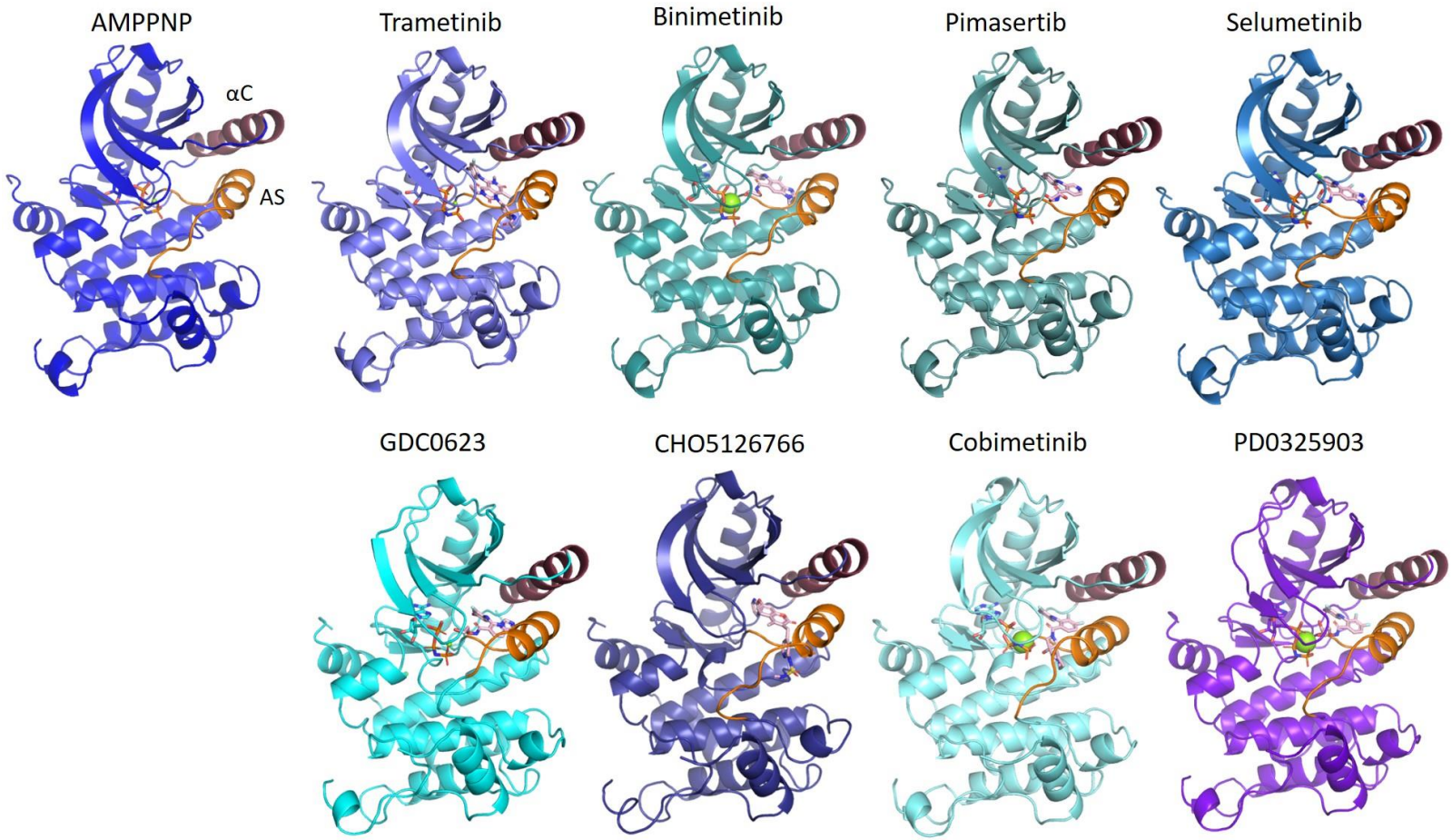

The MEK1 structures can be broadly classified into two groups depending on the orientation of the activation segment (AS, orange) helical portion. The top row shows structures where the end of the activation segment helix faces forward. The structures in the bottom row have an AS helix whose end swings inward. The top row inhibitors tend to have bulky ring systems that extend toward the AS helix, whereas the bottom row inhibitor ring systems are packed away from the end of the helix.

Figure 16. MEK inhibitor difference map densities show clear occupancy in the allosteric binding pocket.

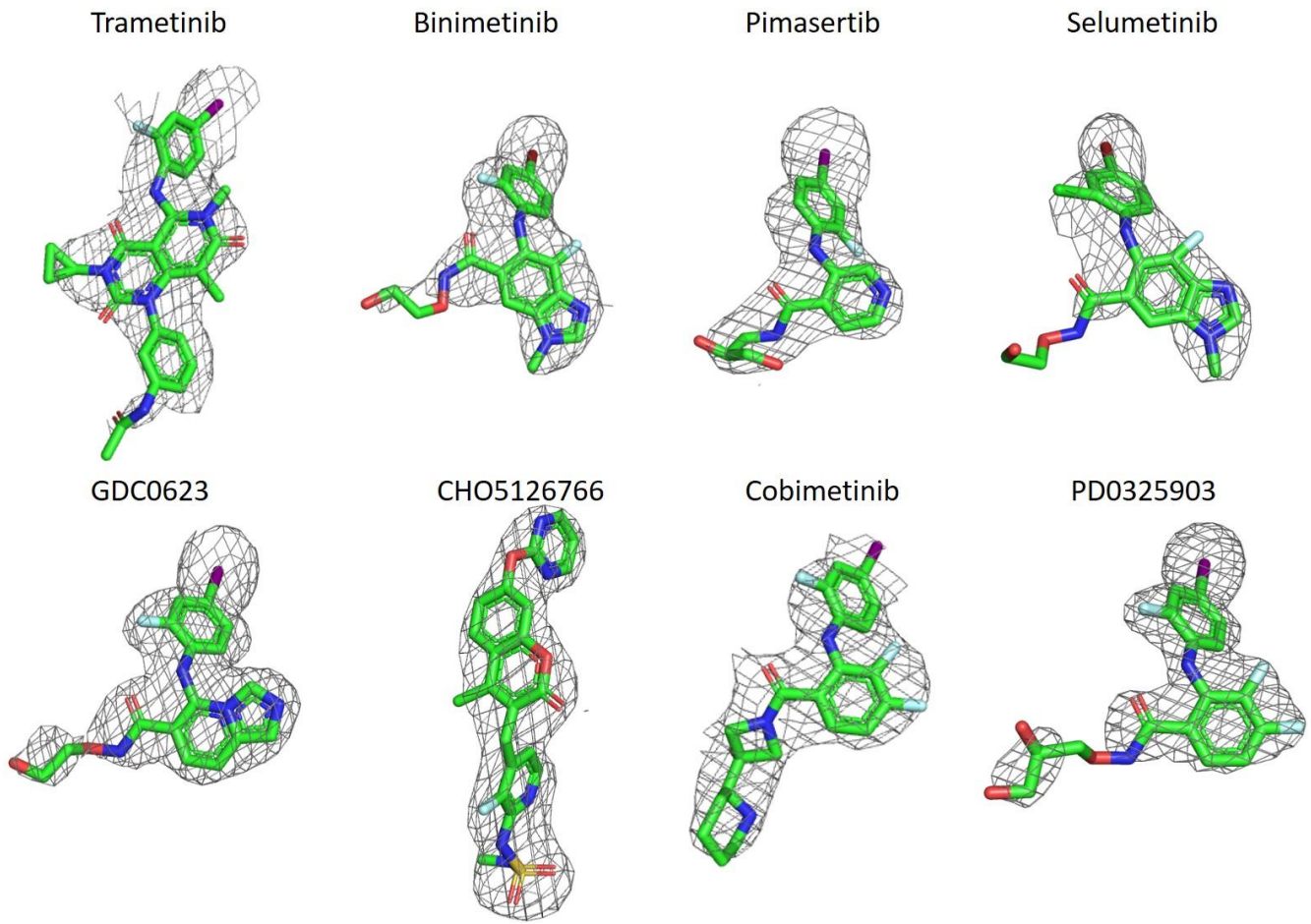

Difference maps were generated using the CCP4 suite by subtracting the AMPPNP-only map from the MEK inhibitor-bound maps. The maps were contoured to 3σ, and the isomesh carved to a distance of 2 Å in PyMol.

CH5126766 structure does not contain nucleotide density

CH5126766 is the one outlier in the nine structures of the BRAF:MEK1 kinase module we solved, as it does not contain AMPPNP density in the MEK1 active site. It is not entirely clear how CH5126766 disrupts nucleotide binding – the allosteric binding pocket it occupies does not

Figure 17. MEK inhibitors bind an allosteric pocket adjacent to the ATP-binding site and interact with the C-helix and activation segment.

17a.

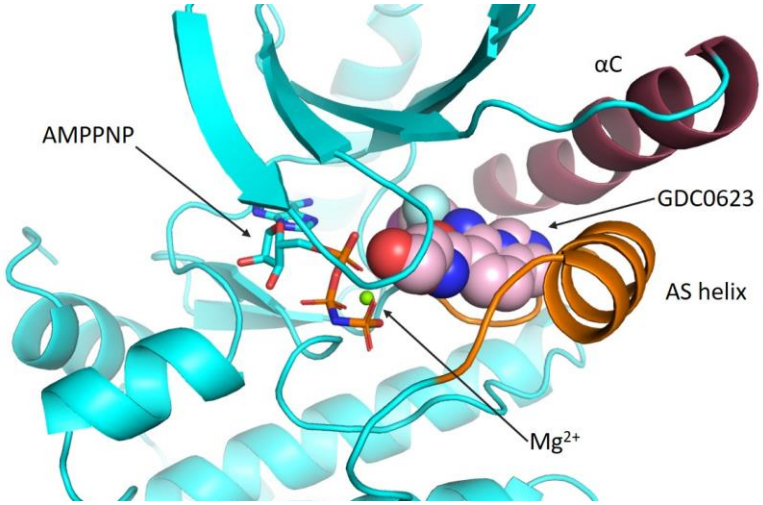

17b.

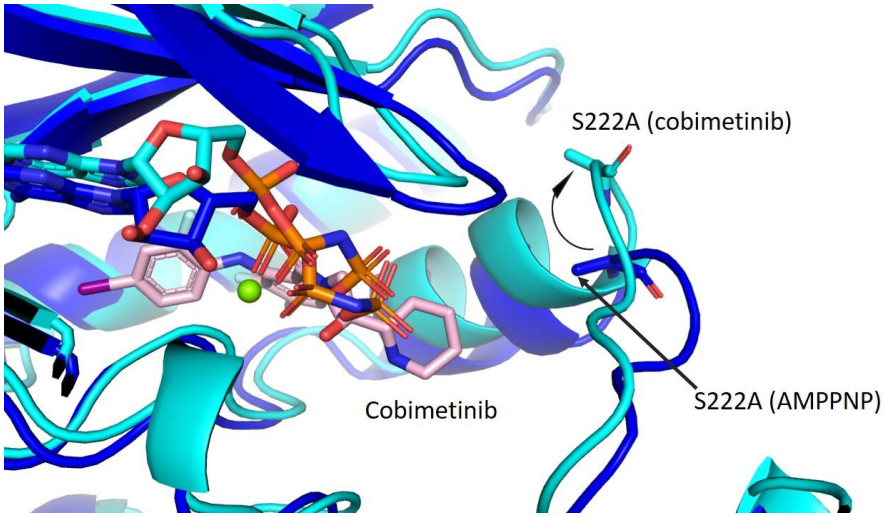

17a. Allosteric MEKis bind adjacent to and, with one exception, concurrently with nucleotide in MEK1. GDC0623 is shown as a representative example in pink spheres. The C-helix is colored dark pink, and the activation segment in orange. 17b. GDC0623, cobimetinib, and PD0325901 cause a ~56^{o} upward rotation of S222, one of two serine sites phosphorylated in the MEK1 activation segment; the cobimetinib structure is in light cyan, and the AMPPNP structure is in blue.

overlap with the ATP-binding site (Figure 18a). In fact, CH5126766 is the only inhibitor that does not extend a functional group toward the AMPPNP-Mg^{2+} conjugate. This compound's sulfonamide substituent makes polar contacts with two arginine residues in the MEK1 C-lobe (Arg 189 and 234) as well as two asparagine residues in the BRAF G-helix (Asn 660/661) (Figure 18b). This phenomenon may be peculiar to the BRAF:MEK1 complex or an artefact of soaking inhibitor into AMPPNP-only crystals, given that structures of MEK1 alone in complex with CH5126766 does include nucleotide density[42].

Figure 18. CH5126766 displaces ATP and interacts with the BRAF G-helix.
18a.

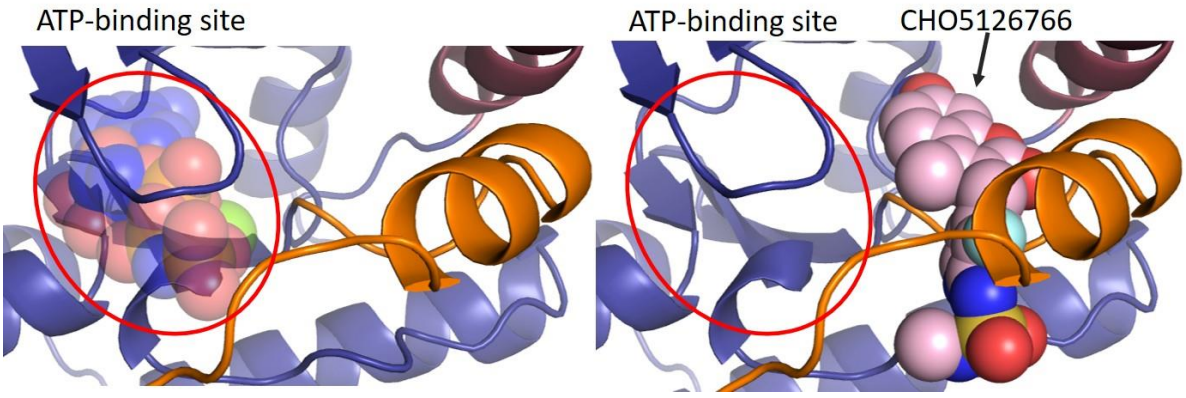

18b.

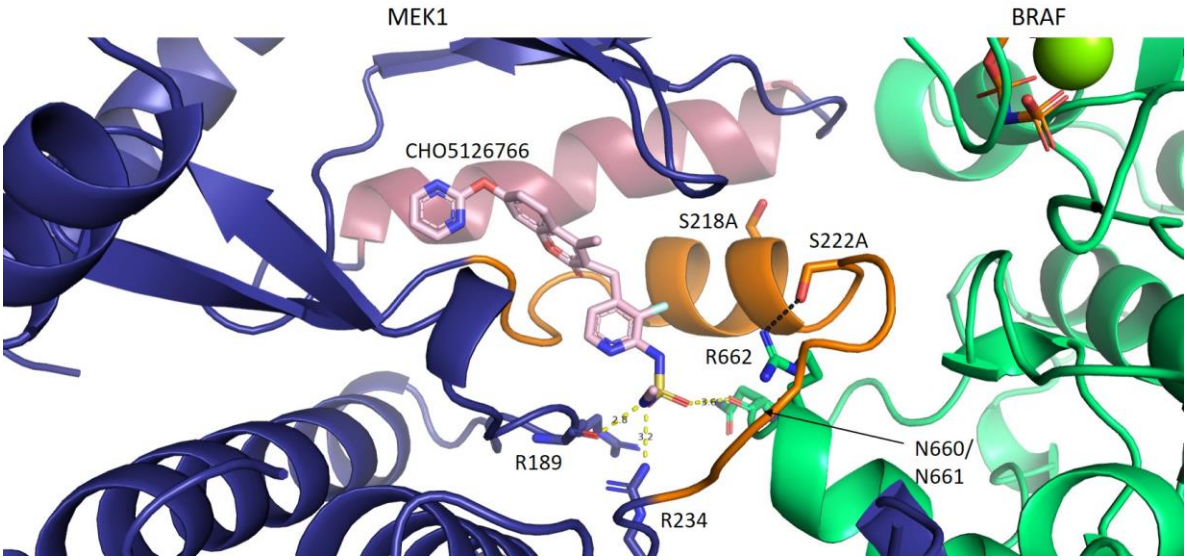

18a. CH5126766 displaces the MEK1 nucleotide but does not sterically overlap with the ATP-binding site.18b. CH5126766 interacts directly with the BRAF G-helix. The MEK1 C-helix is highlighted in dark pink, and the activation segment in orange.

Trametinib interacts with BRAF G-helix Arg 662, which normally contacts the MEK1 S222

Previous work by the Rosen group, together with our own biolayer interferometry data in Table 2 shows that trametinib decreases the affinity of BRAF for MEK1[31]. We determined the

structure of trametinib bound to the BRAF:MEK1:AMPPNP kinase module, and found that the BRAF arginine 662 forms a salt bridge with the trametinib acetamide carbonyl (Figure 19a). The importance of this interaction is not yet clear, but I suspect that trametinib is redirecting the arginine away from its polar interaction with the MEK activation loop serine 222, eliminating one of several contact points that make up the avidity network between the two kinases.

PD0325901 stabilizes the MEK1 Glu 102 interaction with the BRAF nucleotide

PD0325901 is the only MEK inhibitor we tested that increases BRAF:uMEK1 affinity. Our results agree with the Rosen group's SPR measurements, and our co-crystal structure sheds light on how this may be occurring. In other structures we obtained of the kinase module, the distance between the MEK1 Glu 102 carboxyl group and the AMPPNP ribose 3' hydroxyl group ranges from ~3.2-3.6 Å. PD0325901 shortens that distance to 2.9 Å – ideal for hydrogen bonding (Figure 19b). This polar contact appears to be important for maintaining BRAF and MEK1 locked in their mutually autoinhibited state, as mutations in MEK1 that delete residues 102 and 103 cause its constitutive activation and upregulated ERK phosphorylation[60].

Figure 19. BRAF:MEK1 in complex with MEK inhibitors trametinib and PD0325901.
19a.

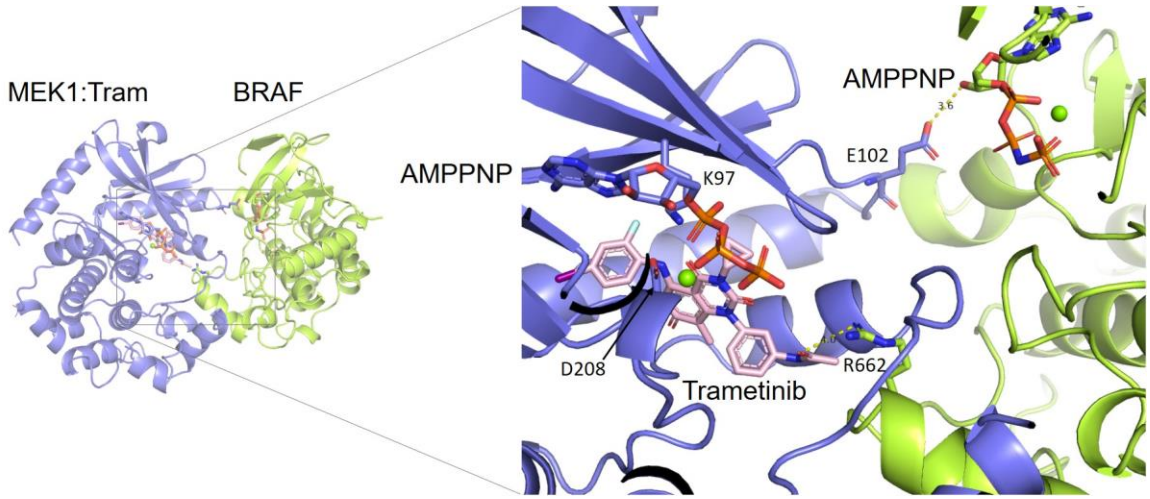

19b.

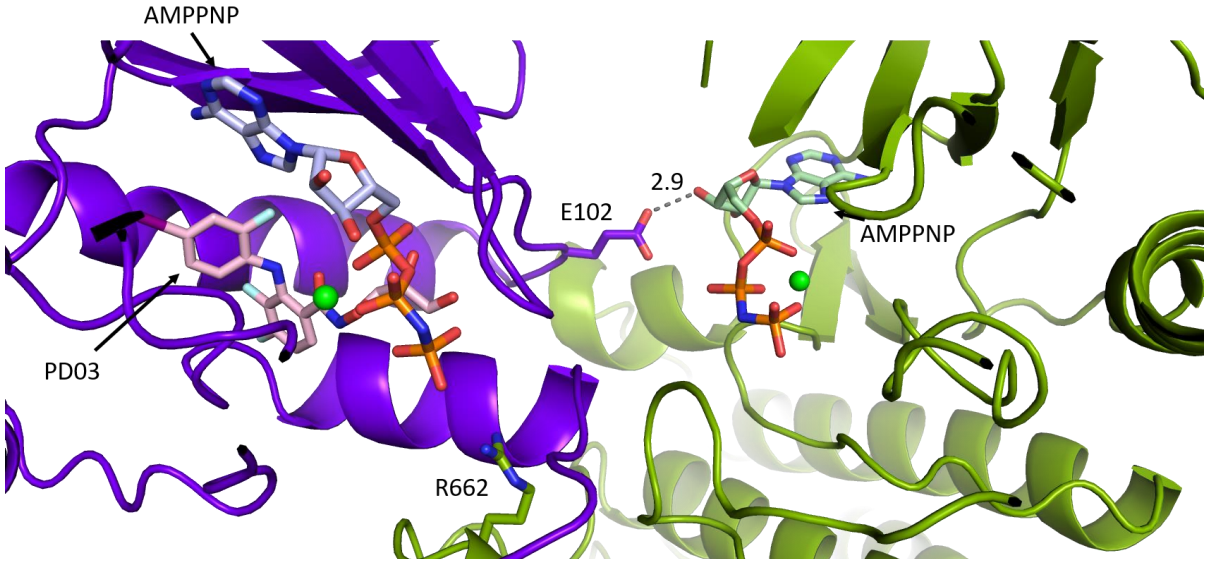

Although all MEK inhibitors characterized here bind in the same allosteric pocket, subtle differences in their interactions with the complex could help explain their mechanisms of action. 19a. Trametinib interacts directly with the BRAF R662, pulling it away from the activation segment S222. 19b. PD0325901 (PD03) shortens the E102:BRAF-AMPPNP bond, from ~3.4 Å to 2.8 Å, possibly leading to a higher affinity between BRAF and MEK1.

Discussion

The discovery of the autoinhibited BRAF:MEK:14-3-3 complex adds a new layer of possible ways MAPK pathway inhibitors could work. There are at least four ways we envision MAPK inhibitors prevent signaling through ERK: 1) they could prevent the recruitment of MEK1 to RAF, decreasing the pool of pMEK that could activate ERK; 2) they could prevent the phosphorylation of MEK by RAF once the complex is activated; 3) they could trap pMEK in the RAF:14-3-3 complex, thereby preventing it from phosphorylating ERK; or 4) they could directly inactivate free pMEK, thus preventing ERK activation (Figure 20). In this study, we have begun to unravel the complex pharmacology of the MAPK pathway by systematically characterizing a battery of inhibitors through biochemical, biophysical, and structural means.

Kunhua Li's reconstitution of the MAPK cascade for radiometric inhibition assays gave us the first insights into how MEKis exhibit differential potency depending on whether MEK1 is unphosphorylated and in the presence of BRAF or prephosphorylated and already active. Strikingly, all MEKis lose potency once MEK1 has been phosphorylated. PD0325901, Pimasertib, and CH5126766 see the most drastic decrease in their inhibitory effect, with the first two compounds losing ~100x potency, and the last losing all potency in the presence of pMEK. This experiment begins to rule out direct inhibition of active MEK1 as a plausible mechanism of action for at least the three inhibitors mentioned above.

Figure 20. Initial characterization of the pharmacology of MEK inhibitors.

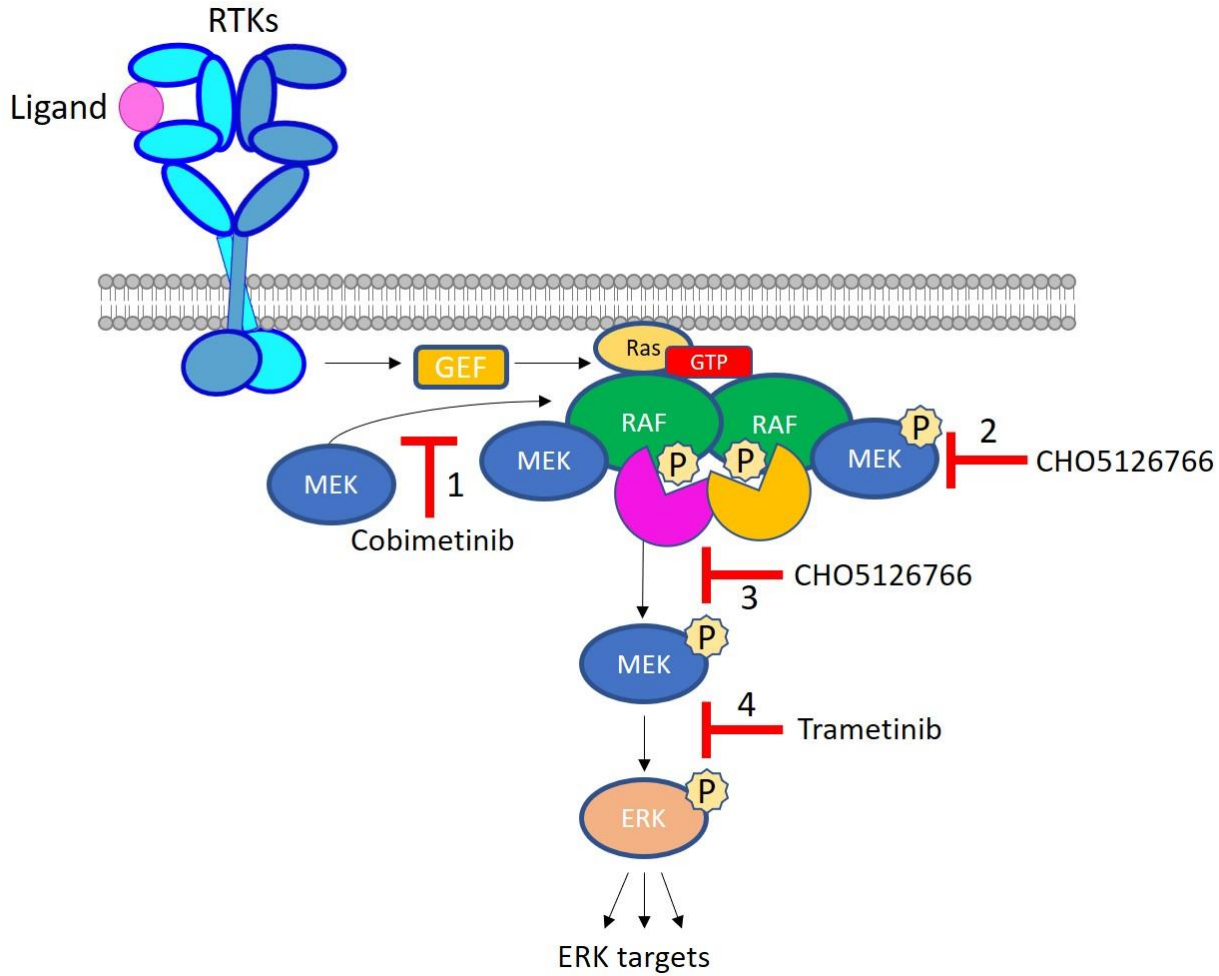

Our initial inhibition and binding experiments have begun to unravel the mechanisms of action for MEK inhibitors. Cobimetinib appears to decrease uMEK affinity for BRAF, likely impairing uMEK recruitment to the active BRAF complex. CH5126766 increases pMEK affinity for BRAF, and hinders MEK phosphorylation according to previous work

The binding experiments I performed at the CMI give us an even clearer picture of the biology and pharmacology of the MAPK pathway. The marked difference in MEK1's affinity for BRAF caused by phosphorylation of the MEK1 activation segment serines (S218/222) is the best evidence to-date that phosphorylation of the MEK activation loop promotes its release from BRAF: once MEK is phosphorylated, its interaction with BRAF transitions from slow-on, slow-off kinetics to fast-on, fast-off kinetics. This leads to a release of phosphorylated MEK1 from the active BRAF:14-3-3 complex, and any non-productive BRAF:pMEK complexes dissociate quickly, leaving BRAF active sites available for phosphorylating and activating more uMEK1. To our knowledge, this is the first direct evidence that phosphorylation of MEK1 promotes its release from BRAF.

All the clinical BRAF inhibitors we tested slightly decrease the affinity of the BRAF:uMEK interaction. As mentioned in Chapter 2 and our article recently published in *Nature*, we hypothesize that BRAF-bound nucleotide is an essential component of the autoinhibited complex. The fact that all BRAF inhibitors displace nucleotide fits well with our binding assay results, and indicates how TAK580, currently in clinical trials, could be a promising treatment for pediatric low-grade actrocytomas.

These binding assays also elucidated the mechanism of action for another set of MEKis. In the presence of CH5126766, pMEK's affinity for BRAF is increased from 334nM to 10nM, recapitulating the affinity of the BRAF:uMEK interaction. We thus surmise that CH5126766

inhibits ERK phosphorylation, at least in part, by "gluing" pMEK1 to the BRAF:14-3-3 complex, which neutralizes both an active MEK1 molecule as well as one half of the active BRAF:14-3-3 complex. This observation aligns well with the initial characterization of this compound by Ishii and colleagues in 2013 reported in *Cancer Research*, where they found that CH5126766 prevents MEK phosphorylation, and promotes a stable BRAF:MEK1 complex[59].

PD0325901 appears to increase the affinity of uMEK1 for BRAF by almost ten-fold, continuing the theme of inhibition by gluing BRAF and MEK1 together. Cobimetinib, in contrast, appears to slow down recruitment of uMEK to the BRAF kinase, dampening MAPK signaling by decreasing the pool of active MEK1 in the cell.

The structures we solved of the BRAF:MEK1 kinase module in complex with the MEK inhibitors tested here add even more fine details to their mechanisms of action. All allosteric MEKis bind the MEK kinase in the same, preformed, ATP-adjacent pocket, but differences in their specific poses and chemical contacts with the complex inform how they work. GDC0623, cobimetinib, and PD0325901 cause S222 in the MEK1 activation segment to flip upward, closer to the BRAF active site. This may explain why PD0325901 and cobimetinib induce MEK1 phosphorylation, as reported by Ishii *et al* and others. PD0325901 concurrently increases the interaction between the MEK1 Glu 102 and the BRAF nucleotide, while cobimetinib does not. This observation, along with the fact that deletion of residues 102 and 103 in MEK1 causes

constitutive ERK phosphorylation, leads me to postulate that this cross-active site interaction is crucial for maintaining the complex locked in its autoinhibited state.

Of all the inhibitors we crystallized with the BRAF:MEK1 kinase complex, CH5126766 stood out in one major way: it did not contain the MEK1-bound nucleotide. I speculate that maintaining nucleotide in the ATP-pocket when inhibitors are present in the allosteric site requires stabilizing interactions between the two ligands. The sulfonamide moiety of this compound serves as a bridge between two arginines in the MEK1 C-lobe and two asparagines in the BRAF G-helix through polar interactions, which could explain the increased affinity of pMEK for BRAF when exposed to CH5126766.

Trametinib's interaction with the kinase module can be compared to that of CH5126766, although with two main differences. Trametinib does not displace the MEK1 nucleotide and interacts directly with a BRAF G-helix arginine, which in the AMPPNP-only structure is in contact with the phosphorylatable S222 of the MEK1 activation segment. This could explain how trametinib destabilizes the BRAF:uMEK1 complex, as it is removing a contact point between the two kinases.

We are currently in the process of developing a lanthanide-based TR-FRET assay to measure MEK1 and ERK2 phosphorylation in the presence of the inhibitors we studied here. We hope to validate and expand on the radiometric assay presented here by identifying which

inhibitors prevent MEK1 phosphorylation, which prevent ERK2 phosphorylation. This assay will help us to fill in the final blanks in the MAPK pathway and pharmacology map.

Chapter four: Structure of the wild-type and V600E BRAF kinase in complex with TAK580

Part of this work was completed in collaboration with Dr. Kunhua Li in the Eck lab. K.L. instructed me in the art of crystal screening and guided me through structure refinement.

Introduction

As laid out in chapter one, potent inhibition of mutant BRAF has not always led to effective treatment of MAPK-driven tumors. Vemurafenib, dabrafenib, and sorafenib have all been shown to cause secondary lesions and have shown little efficacy in treating mutant RAS-driven cancers[27,28,35]. Although combination therapies are now the standard of care for BRAF-mutant melanoma and certain colorectal cancers, adverse events in patients and the difficulty with managing MAPK-driven tumors demand new ways of targeting BRAF.

Of the three inhibitors mentioned above, vemurafenib and dabrafenib are representatives of the Type I class of kinase inhibitor. These compounds are ATP-competitive, and bind the kinase in its inactive, C-helix "out," conformation. Zhang and colleagues showed in 2015 that Type I inhibitors exhibit differential potency toward the two subunits of the active BRAF dimer. The RAF dimer encourages the C-helix "in" conformation, whereas vemurafenib and dabrafenib induce the C-helix "out" conformation[37]. Their inability to completely abrogate activity of the BRAF dimer offers one possible explanation for paradoxical activation: although they are potent inhibitors of monomeric, constitutively active $BRAF^{V600E}$, they cannot efficiently inhibit BRAF in its dimeric form[69]. Indeed, capturing BRAF in its C-helix "out" conformation may serve to allosterically activate another RAF protein through the canonical back-to-back interface[29]. Type II inhibitors like sorafenib, on the other hand, bind kinases in the C-helix "in" conformation adopted by active enzymes.

One particularly difficult problem to address is the prevalence of BRAF-driven low-grade gliomas. This type of tumor's location in the brain makes it a difficult disease to treat with most conventional medicines. The blood-brain barrier (BBB) serves as an efficient filter, excluding almost all foreign substances from crossing into the brain from the general circulatory system. TAK580, a new, pan-RAF inhibitor acquired by Takeda and subsequently licensed to DayOne Tx that is currently in clinical trials, penetrates the BBB and is effective at shutting down signaling from both V600E and KIAA truncation/fusion mutations.

In this chapter, I describe the structure of TAK580 bound to both wild-type and V600E species of the BRAF kinase. It preferentially binds the BRAF kinase in the C-helix "in" conformation. Its binding pose is incompatible with the C-helix "out" conformation of the BRAF kinase, as it inserts a halogen-substituted ring system into an induced hydrophobic pocket under the C-helix, normally occupied by the inhibitory turn of the activation loop. This structure provides structural and mechanistic understanding of why this inhibitor shows promise in the treatment of both V600E- and truncation/fusion-cancers, such as pediatric low-grade astrocytomas.

Materials and Methods

Bacterial expression and purification of $BRAF^{14M}$ WT and V600E

A bacterial construct encoding residues 445-723 of the BRAF kinase domain was engineered with an N-terminal, TEV-cleavable His_6 tag for purification purposes, along with fourteen solubilizing mutations ($BRAF^{14M}$) for initial crystallization trials, as described previously[61]. We also cloned and expressed a V600E variant to explore differences in inhibitor binding between the WT and mutant proteins. We expressed these constructs in BL21 DE3 *E. coli* by growing cells at 37C at 180rpm agitation until OD 0.5-0.7, at which point the flasks were cooled by immersion in ice water for 10-15 minutes. Expression was induced by addition of 0.5mM IPTG and overnight incubation at 18C with agitation.

Cells were harvested and pelleted by centrifugation at 2500g for 20 minutes. The pellets were resuspended in roughly 20mL per L of culture of Bind/Wash buffer (50mM Tris pH 7.0, 250mM sodium chloride, 30mM imidazole, and 1mM TCEP) with 1mM phenylmethylsulfonyl fluoride to inhibit serine protease activity. Cells were disrupted in a steel beaker on wet ice using a sonicator between settings 7-8 using 2s on/8s off pulses for 1.5-2 minutes. All proceeding steps were done on ice. The lysate was clarified by centrifugation in a Sorvall floor centrifuge for 1.5-2h at 17,000rpm. After centrifugation, the cleared lysate (CL) was carefully pipetted from the centrifuge tubes, sacrificing the last 1-2 mLs of cloudy, suspended lipids and particulates. CL was then filtered using syringe-driven, 0.8µm filters. Care was taken to replace the filter when resistance to pressure became significant. The cleared lysate was then applied to a pre-

equilibrated 5mL bed volume HisTrap column using a P1 peristaltic pump between speed settings 2-3 in the 10x configuration. When all the lysate was passed through the column, the nonspecific impurities were removed by washing the column with 50-80mL Bind/Wash buffer on an AKTA explorer FPLC, at 2.5-3mL/min flow, or until a relatively flat UV reading was reached. The BRAF kinases were eluted along a 100mL gradient from 0-50% Elution buffer (50mM Tris pH 7.0, 250mM sodium chloride, 250mM imidazole, and 1mM TCEP) and collected in 10mL fractions. The relevant peak eluted between 25-32% Elution buffer. Fractions were pooled (normally ~50mL for the whole peak), and the His_6 tag was then cleaved by addition of homemade TEV protease and incubation overnight at 4C in the cold room or refrigerator. The next day, the BRAF/TEV mixture was concentrated using a 15mL, 30,000 NMWCO Amicon spin concentrator that had been pre-rinsed with Bind/wash buffer to no more than 15mg/mL. During the concentration step, a GE S75 10/300 size exclusion column was equilibrated with 1.5 column volumes of Sizing buffer (Tris pH 7.0, 250mM sodium chloride, 1mM TCEP). Concentrated protein was injected into the FPLC in 500µL volumes using a 1mL injection loop, and 0.5mL fractions were collected. The resulting fractions were analyzed by SDS-PAGE, and relevant fractions were pooled and concentrated to 20-25mg/mL and frozen in 20 and 50µL aliquots. Final yield for the WT and V600E preparations were ~15mg and ~10mg per liter of culture, respectively.

Crystallization and structure determination.

For TAK580 complex crystal structures, aliquots of BRAF kinase were diluted 1:1 with Sizing buffer and mixed with 200nM TAK580, 5mM $MgCl_2$. Urchin-like crystal clusters initially

grew in 150nL sitting drops mixed 1:1 with a reservoir solution containing 8% Tacsimate, pH 8, and 20% PEG 3350. Preliminary analysis of these crystals with our rotating-anode X-ray source indicated that they were not suitable for structure determination. We therefore set optimization trays using the Hampton Additive Screen. From those sitting drop trays, two conditions showed promising improvements in crystal morphology: B9 (Sodium thiocyanate) and F9 (Benzamidine HCl). These conditions were further optimized in 2µL hanging drops, where PEG 3350 percentages were varied between 16-26%. After optimization, the thiocyanate condition yielded rhomboidal crystals between 50-80µm across, and the benzamidine condition yielded large plates between 100-300µm across. Crystals were harvested and flash frozen in liquid nitrogen using additional 20-22% glycerol as a cryoprotectant. X-ray diffraction data were collected at 100 K using NE-CAT beamline ID-24-C at the Advance Photon Source, Argonne National Laboratory, at a wavelength of 0.9786 Å. Data were integrated and merged using XDS and scaled using Aimless in the CCP4 suite, or by the Xia2 suite using the Dials mode. Data from the small, rhomboidal crystals diffracted to 3.5 Å. The structure was phased by molecular replacement in PHASER using a previously-determined structure of the BRAF kinase bound to a Novartis compound (LXH254) as an initial search model. Inhibitors were placed into positive density in an initial F_o-F_c map and included in subsequent rounds of refinement using PHENIX.REFINE. Successive manual refinement was performed using COOT. The data collection and refinement statistics are presented in Table 6.

Table 6. Resolution and refinement statistics of the WT and V600E kinase in complex with TAK580

	WT TAK580	V600E TAK
Wavelength	0.9787	0.9787
Resolution range	47.64 - 3.54 (3.667 - 3.54)	24.92 - 3.15 (3.263 - 3.15)
Space group	P 2 21 21	P 21 21 21
Unit cell	57.267 85.831 121.023 90 90 90	48.802 85.244 122.905 90 90 90
Total reflections	94831 (9739)	55848 (5314)
Unique reflections	7567 (732)	9189 (893)
Multiplicity	12.5 (13.3)	6.1 (6.0)
Completeness (%)	98.01 (97.98)	96.70 (95.55)
Mean I/sigma(I)	3.99 (1.12)	7.56 (1.55)
Wilson B-factor	66.97	73.37
R-merge	0.455 (2.005)	0.2515 (1.569)
R-meas	0.475 (2.084)	0.2765 (1.721)
R-pim	0.1336 (0.563)	0.1126 (0.6916)
CC1/2	0.972 (0.55)	0.989 (0.708)
CC*	0.993 (0.842)	0.997 (0.911)
Reflections used in refinement	7551 (729)	9046 (880)
Reflections used for R-free	344 (25)	481 (37)
R-work	0.2390 (0.3030)	0.2540 (0.3562)
R-free	0.2878 (0.3662)	0.2881 (0.3871)
CC(work)	0.844 (0.680)	0.949 (0.698)
CC(free)	0.801 (0.559)	0.972 (0.629)
Number of non-hydrogen atoms	4256	4087
macromolecules	4192	4023
ligands	64	64
Protein residues	526	503
RMS(bonds)	0.003	0.002
RMS(angles)	0.57	0.45
Ramachandran favored (%)	93.22	94.25
Ramachandran allowed (%)	6.78	5.75
Ramachandran outliers (%)	0.00	0.00
Rotamer outliers (%)	3.92	0.00
Clashscore	8.03	4.30
Average B-factor	70.68	78.50
macromolecules	70.77	78.79
ligands	64.38	60.10

Results

Expression and purification of the WT and V600E BRAF kinase.

For crystallization of TAK580 in complex with its target, Dr. Kunhua Li and I generated a BRAF kinase domain construct containing 14 solubilizing mutations required for expression in *E. coli*. Although not suitable for enzyme kinetic studies, this BRAF species has been used numerous times for structural studies of BRAF binding to inhibitors[57,61]. Figure 21a shows a representative S75 size exclusion chromatogram with corresponding SDS-PAGE analysis of the collected fractions.

Crystallization and structure determination

Urchin-like crystal clusters initially grew in 150nL sitting drops mixed 1:1 with a reservoir solution containing 8% Tacsimate, pH 8, and 20% PEG 3350 (Figure 21b). Preliminary diffraction analysis of these crystals with our rotating-anode X-ray source indicated that they were not suitable for structure determination. We therefore set optimization trays using the Hampton Additive Screen. From those sitting drop trays, two conditions showed promising improvements in crystal morphology: B9 (Sodium thiocyanate) and F9 (Benzamidine HCl). These conditions were further optimized in 2µL hanging drops, where PEG 3350 percentages were varied between 16-26%. After optimization, the thiocyanate condition yielded rhomboidal crystals between 50-80µm across, and the benzamidine condition yielded large plates between 100-300µm across.

Crystals were harvested and flash frozen in liquid nitrogen using additional 20-22% glycerol as a cryoprotectant. X-ray diffraction data were collected at 100 K using NE-CAT beamline ID-24-C at the Advance Photon Source, Argonne National Laboratory, at a wavelength of 0.9786 Å. Diffraction data were integrated and merged using XDS and scaled using Aimless in the CCP4 suite, or by the Xia2 suite using the Dials mode. Data from the small, rhomboidal crystals extended to 3.5 Å resolution. The structure was phased by molecular replacement in PHASER using a previously-solved structure of the BRAF kinase bound to a Novartis compound as an initial search model. Inhibitors were placed into positive density in an initial F_o-F_c map and included in subsequent rounds of refinement using PHENIX.REFINE. Successive manual refinement was performed using COOT. The data collection and refinement statistics are presented in Table 3.

Figure 21. Expression, purification, and crystallization of BRAF^{14N} with TAK580.

21a. **21b.**

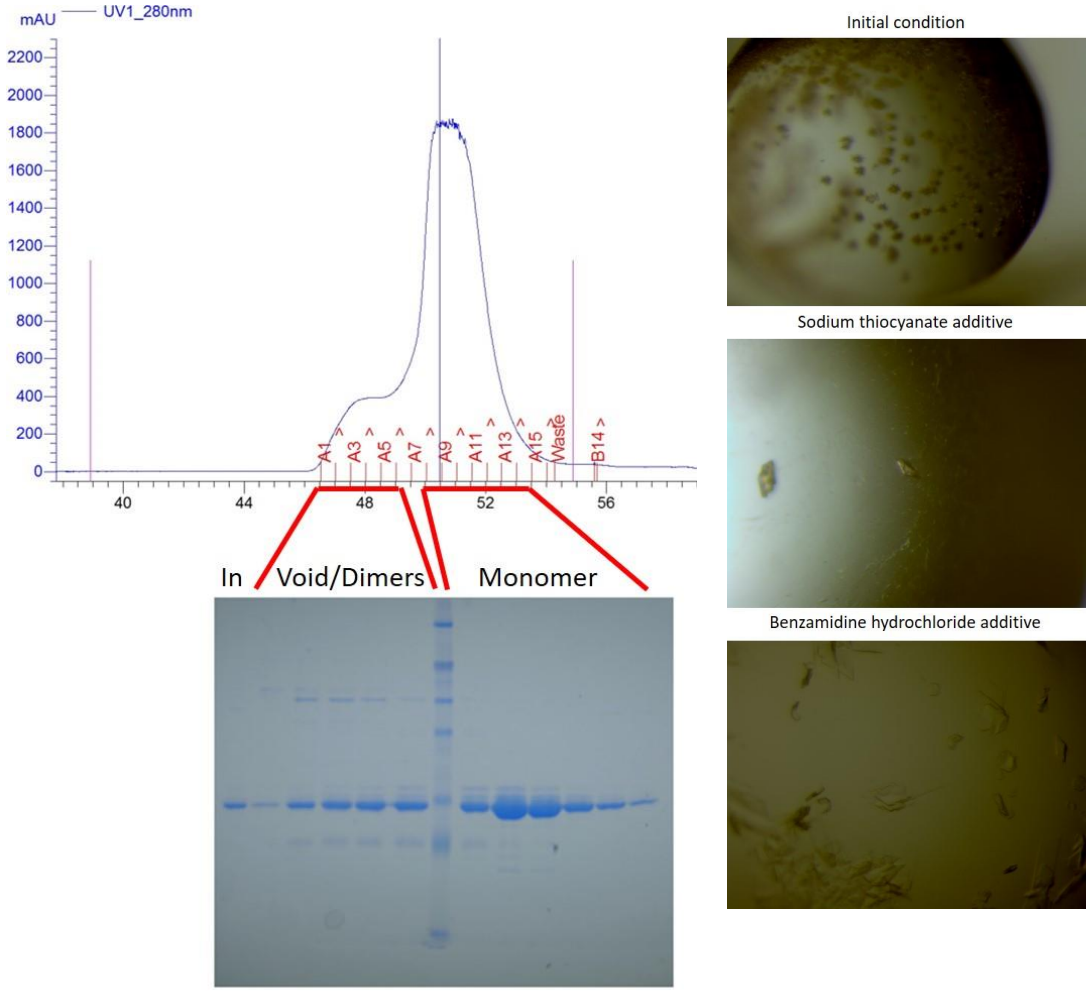

21a. Size exclusion chromatography and representative SDS-PAGE analysis of purified BRAF^{14M} kinase. 21b. Initial crystallization conditions and optimization of BRAF:TAK580 cocrystals. Although the benzamidine hydrochloride additive yielded more plentiful, plate-like crystals, the more rare, rhomboidal crystals produced in the sodium thiocyanate condition yielded higher quality diffraction data and therefore better resolution and statistics. In: Input.

Structures of the wild-type and V600E BRAF kinase in complex with TAK580

The asymmetric unit of both wild-type and V600E BRAF bound to TAK580 contains two copies of the kinase in the back-to-back configuration indicative of the active state (referenced in Chapters 1 and 2, PDBID: 4MNE) (Figure 22a). Contrary to structures solved in complex with

vemurafenib[37], both protomers in the asymmetric unit contained clear inhibitor density. Like all other BRAF inhibitors, TAK580 is an ATP-competitive inhibitor that spans across the nucleotide binding site. It inserts its bi-substituted pyrimidine ring where the nucleotide adenine base binds, forming a T-interaction with the pyrimidine substituent. The central thiazole ring fits between the catalytic Lys 483 and the DFG motif. The lysine-glutamate electrostatic interaction is stabilized by hydrogen bonding between the glutamate and an inhibitor amide. On the right side of the inhibitor, the trifluoromethyl-substituted pyridine ring binds a hydrophobic pocket generated by the extension of the activation loop inhibitory turn (Figure 22b).

As TAK580 is a Type II inhibitor, it binds the kinase in the C-helix "in," DFG loop "out" conformation. An overlay of my TAK580-bound structure with a vemurafenib-bound structure clearly illustrates the difference in BRAF conformations bound by Type I versus Type II inhibitors (Figure 22c). Vemurafenib induces a C-helix-outward conformation and binds the kinase with the activation loop inhibitory turn intact. TAK580, on the other hand, clashes with the DFG motif when it is in the inactive, “in” conformation (22c, red ribbon).

The TAK580:BRAF^{V600E} structure is virtually identical to the wild-type structure at the resolutions we were able to obtain. Density for the activation loops in both structures was not clearly continuous between residues 599-612, so the status of position 600 of the kinase when bound to this inhibitor remains elusive.

Figure 22. Structure of the WT and V600E BRAF kinase in complex with TAK580.
22a.

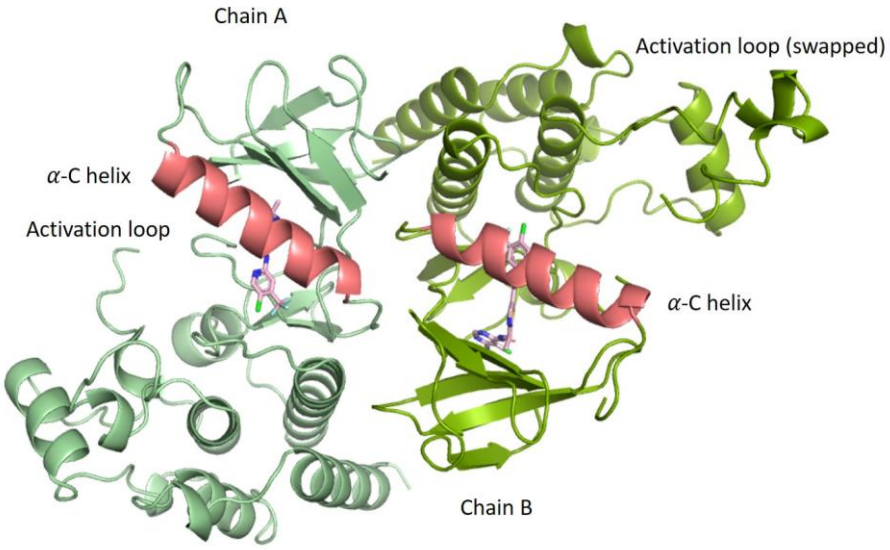

22b.

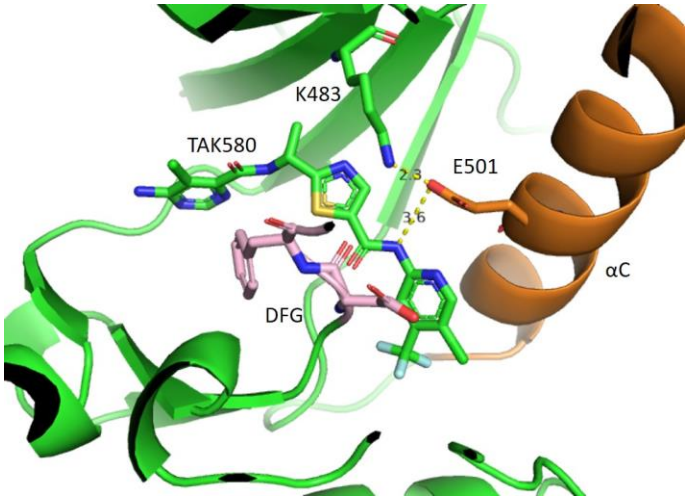

Figure 22 (contd.)

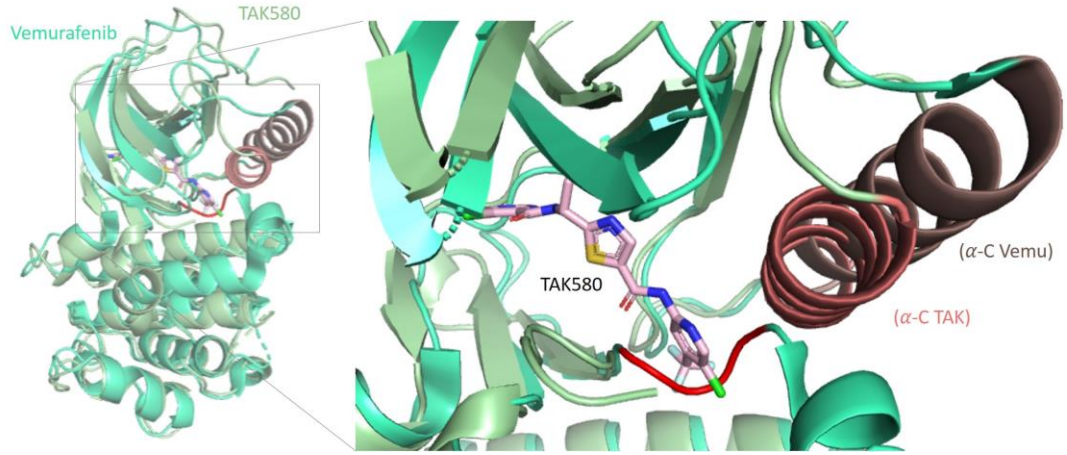

Figure 22 (contd.) 22a. The crystallographic back-to-back BRAF dimer binds TAK580 in both protomers. 22b. TAK580 spans across the nucleotide binding site and displaces the inhibitory helix-like turn. 22c. TAK580 binds the C-helix "in" conformation of BRAF, making it competent to inhibit both the monomeric and dimeric kinases. My structure is contrasted with a vemurafenib-bound structure (PDBID: 3OG7).

Discussion

The structures described above shed light on how a new, promising approach to treating BRAF-driven cancers achieves inhibition of the MAPK pathway. As discussed by Zhang, Bollag and colleagues, Type I kinase inhibitors are effective at inhibiting the monomeric, mutant BRAF, but can only potently inhibit one BRAF subunit of the active, back-to-back dimer[37]. Vemurafenib crystal structures show incomplete inhibitor density in one of two chains in the asymmetric unit[57], providing a potential mechanistic explanation for paradoxical activation of wild-type BRAF in cells: vemurafenib somehow increases the population of dimerization-competent BRAF that can serve as an allosteric activator of a back-to-back wild type BRAF or CRAF partner.

As Sun and colleagues have demonstrated, TAK580 is effective at inhibiting both the V600E and KIAA:1543 species of BRAF in cells[38]. My analysis provides a structural explanation for these observations. The fact that this molecule binds the C-helix “in” conformation of BRAF allows it to shut down both protomers of the active kinase dimer, as well as monomeric, constitutively active V600E mutant. Interestingly, TAK580 also has remarkable potency against CRAF, providing an almost complete blockade of MAPK signals at the RAF level (Sunesis ESMO poster presentation, Madrid 2017).

Chapter five: Conclusions and future directions

For the entirety of my scientific career, my interests have centered on the form and function of molecular machines. I am attracted to cancer research specifically because one of the clearest ways to discover how a cellular machine works is to study what happens when it is broken – in the case of protein machinery, via mutations in the genes that code for it. Throughout my PhD, I have focused on the proteins responsible for transliterating chemical messages that mediate intra- and inter-cellular communication. Most of the work presented in Chapter 2 was published in Park *et al.*[56] and I am currently preparing additional papers based on the work in Chapters 3 and 4.

The particular system I have applied my efforts to understand is the mitogen-activated protein kinase (MAPK) cascade. This pathway is currently represented in textbook diagrams as a linear sequence of activation events – often the transfer of a phosphate from ATP to a downstream kinase – which turn on each subsequent protein in the series.

The Eck lab recently made a discovery that changes the way we see and potentially treat dysregulation of the MAPK pathway. Using a combination of cryo-electron microscopy and X-ray crystallography, we determined the structure of an inactive BRAF:MEK1 complex bound to a 14-3-3 dimer. In a recent *Nature* article, we propose a model in which the MAPK pathway is tightly regulated in healthy cells by the mutual autoinhibition of the RAF and MEK kinases in this complex. Crystal structures of the BRAF:MEK1 kinase module I solved in collaboration with Dr. Kunhua Li afforded us a higher-resolution view of the amino acid residue-level interactions that

enforce the “off” state of this kinase dimer. This has further informed how oncogenic mutations can destabilize this inactive complex. For example, the most common oncogenic mutation in the MAPK pathway introduces an acidic residue in BRAF that disrupts a van der Waals network keeping an alpha-helix from swinging inward and completing the catalytic site. We have also solved the structures of the BRAF:MEK1 kinase dimer in complex with a panel of eight clinical-stage and preclinical MEK inhibitors. These structures, combined with a thorough biochemical characterization of the complex, suggest that the actual pharmacological target of MEK inhibitors is not simply the MEK kinase freely diffusing in the cytoplasm. Binding and activity experiments paint a more complex picture, where different MEK inhibitors act on the MAPK pathway at distinct stages: some inhibitors prevent phosphorylation of MEK by RAF proteins, others prevent the release of phosphorylated MEK from the BRAF-chaperone complex, while yet another class of inhibitors prevents active MEK from phosphorylating ERK.

These insights into the regulation and dysregulation of the MAPK pathway highlight the importance of understanding proteins in a relevant molecular context rather than as linear circuits. Contrary to how most signal transduction diagrams portray them, cellular pathways are not simple cascades where A activates B, which activates C, and so forth. The wealth of knowledge unlocked by structural studies can be leveraged to design more effective anticancer drugs: now that we know that MEK by itself is not the only pharmacological target of MEK inhibitors, we can rationally improve on their initially serendipitous mechanisms of action for the treatment of disease. The results of our coupled BRAF:MEK:ERK activity assays and the BLI-based

binding assays may suggest more effective adjuvant therapy combinations. Currently, vemurafenib and cobimetinib, as well as dabrafenib and trametinib, are being used in tandem to treat melanoma[40,50]. Combining MEK and RAF inhibitors that both increase the affinity of MEK for BRAF would seem to be more effective at shutting down aberrant ERK signaling than treating patients with inhibitors that work at cross purposes to each other. Furthermore, the discovery of the autoinhibited BRAF:MEK1 complex provides a new way of inhibiting the MAPK pathway at the top of the cascade: "gluing" MEK to BRAF, either by using a PROTAC-based strategy[78] or by extending a covalent warhead from the MEK allosteric site to ARAF, BRAF, or CRAF. This approach demonstrates that understanding how a machine's form dictates its function can be directly applied to improving human health.

References

1. Rosen, L. B., Ginty, D. D., Weber, M. J. & Greenberg, M. E. Membrane depolarization and calcium influx stimulate MEK and MAP kinase via activation of Ras. *Neuron* **12**, 1207–1221 (1994).

2. Luttrell, L. M., Daaka, Y., Rocca, G. J. D. & Lefkowitz, R. J. G Protein-coupled Receptors Mediate Two Functionally Distinct Pathways of Tyrosine Phosphorylation in Rat 1a Fibroblasts. *J Biol Chem* **272**, 31648–31656 (1997).

3. Porfiri, E. & McCormick, F. Regulation of Epidermal Growth Factor Receptor Signaling by Phosphorylation of the Ras Exchange Factor hSOS1. *J Biol Chem* **271**, 5871–5877 (1996).

4. Schechter, A. L. *et al.* The neu oncogene: an erb-B-related gene encoding a 185,000-Mr tumour antigen. *Nature* **312**, 513–516 (1984).

5. Jay, G., Shiu, R. P. C., Jay, F. T., Levine, A. S. & Pastan, I. Identification of a transformation-specific protein induced by a rous sarcoma virus. *Cell* **13**, 527–534 (1978).

6. Chang, E. H., Furth, M. E., Scolnick, E. M. & Lowy, D. R. Tumorigenic transformation of mammalian cells induced by a normal human gene homologous to the oncogene of Harvey murine sarcoma virus. *Nature* **297**, 479–483 (1982).

7. Lammers, R., Obberghen, E. V., Ballotti, R., Schlessinger, J. & Ullrich, A. Transphosphorylation as a possible mechanism for insulin and epidermal growth factor receptor activation. *J Biological Chem* **265**, 16886–90 (1990).

8. Qian, X., LeVea, C. M., Freeman, J. K., Dougall, W. C. & Greene, M. I. Heterodimerization of epidermal growth factor receptor and wild-type or kinase-deficient Neu: a mechanism of interreceptor kinase activation and transphosphorylation. *Proc National Acad Sci* **91**, 1500–1504 (1994).

9. Lowenstein, E. J. *et al.* The SH2 and SH3 domain-containing protein GRB2 links receptor tyrosine kinases to ras signaling. *Cell* **70**, 431–42 (1992).

10. Gale, N. W., Kaplan, S., Lowenstein, E. J., Schlessinger, J. & Bar-Sagi, D. Grb2 mediates the EGF-dependent activation of guanine nucleotide exchange on Ras. *Nature* **363**, 88–92 (1993).

11. Egan, S. E. *et al.* Association of Sos Ras exchange protein with Grb2 is implicated in tyrosine kinase signal transduction and transformation. *Nature* **363**, 45–51 (1993).

12. Weber, C. K., Slupsky, J. R., Kalmes, H. A. & Rapp, U. R. Active Ras induces heterodimerization of cRaf and BRaf. *Cancer Res* **61**, 3595–8 (2001).

13. Rajakulendran, T., Sahmi, M., Lefrançois, M., Sicheri, F. & Therrien, M. A dimerization-dependent mechanism drives RAF catalytic activation. *Nature* **461**, 542–545 (2009).

14. Haling, J. R. *et al.* Structure of the BRAF-MEK Complex Reveals a Kinase Activity Independent Role for BRAF in MAPK Signaling. *Cancer Cell* **26**, 402–413 (2014).

15. Wan, P. T. C. *et al.* Mechanism of Activation of the RAF-ERK Signaling Pathway by Oncogenic Mutations of B-RAF. *Cell* **116**, 855–867 (2004).

16. Zheng, J. *et al.* 2.2 Å refined crystal structure of the catalytic subunit of cAMP-dependent protein kinase complexed with MnATP and a peptide inhibitor. *Acta Crystallogr Sect D Biological Crystallogr* **49**, 362–365 (1993).

17. Gardner, A. M., Vaillancourt, R. R. & Johnson, G. L. Activation of mitogen-activated protein kinase/extracellular signal-regulated kinase kinase by G protein and tyrosine kinase oncoproteins. *J Biological Chem* **268**, 17896–901 (1993).

18. Ely, C. M. *et al.* A 42-kD tyrosine kinase substrate linked to chromaffin cell secretion exhibits an associated MAP kinase activity and is highly related to a 42-kD mitogen-stimulated protein in fibroblasts. *J Cell Biology* **110**, 731–742 (1990).

19. Davis, R. J. Transcriptional regulation by MAP kinases. *Mol Reprod Dev* **42**, 459–467 (1995).

20. Yoon, S. & Seger, R. The extracellular signal-regulated kinase: Multiple substrates regulate diverse cellular functions. *Growth Factors* **24**, 21–44 (2006).

21. Buchdunger, E. *et al.* Inhibition of the Abl protein-tyrosine kinase in vitro and in vivo by a 2-phenylaminopyrimidine derivative. *Cancer Res* **56**, 100–4 (1996).

22. Robertson, D. Genentech's anticancer Mab expected by November. *Nat Biotechnol* **16**, 615–615 (1998).

23. Bugaj, L. J. *et al.* Cancer mutations and targeted drugs can disrupt dynamic signal encoding by the Ras-Erk pathway. *Sci New York N Y* **361**, eaao3048 (2018).

24. Langbeheim, H., Shih, T. Y. & Scolnick, E. M. Identification of a normal vertebrate cell protein related to the p21 src of harvey murine sarcoma virus. *Virology* **106**, 292–300 (1980).

25. Tsimberidou, A. M., Eggermont, A. M. M. & Schilsky, R. L. Precision cancer medicine: the future is now, only better. *Am Soc Clin Oncol Educ Book Asco Am Soc Clin Oncol Meet* 61–9 (2014) doi:10.14694/edbook_am.2014.34.61.

26. Bailey, M. H. *et al.* Comprehensive Characterization of Cancer Driver Genes and Mutations. *Cell* **173**, 371-385.e18 (2018).

27. Prior, I. A., Lewis, P. D. & Mattos, C. A comprehensive survey of Ras mutations in cancer. *Cancer Res* **72**, 2457–67 (2012).

28. Parker, J. A., Volmar, A. Y., Pavlopoulos, S. & Mattos, C. K-Ras Populates Conformational States Differently from Its Isoform H-Ras and Oncogenic Mutant K-RasG12D. *Struct Lond Engl 1993* **26**, 810-820.e4 (2018).

29. Ostrem, J. M., Peters, U., Sos, M. L., Wells, J. A. & Shokat, K. M. K-Ras(G12C) inhibitors allosterically control GTP affinity and effector interactions. *Nature* **503**, 548–51 (2013).

30. Canon, J. *et al.* The clinical KRAS(G12C) inhibitor AMG 510 drives anti-tumour immunity. *Nature* **575**, 217–223 (2019).

31. Janes, M. R. *et al.* Targeting KRAS Mutant Cancers with a Covalent G12C-Specific Inhibitor. *Cell* **172**, 578-589.e17 (2018).

32. Simanshu, D. K., Nissley, D. V. & McCormick, F. RAS Proteins and Their Regulators in Human Disease. *Cell* **170**, 17–33 (2017).

33. Robert, C. *et al.* Cutaneous side-effects of kinase inhibitors and blocking antibodies. *Lancet Oncol* **6**, 491–500 (2005).

34. Lacouture, M. E. *et al.* Inflammation of actinic keratoses subsequent to therapy with sorafenib, a multitargeted tyrosine-kinase inhibitor. *Clin Exp Dermatol* **31**, 783–5 (2006).

35. Poulikakos, P. I., Zhang, C., Bollag, G., Shokat, K. M. & Rosen, N. RAF inhibitors transactivate RAF dimers and ERK signalling in cells with wild-type BRAF. *Nature* **464**, 427–30 (2010).

36. Posada, J. & Cooper, J. A. Requirements for phosphorylation of MAP kinase during meiosis in Xenopus oocytes. *Sci New York N Y* **255**, 212–5 (1992).

37. Banks, M., Crowell, K., Proctor, A. & Jensen, B. C. Cardiovascular Effects of the MEK Inhibitor, Trametinib: A Case Report, Literature Review, and Consideration of Mechanism. *Cardiovasc Toxicol* **17**, 487–493 (2017).

38. Daud, A. & Tsai, K. Management of Treatment-Related Adverse Events with Agents Targeting the MAPK Pathway in Patients with Metastatic Melanoma. *Oncol* **22**, 823–833 (2017).

39. Méndez-Martínez, S. *et al.* OCULAR ADVERSE EVENTS ASSOCIATED WITH MEK INHIBITORS. *Retin* **39**, 1435–1450 (2019).

40. Heinzerling, L. *et al.* Tolerability of BRAF/MEK inhibitor combinations: adverse event evaluation and management. *Esmo Open* **4**, e000491 (2019).

41. Hatzivassiliou, G. *et al.* Mechanism of MEK inhibition determines efficacy in mutant KRAS- versus BRAF-driven cancers. *Nature* **501**, 232–6 (2013).

42. Lito, P. *et al.* Disruption of CRAF-mediated MEK activation is required for effective MEK inhibition in KRAS mutant tumors. *Cancer Cell* **25**, 697–710 (2014).

43. Holderfield, M., Deuker, M. M., McCormick, F. & McMahon, M. Targeting RAF kinases for cancer therapy: BRAF-mutated melanoma and beyond. *Nat Rev Cancer* **14**, 455–67 (2014).

44. Dankner, M., Rose, A. A. N., Rajkumar, S., Siegel, P. M. & Watson, I. R. Classifying BRAF alterations in cancer: new rational therapeutic strategies for actionable mutations. *Oncogene* **37**, 3183–3199 (2018).

45. Gear, H., Williams, H., Kemp, E. G. & Roberts, F. BRAF Mutations in Conjunctival Melanoma. *Investigative Opthalmology Vis Sci* **45**, 2484 (2004).

46. Nieto, P. *et al.* A Braf kinase-inactive mutant induces lung adenocarcinoma. *Nature* **548**, 239–243 (2017).

47. Kaul, A., Chen, Y.-H., Emnett, R. J., Dahiya, S. & Gutmann, D. H. Pediatric glioma-associated KIAA1549:BRAF expression regulates neuroglial cell growth in a cell type-specific and mTOR-dependent manner. *Gene Dev* **26**, 2561–6 (2012).

48. Hirschi, B., Gallmeier, E., Ziesch, A., Marschall, M. & Kolligs, F. T. Genetic targeting of B-RafV600E affects survival and proliferation and identifies selective agents against BRAF-mutant colorectal cancer cells. *Mol Cancer* **13**, 122 (2014).

49. Hall-Jackson, C. A. *et al.* Paradoxical activation of Raf by a novel Raf inhibitor. *Chem Biol* **6**, 559–568 (1999).

50. Atkinson, V. *et al.* Dabrafenib plus trametinib is effective in the treatment of BRAF V600-mutated metastatic melanoma patients: analysis of patients from the dabrafenib plus trametinib Named Patient Program (DESCRIBE II). *Melanoma Res* 1 (2019) doi:10.1097/cmr.0000000000000654.

51. Zhang, C. *et al.* RAF inhibitors that evade paradoxical MAPK pathway activation. *Nature* **526**, 583–586 (2015).

52. Sun, Y. *et al.* A brain-penetrant RAF dimer antagonist for the noncanonical BRAF oncoprotein of pediatric low-grade astrocytomas. *Neuro-oncology* **19**, 774–785 (2017).

53. Lake, D., Corrêa, S. A. L. & Müller, J. Negative feedback regulation of the ERK1/2 MAPK pathway. *Cell Mol Life Sci* **73**, 4397–4413 (2016).

54. English, J. M. & Cobb, M. H. Pharmacological inhibitors of MAPK pathways. *Trends Pharmacol Sci* **23**, 40–45 (2002).

55. Flaherty, K. T. *et al.* Combined BRAF and MEK inhibition in melanoma with BRAF V600 mutations. *New Engl J Medicine* **367**, 1694–703 (2012).

56. Fischmann, T. O. *et al.* Crystal Structures of MEK1 Binary and Ternary Complexes with Nucleotides and Inhibitors. *Biochemistry-us* **48**, 2661–2674 (2009).

57. Ohren, J. F. *et al.* Structures of human MAP kinase kinase 1 (MEK1) and MEK2 describe novel noncompetitive kinase inhibition. *Nat Struct Mol Biol* **11**, 1192–1197 (2004).

58. Lavoie, H. & Therrien, M. Regulation of RAF protein kinases in ERK signalling. *Nat Rev Mol Cell Bio* **16**, 281–298 (2015).

59. Sievert, A. J. *et al.* Paradoxical activation and RAF inhibitor resistance of BRAF protein kinase fusions characterizing pediatric astrocytomas. *P Natl Acad Sci Usa* **110**, 5957–62 (2013).

60. Hatzivassiliou, G. *et al.* RAF inhibitors prime wild-type RAF to activate the MAPK pathway and enhance growth. *Nature* **464**, 431–435 (2010).

61. Heidorn, S. J. *et al.* Kinase-dead BRAF and oncogenic RAS cooperate to drive tumor progression through CRAF. *Cell* **140**, 209–21 (2010).

62. Lito, P. *et al.* Relief of Profound Feedback Inhibition of Mitogenic Signaling by RAF Inhibitors Attenuates Their Activity in BRAFV600E Melanomas. *Cancer Cell* **22**, 668–682 (2012).

63. Yao, Z. *et al.* RAF inhibitor PLX8394 selectively disrupts BRAF dimers and RAS-independent BRAF-mutant-driven signaling. *Nat Med* **25**, 284–291 (2018).

64. Park, E. *et al.* Architecture of autoinhibited and active BRAF-MEK1-14-3-3 complexes. *Nature* **575**, 545–550 (2019).

65. Roberts, P. J. & Der, C. J. Targeting the Raf-MEK-ERK mitogen-activated protein kinase cascade for the treatment of cancer. *Oncogene* **26**, 3291–3310 (2007).

66. Greaves, W. O. *et al.* Frequency and Spectrum of BRAF Mutations in a Retrospective, Single-Institution Study of 1112 Cases of Melanoma. *J Mol Diagnostics* **15**, 220–226 (2013).

67. Davies, H. *et al.* Mutations of the BRAF gene in human cancer. *Nature* **417**, 949–954 (2002).

68. Zhang, X., Gureasko, J., Shen, K., Cole, P. A. & Kuriyan, J. An Allosteric Mechanism for Activation of the Kinase Domain of Epidermal Growth Factor Receptor. *Cell* **125**, 1137–1149 (2006).

69. Xu, W., Doshi, A., Lei, M., Eck, M. J. & Harrison, S. C. Crystal Structures of c-Src Reveal Features of Its Autoinhibitory Mechanism. *Mol Cell* **3**, 629–638 (1999).

70. Kim, M.-S. *et al.* A draft map of the human proteome. *Nature* **509**, 575–81 (2014).

71. Liau, N. P. D. *et al.* Negative regulation of RAF kinase activity by ATP is overcome by 14-3-3-induced dimerization. *Nat Struct Mol Biol* **27**, 134–141 (2020).

72. Fernández-Medarde, A. & Santos, E. Ras in cancer and developmental diseases. *Genes Cancer* **2**, 344–58 (2011).

73. Hymowitz, S. G. & Malek, S. Targeting the MAPK Pathway in RAS Mutant Cancers. *Csh Perspect Med* **8**, a031492 (2018).

74. Bollag, G. *et al.* Clinical efficacy of a RAF inhibitor needs broad target blockade in BRAF-mutant melanoma. *Nature* **467**, 596–9 (2010).

75. Grimaldi, A. M. *et al.* MEK Inhibitors in the Treatment of Metastatic Melanoma and Solid Tumors. *Am J Clin Dermatol* **18**, 745–754 (2017).

76. Ishii, N. *et al.* Enhanced Inhibition of ERK Signaling by a Novel Allosteric MEK Inhibitor, CH5126766, That Suppresses Feedback Reactivation of RAF Activity. *Cancer Res* **73**, 4050–4060 (2013).

77. Gao, Y. *et al.* Allele-Specific Mechanisms of Activation of MEK1 Mutants Determine Their Properties. *Cancer Discov* **8**, 648–661 (2018).

78. Karoulia, Z., Gavathiotis, E. & Poulikakos, P. I. New perspectives for targeting RAF kinase in human cancer. *Nat Rev Cancer* **17**, 676–691 (2017).

79. Tsai, J. *et al.* Discovery of a selective inhibitor of oncogenic B-Raf kinase with potent antimelanoma activity. *Proc National Acad Sci* **105**, 3041–3046 (2008).

80. Neklesa, T. K., Winkler, J. D. & Crews, C. M. Targeted protein degradation by PROTACs. *Pharmacol Therapeut* **174**, 138–144 (2017).

Figure A1. Size exclusion chromatography analysis of the oligomerization state of the BRAF:MEK1 kinase module in the presence of nucleotide, RAF inhibitors, and MEK inhibitors.

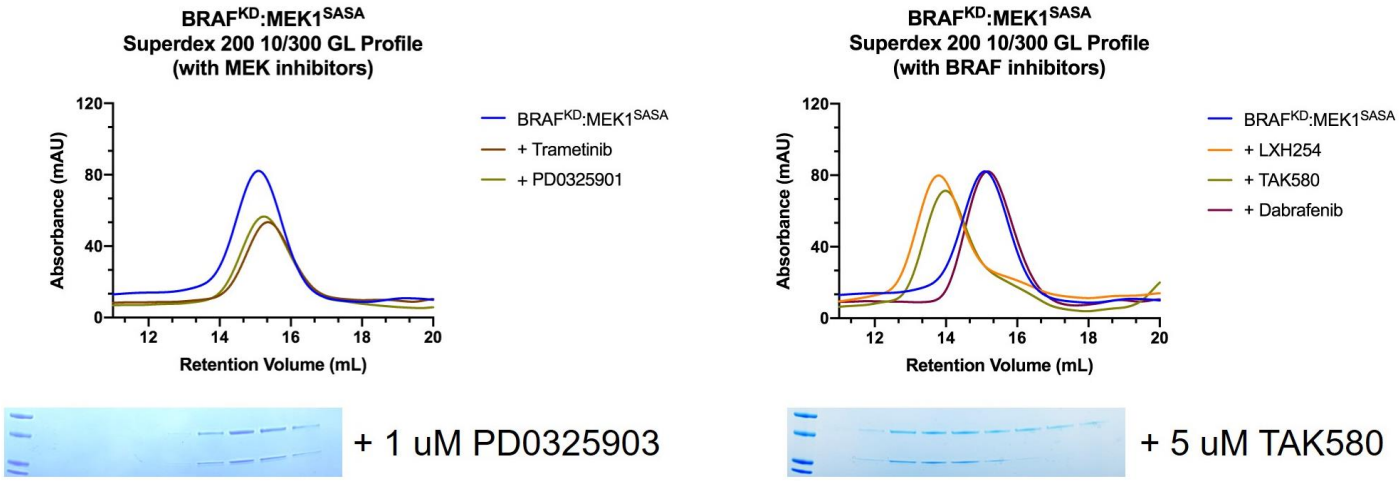

Figure A2. BRAF:MEK1 Biolayer interferometry data processed by kinetic and steady state fitting. Binding assays were performed as described in the Methods for chapter 3. Binding of unphosphorylated and phosphorylated MEK1 to the BRAF kinase in the presence of nucleotide and a battery of RAF and MEK inhibitors. Values summarized in Table 2 are an average of kinetic fits taken from MEK1 concentration conditions with an R^2 value >0.95. For pMEK experiments, 2:1 heterologous ligand fits were used, since a fraction of our sample was unphosphorylated. For these experiments, I averaged the KD2 values, which correspond to the fast kinetic regime, for conditions with an R^2 value >0.95.

Figure A2a. Unphosphorylated MEK1 binding to BRAF in the presence of ATP.

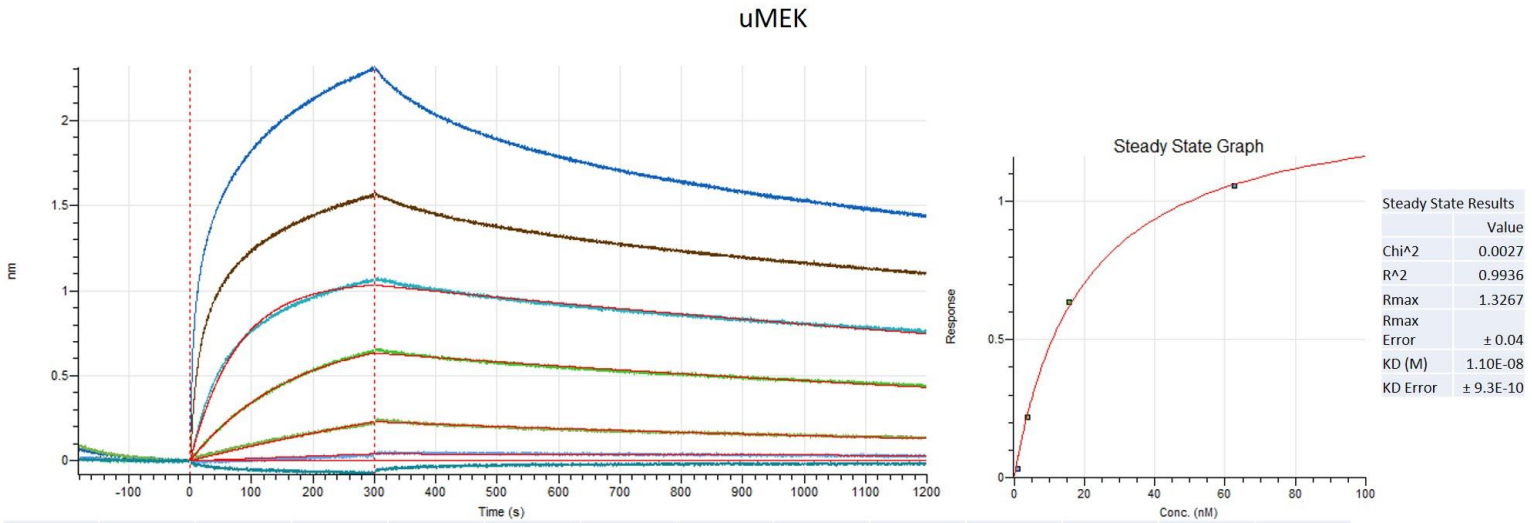

Conc. (nM)	Response	KD (M)	KD Error	ka (1/Ms)	ka Error	kdis (1/s)	kdis Error	Rmax	Rmax Error	Req	Req/Rmax(%)	Full X^2	Full R^2
1000	2.2923												
250	1.5543												
62.5	1.0555	1.75E-09	5.53E-12	2.05E+05	4.42E+02	3.60E-04	8.31E-07	1.0831	0.0006	1.0535	97.3	1.2543	0.9912
15.6	0.6378	1.19E-09	3.67E-12	3.58E+05	9.29E+02	4.26E-04	7.11E-07	0.8171	0.0011	0.7592	92.9	0.3002	0.9962
3.91	0.2185	3.83E-09	1.88E-10	1.64E+05	8.01E+03	6.27E-04	1.99E-06	1.4411	0.065	0.728	50.5	0.2478	0.9789
0.98	0.0326	2.76E-09	4.76E-09	9.99E+04	1.72E+05	2.76E-04	9.57E-06	1.4867	2.5303	0.3894	26.2	0.2518	0.7903
0.244	-7.04E-02	1.00E-07	<1.0E-12	1.00E+04	0.00E+00	1.00E-03	<1.0E-07	0		0		7.3937	

Figure A2 (contd.).

Figure A2b. Unphosphorylated MEK1 binding to BRAF in the presence of ATP and GDC0623.

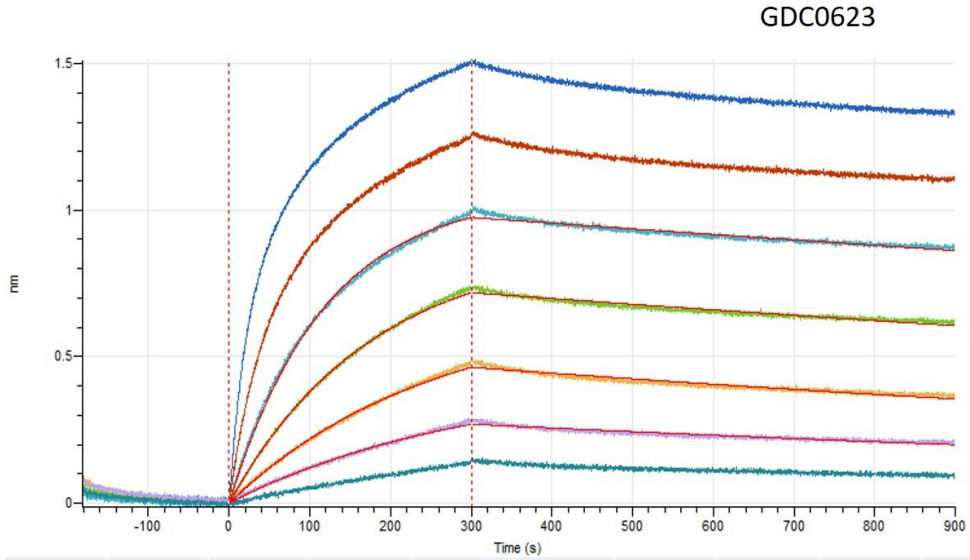

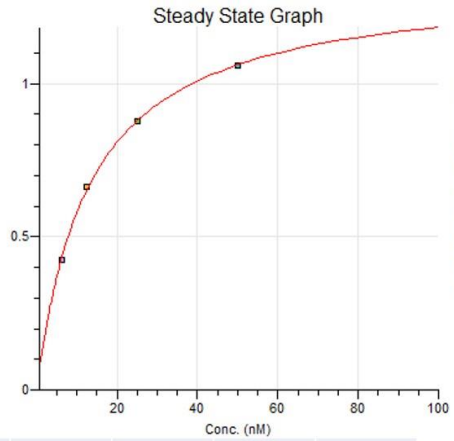

Steady State Results	
	Value
Chi^2	0.0002
R^2	0.9993
Rmax	1.3396
Rmax Error	± 0.013
KD (M)	1.30E-08
KD Error	± 3.5E-10

Conc. (nM)	Response	KD (M)	KD Error	ka (1/Ms)	ka Error	kdis (1/s)	kdis Error	Rmax	Rmax Error	Req	Req/Rmax(%)	Full X^2	Full R^2
200	1.4963												
100	1.2399												
50	0.9809	1.25E-09	6.14E-12	1.65E+05	2.96E+02	2.06E-04	9.41E-07	1.0856	0.0008	1.0592	97.6	0.3945	0.9976
25	0.7261	1.32E-09	6.08E-12	2.16E+05	5.68E+02	2.85E-04	1.08E-06	0.924	0.0013	0.8778	95	0.2591	0.9976
12.5	0.4714	1.55E-09	1.07E-11	2.86E+05	1.62E+03	4.44E-04	1.73E-06	0.7443	0.0028	0.662	88.9	0.2484	0.9946
6.25	0.2762	1.09E-09	1.15E-11	4.59E+05	4.29E+03	5.01E-04	2.39E-06	0.4975	0.0033	0.4235	85.1	0.1525	0.9903
3.13	0.1348												

Figure A2 (contd.).

Figure A2c. Unphosphorylated MEK1 binding to BRAF in the presence of ATP and PD0325901.

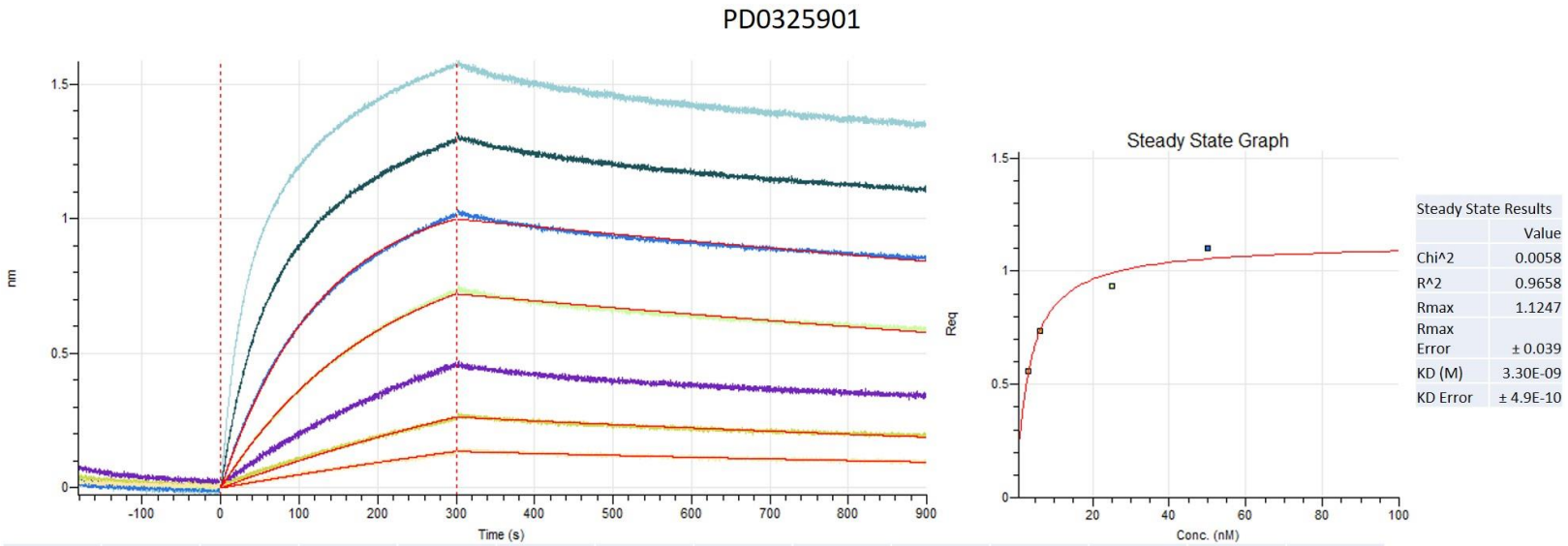

Conc. (nM)	Response	KD (M)	KD Error	ka (1/Ms)	ka Error	kdis (1/s)	kdis Error	Rmax	Rmax Error	Req	Req/Rmax(%)	Full X^2	Full R^2
200	1.5644												
100	1.2847												
50	1.0064	1.87E-09	6.24E-12	1.52E+05	2.47E+02	2.85E-04	8.30E-07	1.1435	0.0008	1.1022	96.4	0.305	0.9983
25	0.7225	2.03E-09	8.17E-12	1.82E+05	5.20E+02	3.68E-04	1.05E-06	1.0106	0.0017	0.9349	92.5	0.232	0.9979
12.5	0.449												
6.25	0.2526	3.73E-09	1.06E-10	1.49E+05	4.15E+03	5.54E-04	2.48E-06	1.1728	0.0293	0.7343	62.6	0.1499	0.9901
3.13	0.1288	5.10E-09	4.89E-10	1.13E+05	1.08E+04	5.79E-04	3.30E-06	1.4672	0.1344	0.5572	38	0.0693	0.9848

Figure A2 (contd.).

Figure A2d. Unphosphorylated MEK1 binding to BRAF in the presence of ATP and CHO5126676.

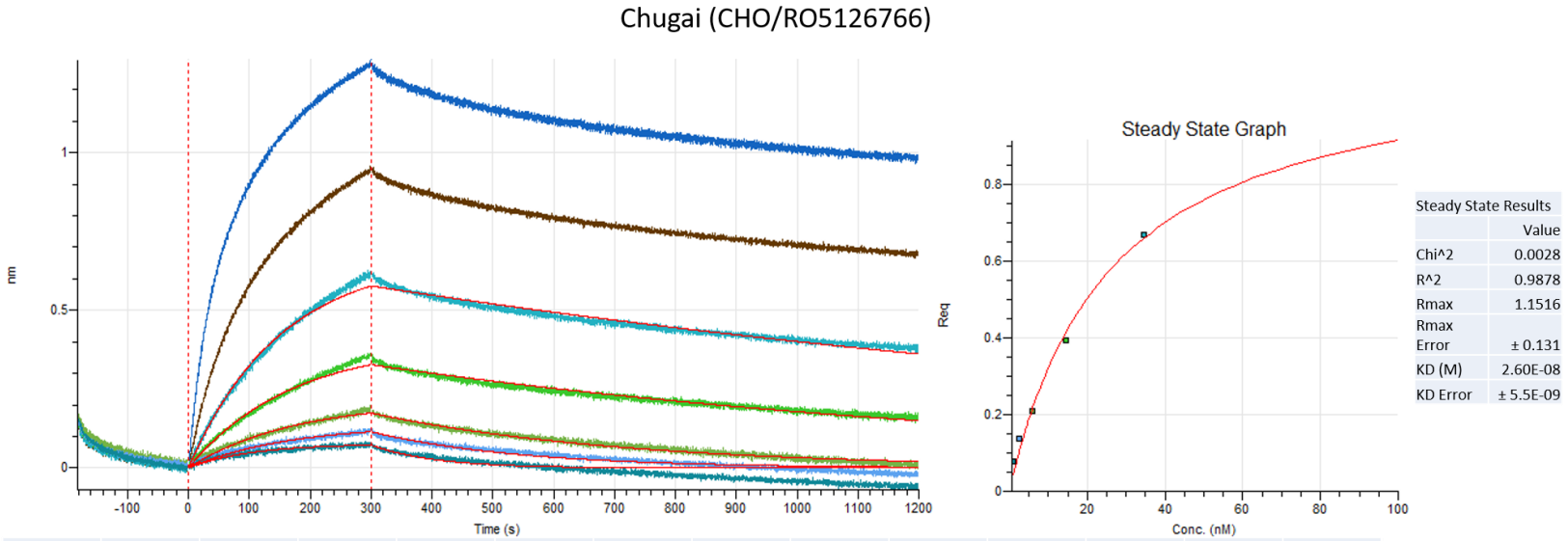

Conc. (nM)	Response	KD (M)	KD Error	ka (1/Ms)	ka Error	kdis (1/s)	kdis Error	Rmax	Rmax Error	Req	Req/Rmax(%)	Full X^2	Full R^2
200	1.273												
83.3	0.9384												
34.7	0.6092	2.95E-09	1.62E-11	1.77E+05	8.40E+02	5.21E-04	1.43E-06	0.7254	0.0016	0.6686	92.2	0.9375	0.9856
14.5	0.3518	2.45E-09	1.92E-11	3.54E+05	2.63E+03	8.68E-04	2.22E-06	0.4591	0.0019	0.3927	85.5	0.5265	0.9788
6.03	0.1839	4.10E-09	6.79E-11	5.79E+05	9.48E+03	2.38E-03	6.11E-06	0.3538	0.0041	0.2105	59.5	0.2897	0.9794
2.51	0.116	5.01E-09	3.22E-10	8.14E+05	5.22E+04	4.07E-03	2.40E-05	0.4095	0.0222	0.1368	33.4	0.5401	0.941
1.05	0.075	5.00E-08	2.13E-07	1.92E+05	8.18E+05	9.57E-03	3.40E-04	3.742	15.826	0.0768	2.1	4.1359	0.589

Figure A2 (contd.).

Figure A2e. Unphosphorylated MEK1 binding to BRAF in the presence of ATP and Trametinib.

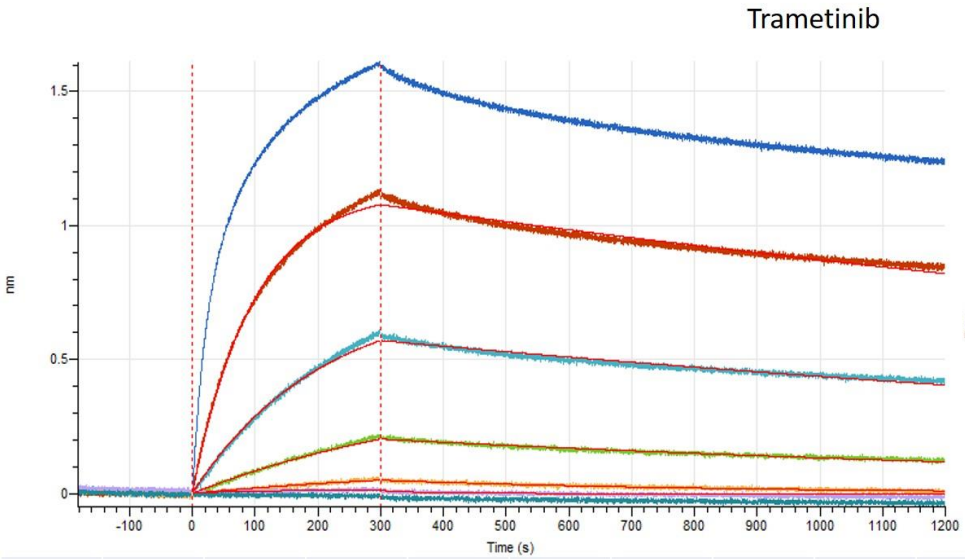

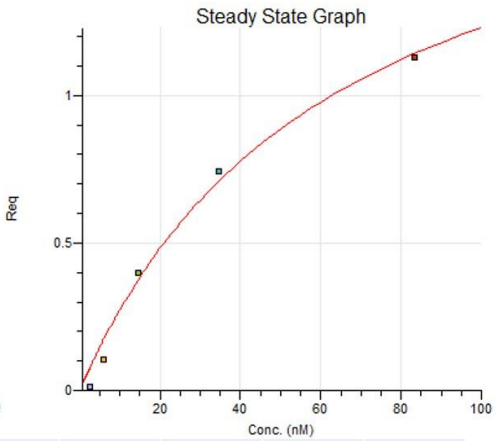

Steady State Results	
	Value
Chi^2	0.0108
R^2	0.9873
Rmax	2.01
Rmax Error	± 0.266
KD (M)	6.30E-08
KD Error	± 1.6E-08

Conc. (nM)	Response	KD (M)	KD Error	ka (1/Ms)	ka Error	kdis (1/s)	kdis Error	Rmax	Rmax Error	Req	Req/Rmax(%)	Full X^2	Full R^2
200	1.5992												
83.3	1.1191	2.51E-09	9.23E-12	1.21E+05	2.86E+02	3.04E-04	8.54E-07	1.162	0.0009	1.128	97.1	1.4621	0.9919
34.7	0.5928	2.94E-09	1.76E-11	1.30E+05	6.67E+02	3.83E-04	1.18E-06	0.804	0.0023	0.7412	92.2	0.687	0.9903
14.5	0.2103	5.02E-09	8.94E-11	1.21E+05	2.12E+03	6.07E-04	1.89E-06	0.538	0.0076	0.3996	74.3	0.1771	0.9828
6.03	0.0521	3.81E-08	1.32E-08	4.82E+04	1.67E+04	1.83E-03	1.02E-05	0.7707	0.259	0.1053	13.7	0.101	0.9079
2.51	0.0142	1.01E-07	6.60E-07	1.47E+05	9.58E+05	1.50E-02	1.20E-03	0.4601	2.9544	0.0111	2.4	0.345	0.2778
1.05	-9.23E-03												

Figure A2 (contd.).

Figure A2f. Unphosphorylated MEK1 binding to BRAF in the presence of ATP and Cobimetinib.

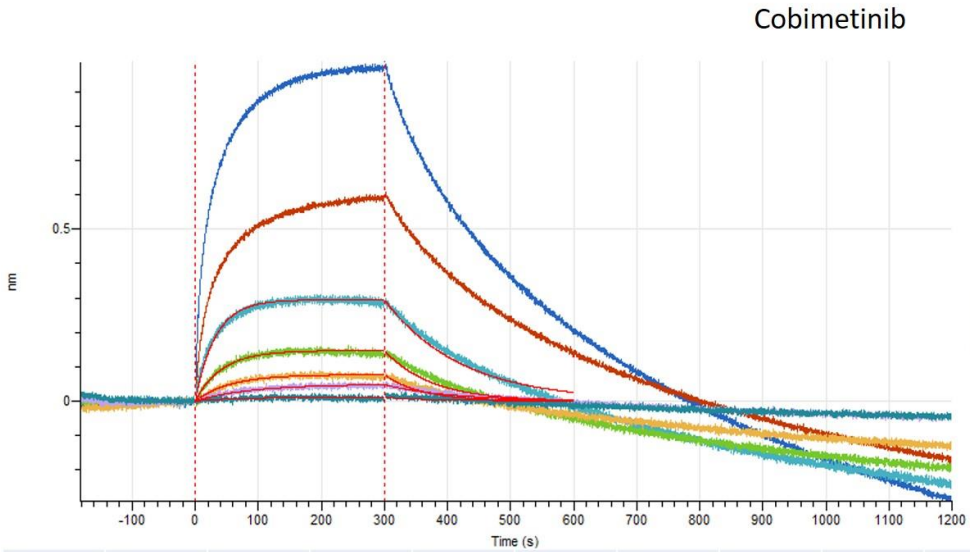

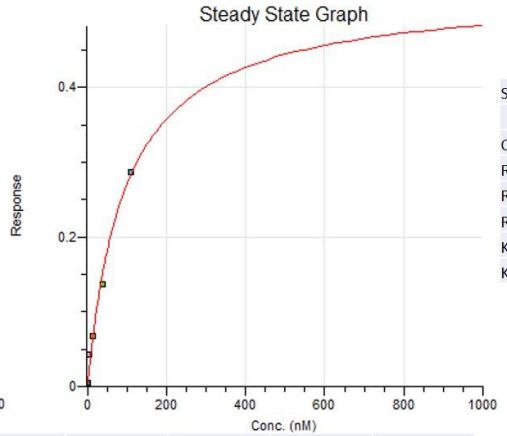

Steady State Results	
	Value
Chi^2	0.0006
R^2	0.9869
Rmax	0.5292
Rmax Error	± 0.079
KD (M)	9.60E-08
KD Error	± 2.6E-08

Conc. (nM)	Response	KD (M)	KD Error	ka (1/Ms)	ka Error	kdis (1/s)	kdis Error	Rmax	Rmax Error	Req	Req/Rmax(%)	Full X^2	Full R^2
1000	0.9709												
333.3	0.5898												
111.1	0.2867	3.99E-08	5.10E-10	2.07E+05	2.50E+03	8.27E-03	3.61E-05	0.4004	0.0019	0.2946	73.6	0.5681	0.9832
37	0.1365	5.03E-08	2.90E-09	2.70E+05	1.51E+04	1.36E-02	1.82E-04	0.3456	0.0137	0.1466	42.4	0.9555	0.928
12.4	0.0683	2.99E-07	3.25E-07	5.73E+04	6.24E+04	1.71E-02	4.02E-04	1.9311	2.0572	0.0766	4	0.6296	0.8608
4.12	0.043	2.50E-08	4.27E-09	3.82E+05	6.51E+04	9.54E-03	1.03E-04	0.3442	0.0544	0.0487	14.1	0.0742	0.9129
1.37	0.0056	8.68E-08	7.80E-07	1.58E+05	1.42E+06	1.37E-02	9.42E-04	0.6858	6.118	0.0107	1.6	0.122	0.4164

Figure A2 (contd.).

Figure A2g. Unphosphorylated MEK1 binding to BRAF in the presence of ATP and Selumetinib.

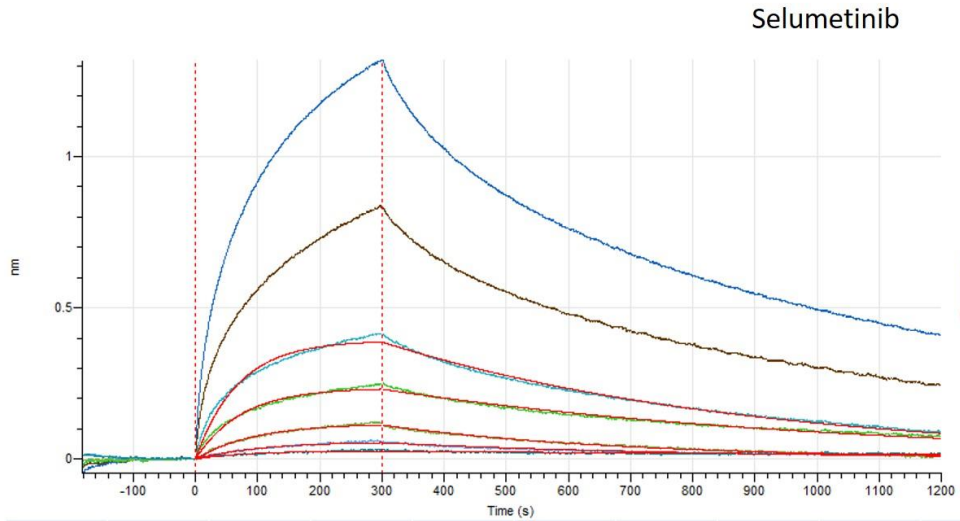

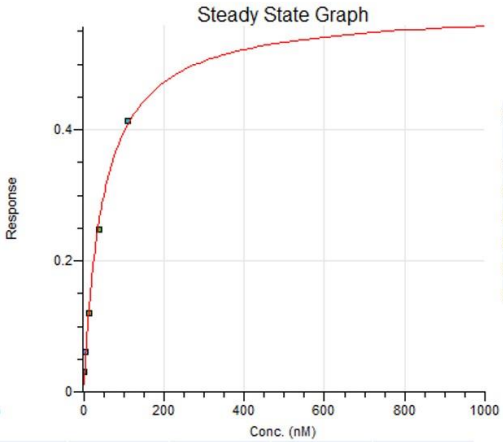

Steady State Results	
	Value
Chi^2	0.0005
R^2	0.995
Rmax	0.585
Rmax Error	± 0.032
KD (M)	4.80E-08
KD Error	± 5.9E-09

Conc. (nM)	Response	KD (M)	KD Error	ka (1/Ms)	ka Error	kdis (1/s)	kdis Error	Rmax	Rmax Error	Req	Req/Rmax(%)	Full X^2	Full R^2
1000	1.3115												
333.3	0.8293												
111.1	0.4126	1.45E-08	6.61E-11	1.16E+05	4.98E+02	1.69E-03	2.62E-06	0.4431	0.0006	0.3919	88.4	0.5318	0.9908
37	0.2469	4.12E-09	2.12E-11	3.29E+05	1.57E+03	1.35E-03	2.58E-06	0.2613	0.0004	0.2352	90	0.2459	0.9852
12.4	0.121	3.91E-09	2.38E-11	6.50E+05	3.82E+03	2.54E-03	4.09E-06	0.155	0.0004	0.1177	76	0.0498	0.9924
4.12	0.0607	9.99E-10	1.16E-11	1.86E+06	2.07E+04	1.86E-03	6.05E-06	0.0713	0.0004	0.0574	80.5	0.045	0.9612
1.37	0.0305	7.31E-11	1.26E-12	8.40E+06	1.20E+05	6.14E-04	5.91E-06	0.0285	0.0001	0.027	94.9	0.0323	0.751

Figure A2 (contd.).

Figure A2h. Unphosphorylated MEK1 binding to BRAF in the presence of ATP and Pimasertib.

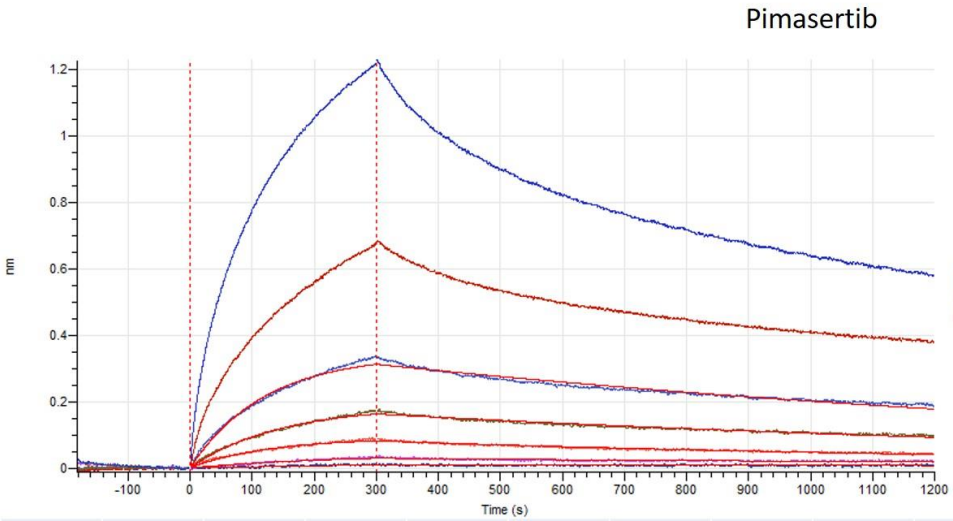

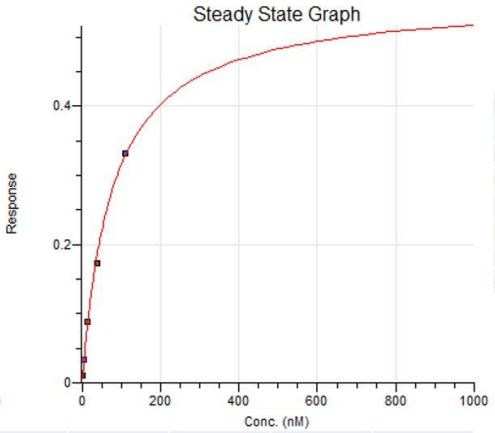

Steady State Results	
	Value
Chi^2	0.0002
R^2	0.9967
Rmax	0.5566
Rmax Error	± 0.035
KD (M)	7.70E-08
KD Error	± 9.6E-09

Conc. (nM)	Response	KD (M)	KD Error	ka (1/Ms)	ka Error	kdis (1/s)	kdis Error	Rmax	Rmax Error	Req	Req/Rmax(%)	Full X^2	Full R^2
1000	1.2086												
333.3	0.6664												
111.1	0.3315	9.04E-09	5.10E-11	6.95E+04	3.40E+02	6.28E-04	1.76E-06	0.3678	0.0007	0.3401	92.5	0.3801	0.9791
37	0.1721	3.63E-09	2.10E-11	1.74E+05	8.97E+02	6.30E-04	1.67E-06	0.2027	0.0005	0.1847	91.1	0.0912	0.9822
12.4	0.0877	1.31E-09	9.68E-12	5.99E+05	4.01E+03	7.84E-04	2.47E-06	0.0984	0.0003	0.089	90.4	0.0444	0.9664
4.12	0.0332	5.48E-10	1.42E-11	9.46E+05	2.27E+04	5.18E-04	5.13E-06	0.045	0.0007	0.0397	88.3	0.0298	0.8718
1.37	0.0105	9.03E-10	4.77E-10	3.06E+05	1.61E+05	2.76E-04	1.24E-05	0.0805	0.0401	0.0486	60.3	0.0205	0.5037

Figure A2 (contd.).

Figure A2i. Unphosphorylated MEK1 binding to BRAF in the presence of ATP and TAK580.

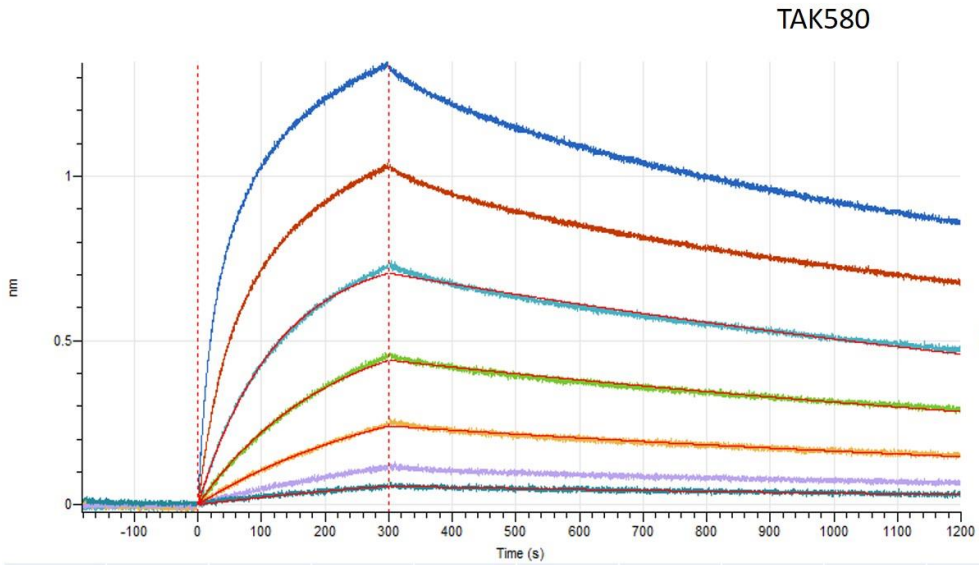

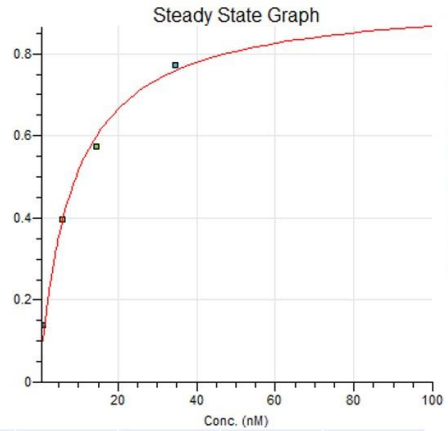

Steady State Results	Value
Chi^2	0.0019
R^2	0.9913
Rmax	0.9385
Rmax Error	± 0.045
KD (M)	8.20E-09
KD Error	± 1.2E-09

Conc. (nM)	Response	KD (M)	KD Error	ka (1/Ms)	ka Error	kdis (1/s)	kdis Error	Rmax	Rmax Error	Req	Req/Rmax(%)	Full X^2	Full R^2
200	1.3333												
83.3	1.0241												
34.7	0.7202	2.18E-09	6.10E-12	2.19E+05	4.99E+02	4.78E-04	7.71E-07	0.8218	0.0008	0.7732	94.1	0.4262	0.9952
14.5	0.4476	1.62E-09	7.40E-12	3.01E+05	1.24E+03	4.89E-04	9.55E-07	0.6381	0.0015	0.5738	89.9	0.2434	0.9941
6.03	0.2408	1.31E-09	1.29E-11	4.20E+05	4.01E+03	5.48E-04	1.41E-06	0.4834	0.0033	0.3974	82.2	0.1479	0.989
2.51	0.1122												
1.05	0.0562	6.54E-10	4.97E-11	1.03E+06	7.81E+04	6.75E-04	5.24E-06	0.2256	0.0149	0.1389	61.6	0.1008	0.8652

Figure A2 (contd.).

Figure A2j. Unphosphorylated MEK1 binding to BRAF in the presence of ATP and Sorafenib.

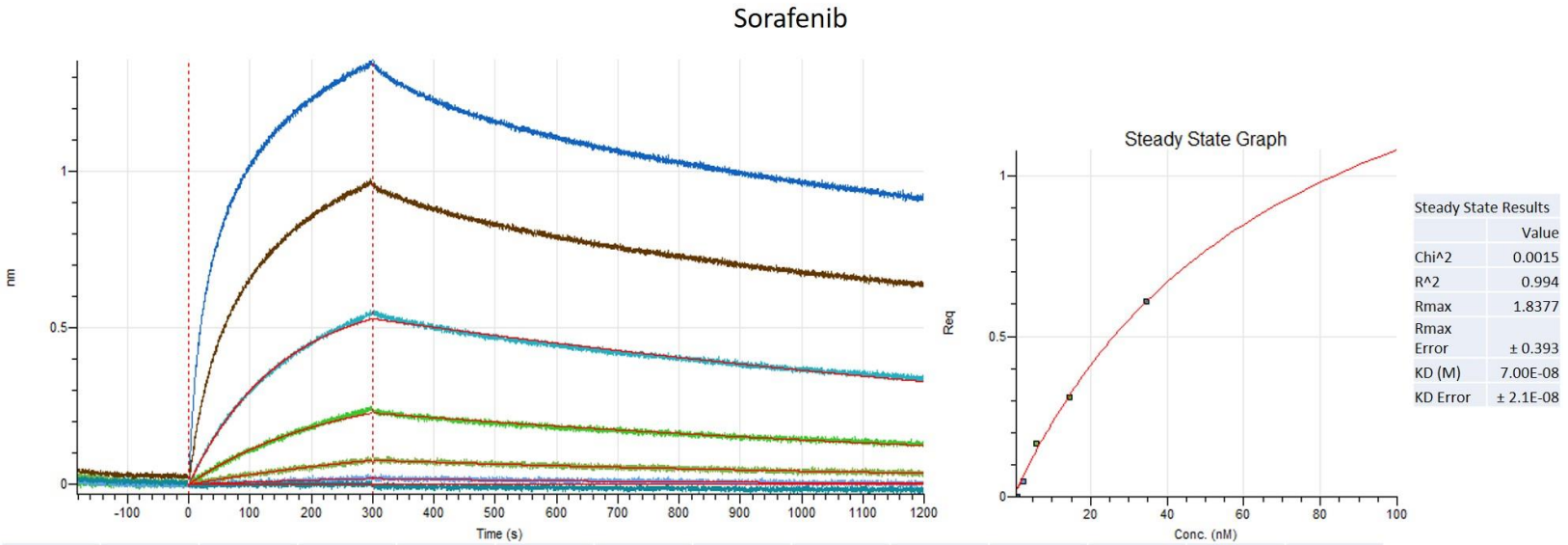

Steady State Results	Value
Chi^2	0.0015
R^2	0.994
Rmax	1.8377
Rmax Error	± 0.393
KD (M)	7.00E-08
KD Error	± 2.1E-08

Conc. (nM)	Response	KD (M)	KD Error	ka (1/Ms)	ka Error	kdis (1/s)	kdis Error	Rmax	Rmax Error	Req	Req/Rmax(%)	Full X^2	Full R^2
200	1.3372												
83.3	0.9594												
34.7	0.5416	2.97E-09	1.02E-11	1.79E+05	5.29E+02	5.31E-04	9.03E-07	0.6617	0.0009	0.6095	92.1	0.3091	0.9943
14.5	0.2392	2.63E-09	2.13E-11	2.58E+05	1.99E+03	6.76E-04	1.69E-06	0.3678	0.0018	0.3113	84.6	0.1716	0.9854
6.03	0.0769	4.13E-09	2.19E-10	2.06E+05	1.09E+04	8.48E-04	4.46E-06	0.2795	0.0127	0.166	59.4	0.1153	0.9288
2.51	0.0206	2.54E-08	4.07E-08	6.47E+04	1.04E+05	1.64E-03	2.46E-05	0.5142	0.8095	0.0464	9	0.1067	0.5983
1.05	0.0017	1.00E-07	<1.0E-12	1.00E+04	0.00E+00	1.00E-03	<1.0E-07	0		0		0.8267	

Figure A2 (contd.).

Figure A2k. Unphosphorylated MEK1 binding to BRAF in the presence of ATP and Dabrafenib.

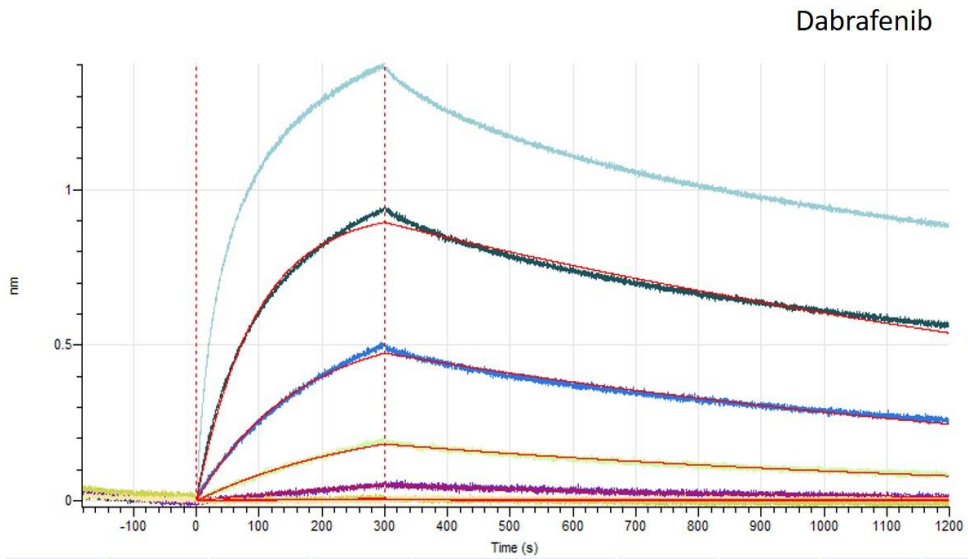

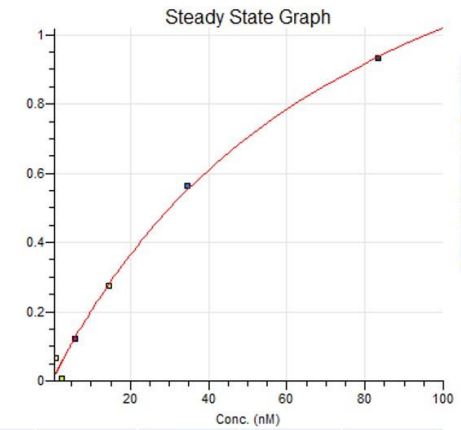

Steady State Results	
	Value
Chi^2	0.0042
R^2	0.9933
Rmax	1.853
Rmax Error	± 0.209
KD (M)	8.20E-08
KD Error	± 1.6E-08

Conc. (nM)	Response	KD (M)	KD Error	ka (1/Ms)	ka Error	kdis (1/s)	kdis Error	Rmax	Rmax Error	Req	Req/Rmax(%)	Full X^2	Full R^2
200	1.3924												
83.3	0.9301	4.61E-09	1.62E-11	1.22E+05	3.51E+02	5.62E-04	1.13E-06	0.984	0.0009	0.9325	94.8	1.4184	0.9893
34.7	0.4937	4.65E-09	2.37E-11	1.57E+05	7.37E+02	7.28E-04	1.40E-06	0.6391	0.0016	0.5635	88.2	0.5006	0.9896
14.5	0.1879	4.94E-09	7.00E-11	1.86E+05	2.58E+03	9.17E-04	2.49E-06	0.371	0.0037	0.2766	74.5	0.1908	0.9776
6.03	0.0482	3.90E-08	2.10E-08	3.87E+04	2.08E+04	1.51E-03	1.13E-05	0.9211	0.483	0.1232	13.4	0.1694	0.8476
2.51	0.0085	2.57E-07	5.70E-06	3.72E+04	8.26E+05	9.55E-03	8.26E-04	0.7423	16.4057	0.0072	1	0.2144	0.1834
1.05	-1.40E-03	<1.0E-12	1.58E-11	2.89E+05	7.49E+05	<1.0E-07	4.56E-06	0.0657	0.163	0.0657	100	0.1315	0.1548

Figure A2 (contd.).

Figure A2l. Unphosphorylated MEK1 binding to BRAF in the presence of ATP and Vemurafenib.

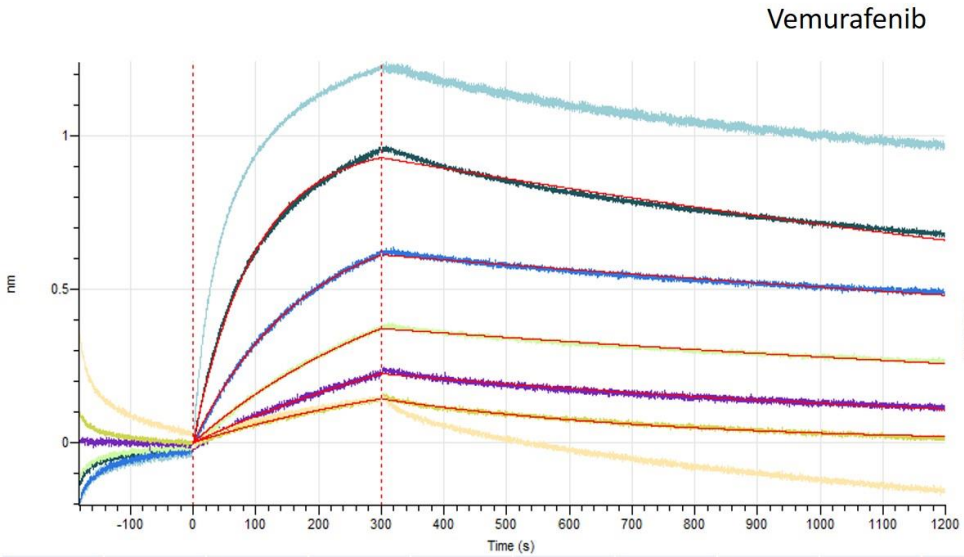

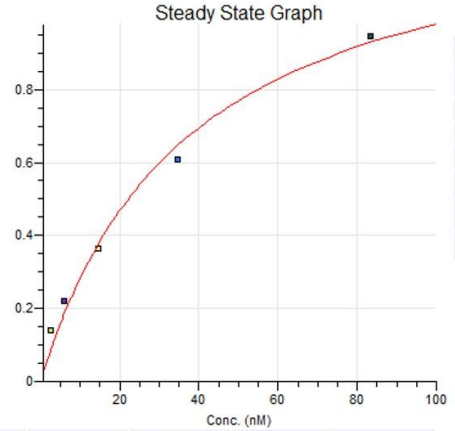

Steady State Results	
	Value
Chi^2	0.006
R^2	0.986
Rmax	1.3472
Rmax Error	± 0.112
KD (M)	3.80E-08
KD Error	± 6.9E-09

Conc. (nM)	Response	KD (M)	KD Error	ka (1/Ms)	ka Error	kdis (1/s)	kdis Error	Rmax	Rmax Error	Req	Req/Rmax(%)	Full X^2	Full R^2
200	1.2166												
83.3	0.9466	3.19E-09	9.66E-12	1.19E+05	2.60E+02	3.80E-04	8.01E-07	1.0103	0.0007	0.973	96.3	0.8939	0.9933
34.7	0.61	1.74E-09	6.01E-12	1.55E+05	3.89E+02	2.69E-04	6.35E-07	0.7884	0.001	0.7507	95.2	0.2555	0.9968
14.5	0.3656	2.59E-09	1.98E-11	1.58E+05	1.15E+03	4.09E-04	9.32E-07	0.7929	0.0043	0.6724	84.8	0.1747	0.995
6.03	0.2212	6.20E-09	2.56E-10	1.30E+05	5.34E+03	8.02E-04	2.18E-06	1.2071	0.0452	0.5953	49.3	0.2429	0.9822
2.51	0.1391	3.12E-08	7.24E-09	6.92E+04	1.61E+04	2.16E-03	4.60E-06	3.8094	0.8669	0.2837	7.4	0.1278	0.9851
1.05	0.141												

Figure A2 (contd.).

Figure A2m. Phosphorylated MEK1 binding to BRAF in the presence of ATP.

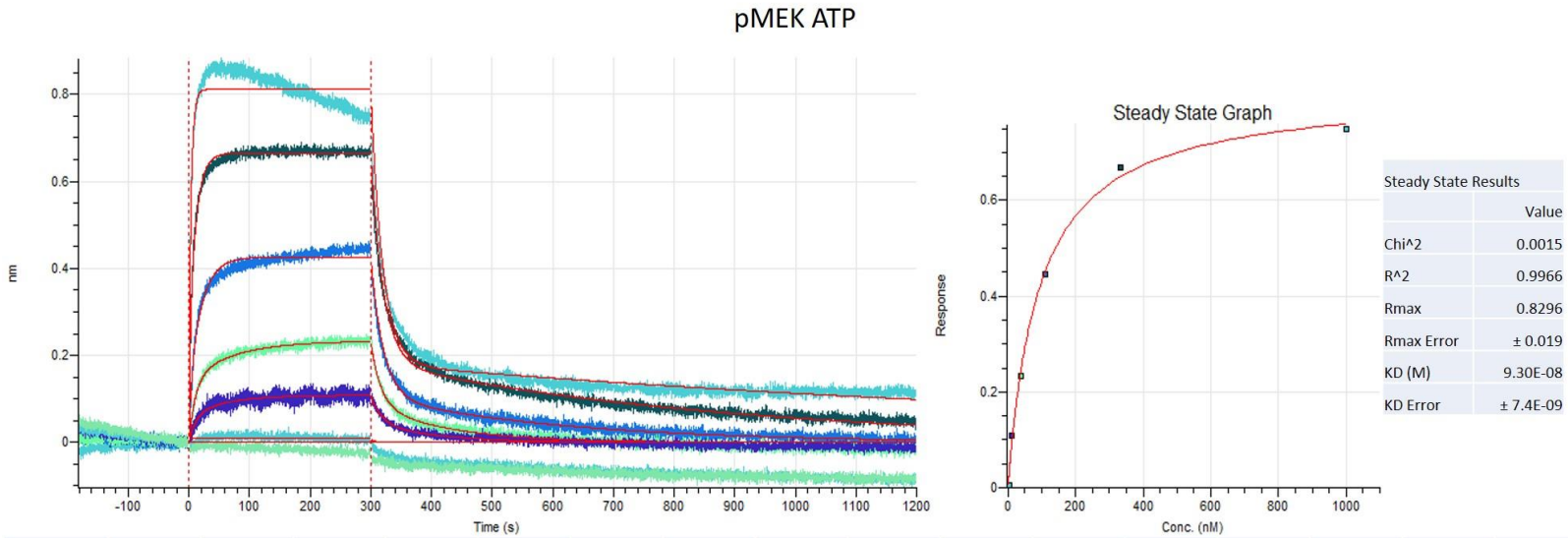

Conc. (nM)	Response	KD (M)	KD2	KD Error	KD2 Error	ka (1/Ms)	ka2	ka Error	ka2 Error	kdis (1/s)	kdis2	kdis Error	kdis2 Error	Full R^2	KD(%)	KD2(%)
1000	0.7479	9.21E-10	2.73E-07	1.17E-10	7.66E-09	7.34E+05	1.88E+05	9.23E+04	5.03E+03	6.76E-04	5.12E-02	1.15E-05	4.32E-04	0.9939	18	82
333	0.6675	1.22E-09	3.98E-07	4.42E-11	6.64E-09	1.40E+06	1.24E+05	5.05E+04	1.98E+03	1.71E-03	4.95E-02	8.19E-06	2.49E-04	0.9984	15	85
111	0.4449	1.48E-09	2.82E-05	7.07E-11	9.07E-05	2.16E+06	1.74E+03	1.01E+05	5.60E+03	3.19E-03	4.90E-02	2.93E-05	4.15E-04	0.9964	0	100
37	0.2338	5.18E-08	7.97E-08	3.72E-09	6.10E-09	1.54E+05	7.84E+05	1.07E+04	5.68E+04	7.96E-03	6.26E-02	1.45E-04	1.56E-03	0.9887	33	67
12.4	0.1081	1.74E-08	2.74E-08	2.29E-09	4.69E-09	5.47E+05	2.14E+06	6.83E+04	3.42E+05	9.51E-03	5.85E-02	4.00E-04	3.55E-03	0.9571	36	64
4.1	0.0051	4.73E-07	<1.0E-12		2.00E-07	4.35E+08	8.66E+11		8.27E+17	2.06E+02	1.81E-01		6.25E-01		57	43
1.4	-2.53E-02	7.80E-12	7.80E-12	<1.0E-12	<1.0E-12	3.57E+06	3.57E+06	0.00E+00	0.00E+00	2.79E-05	2.79E-05	<1.0E-07	<1.0E-07			

Figure A2 (contd.).

Figure A2n. Phosphorylated MEK1 binding to BRAF in the presence of ATP and GDC0623.

pMEK GDC0623

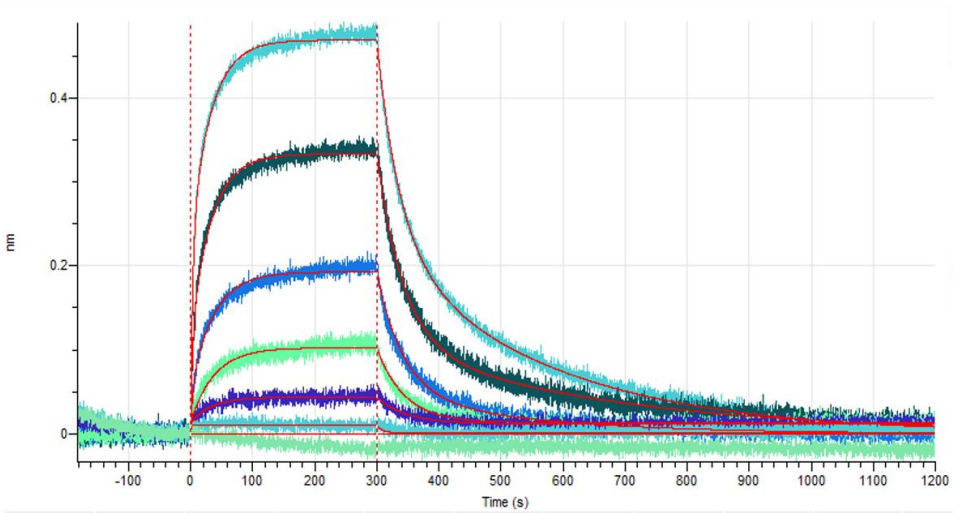

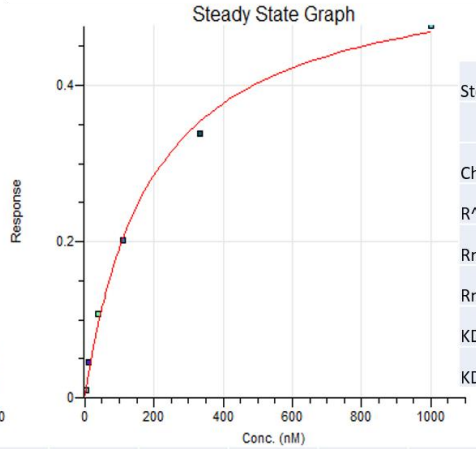

Steady State Results	
	Value
Chi^2	0.0008
R^2	0.9954
Rmax	0.5585
Rmax Error	± 0.019
KD (M)	1.90E-07
KD Error	± 2.0E-08

Conc. (nM)	Response	KD (M)	KD2	KD Error	KD2 Error	ka (1/Ms)	ka2	ka Error	ka2 Error	kdis (1/s)	kdis2	kdis Error	kdis2 Error	Full X^2	Full R^2	KD(%)	KD2(%)
1000	0.4768	1.34E-08	6.10E-06	2.18E-10	4.84E-07	2.79E+05	4.39E+03	4.43E+03	3.47E+02	3.74E-03	2.68E-02	1.41E-05	1.95E-04	0.2526	0.9987	12	88
333.3	0.3388	2.91E-09	1.07E-06	1.12E-10	5.29E-08	9.42E+05	2.21E+04	3.54E+04	1.08E+03	2.75E-03	2.36E-02	2.19E-05	1.88E-04	0.3255	0.9965	11	89
111.1	0.2015	1.84E-09	8.32E-07	1.35E-10	1.47E-07	2.36E+06	2.89E+04	1.68E+05	5.09E+03	4.34E-03	2.40E-02	7.89E-05	3.04E-04	0.2314	0.9931	4	96
37	0.1075	<1.0E-12	2.25E-07	<1.0E-12	2.52E-08	1.63E+08	1.00E+05	1.67E+08	1.12E+04	<1.0E-07	2.26E-02	2.47E-06	2.22E-04	0.2103	0.9724	2	98
12.4	0.0457	<1.0E-12	2.57E-08	<1.0E-12	2.75E-09	2.32E+08	8.11E+05	1.44E+08	8.48E+04	<1.0E-07	2.09E-02	2.26E-06	4.55E-04	0.1395	0.8732	11	89
4.1	0.0102	<1.0E-12	7.86E-10		4.06E-10	8.63E+11	1.52E+08		7.40E+07	6.28E-05	1.19E-01	2.68E-04	2.03E-02	0.1515	0.2297	9	91
1.4	-1.85E-02					3.57E+06	3.57E+06	0.00E+00	0.00E+00			<1.0E-07	<1.0E-07	1.5566			

Figure A2 (contd.).

Figure A2o. Phosphorylated MEK1 binding to BRAF in the presence of ATP and PD0325901.

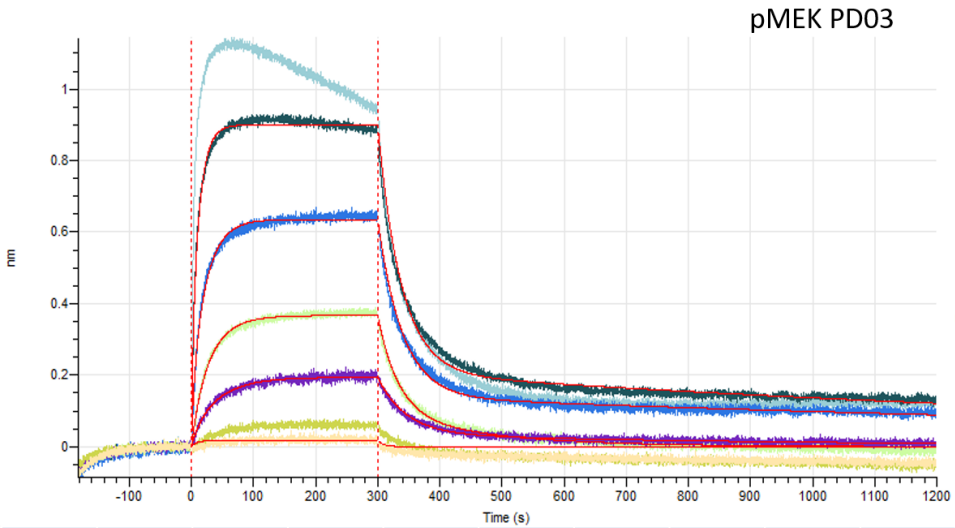

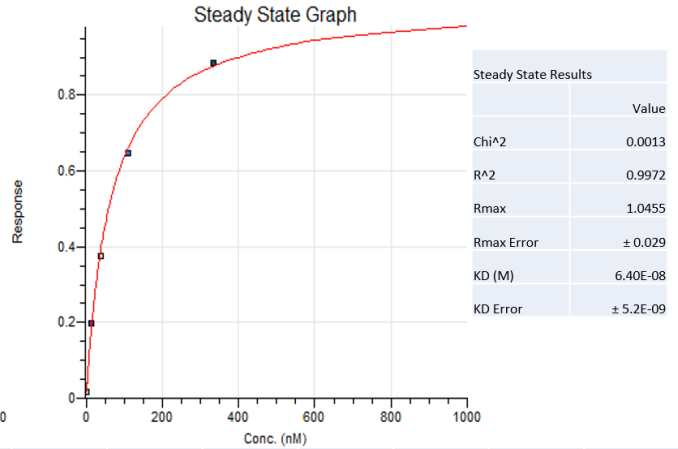

Steady State Results	
	Value
Chi^2	0.0013
R^2	0.9972
Rmax	1.0455
Rmax Error	± 0.029
KD (M)	6.40E-08
KD Error	± 5.2E-09

Conc. (nM)	Response	KD (M)	KD2	KD Error	KD2 Error	ka (1/Ms)	ka2	ka Error	ka2 Error	kdis (1/s)	kdis2	kdis Error	kdis2 Error	Full R^2	KD(%)	KD2(%)
1000	0.9483															
333	0.8859	4.96E-10	1.64E-07	2.18E-11	1.68E-09	1.23E+06	1.62E+05	5.22E+04	1.53E+03	6.07E-04	2.66E-02	6.88E-06	1.04E-04	0.998	17	83
111	0.6456	2.82E-10	1.64E-07	1.05E-11	2.50E-09	1.82E+06	1.55E+05	6.21E+04	2.27E+03	5.12E-04	2.53E-02	7.41E-06	1.03E-04	0.9976	10	90
37	0.3757	4.38E-09	1.18E-05	2.09E-10	7.27E-05	1.35E+06	2.58E+03	6.01E+04	1.59E+04	5.91E-03	3.05E-02	1.00E-04	3.53E-04	0.9968	0	100
12.4	0.1994	2.48E-10	4.53E-07	1.60E-11	2.50E-07	6.14E+06	4.84E+04	3.74E+05	2.67E+04	1.53E-03	2.19E-02	3.32E-05	1.94E-04	0.9911	1	99
4.1	0.059															
1.4	0.017	1.06E-02	2.49E-08		3.48E-07	3.35E+05	4.25E+06	7.55E+18	5.92E+07	3.55E+03	1.06E-01		6.72E-02		6	94

Figure A2 (contd.).

Figure A2p. Phosphorylated MEK1 binding to BRAF in the presence of ATP and CH5126676.

pMEK Chugai

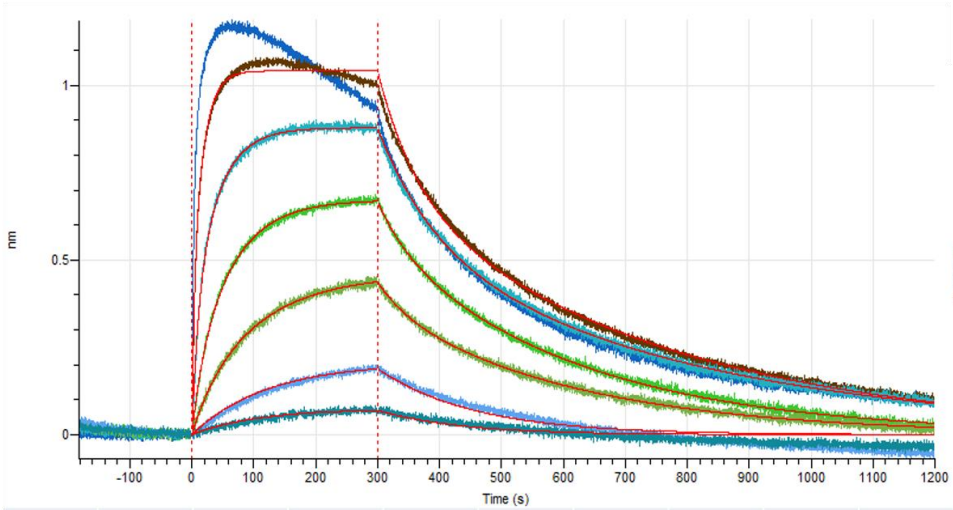

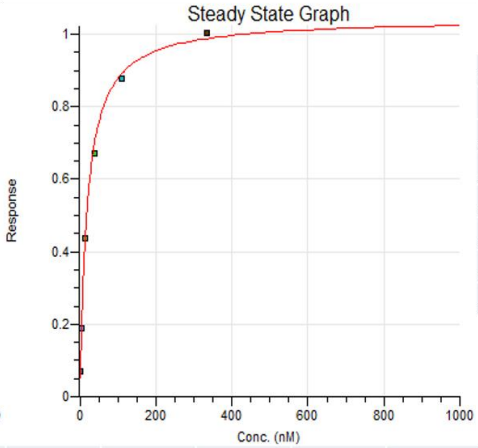

Steady State Results	
	Value
Chi^2	0.0014
R^2	0.998
Rmax	1.044
Rmax Error	± 0.015
KD (M)	1.90E-08
KD Error	± 1.0E-09

Conc. (nM)	Response	KD (M)	KD2	KD Error	KD2 Error	ka (1/Ms)	ka2	ka Error	ka2 Error	kdis (1/s)	kdis2	kdis Error	kdis2 Error	Full R^2	KD(%)	KD2(%)
1000	0.94															
333	1.0053	1.34E-08	2.17E-08	8.26E-11	5.51E-10	1.70E+05	7.54E+05	9.42E+02	1.76E+04	2.27E-03	1.64E-02	6.19E-06	1.61E-04	0.9985	68	32
111	0.8787	9.79E-09	1.48E-08	5.24E-11	2.16E-10	2.10E+05	7.53E+05	9.07E+02	9.24E+03	2.06E-03	1.11E-02	6.51E-06	8.83E-05	0.999	64	36
37	0.6706	8.70E-09	1.86E-08	3.91E-11	6.38E-10	3.63E+05	1.13E+06	1.48E+03	3.30E+04	3.16E-03	2.11E-02	5.94E-06	3.82E-04	0.9989	81	19
12.4	0.4361	6.21E-09	3.57E-08	7.06E-11	4.18E-09	5.13E+05	6.10E+05	5.65E+03	6.92E+04	3.19E-03	2.18E-02	8.92E-06	6.33E-04	0.9971	68	32
4.1	0.1886	1.66E-08	1.35E-08	3.77E-06	1.13E-06	3.70E+05	4.83E+05	8.24E+07	3.91E+07	6.14E-03	6.51E-03	2.64E-01	1.36E-01	0.8975	36	64
1.4	0.0696	5.67E-09	5.48E-09	4.93E-07	4.79E-07	1.36E+06	1.34E+06	4.47E+07	5.05E+07	7.73E-03	7.35E-03	6.22E-01	5.81E-01	0.7495	51	49

Figure A2 (contd.).

Figure A2q. Phosphorylated MEK1 binding to BRAF in the presence of ATP and Trametinib.

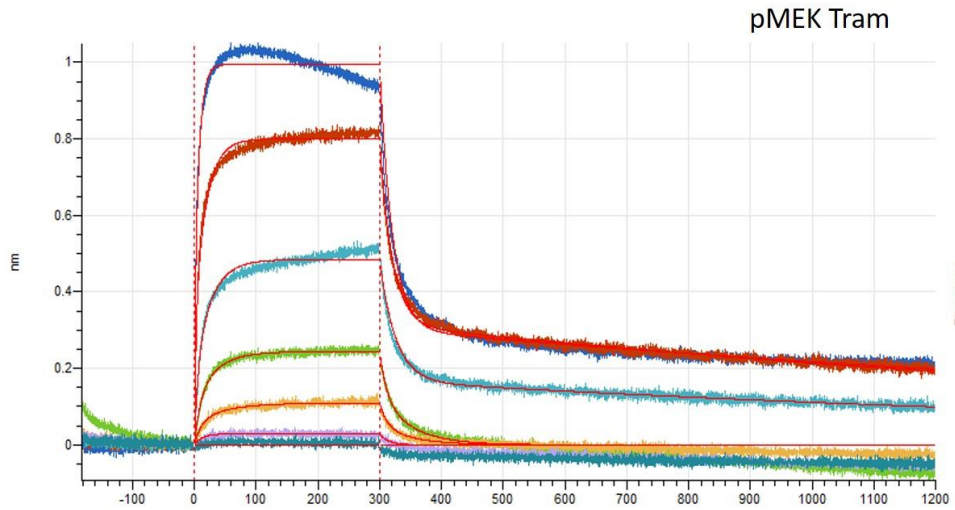

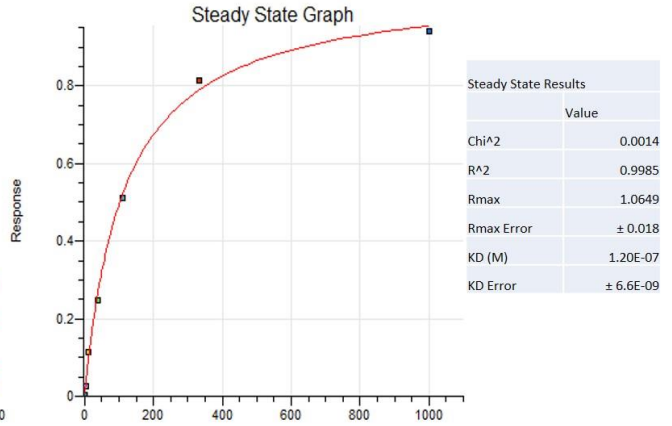

Steady State Results	
	Value
Chi^2	0.0014
R^2	0.9985
Rmax	1.0649
Rmax Error	± 0.018
KD (M)	1.20E-07
KD Error	± 6.6E-09

Conc. (nM)	Response	KD (M)	KD2	KD Error	KD2 Error	ka (1/Ms)	ka2	ka Error	ka2 Error	kdis (1/s)	kdis2	kdis Error	kdis2 Error	Full R^2	KD(%)	KD2(%)
1000	0.9398	6.71E-10	5.71E-07	3.80E-11	1.09E-08	7.10E+05	8.55E+04	3.93E+04	1.52E+03	4.76E-04	4.88E-02	5.59E-06	3.28E-04	0.996	22	78
333	0.8152	4.97E-10	3.38E-06	1.11E-11	3.07E-07	1.10E+06	1.44E+04	2.38E+04	1.30E+03	5.49E-04	4.85E-02	3.23E-06	2.69E-04	0.9974	6	94
111	0.5124	3.66E-10	9.47E-06	1.13E-11	9.72E-06	1.60E+06	4.12E+03	4.66E+04	4.23E+03	5.85E-04	3.90E-02	6.15E-06	2.97E-04	0.9942	1	99
37	0.2473	7.54E-08	2.51E-07	1.82E-08	2.74E-07	2.62E+05	3.57E+05	5.75E+04	3.83E+05	1.97E-02	8.97E-02	1.99E-03	1.81E-02	0.9084	31	69
12.4	0.1126	1.52E-07	1.59E-07	1.44E-07	2.16E-07	1.26E+05	5.29E+05	1.19E+05	7.14E+05	1.91E-02	8.42E-02	1.71E-03	1.14E-02	0.9237	46	54
4.1	0.0252	2.23E-02	3.71E-08		1.45E-07	1.60E+05	1.89E+06	1.24E+20	7.37E+06	3.55E+03	7.01E-02		2.30E-02		0	100
1.4	0.0022	7.76E-12	7.76E-12	<1.0E-12	<1.0E-12	3.57E+06	3.57E+06	0.00E+00	0.00E+00	2.77E-05	2.77E-05	<1.0E-07	<1.0E-07			

Figure A2 (contd.).

Figure A2r. Phosphorylated MEK1 binding to BRAF in the presence of ATP and Binimetinib.

pMEK MEK162 (Binimetinib)

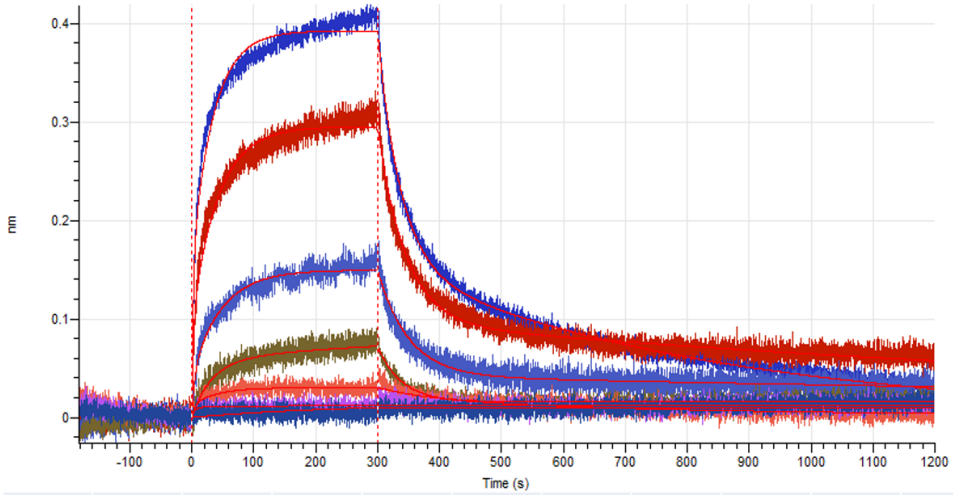

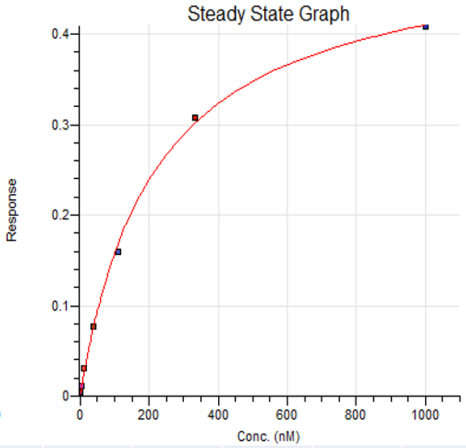

Steady State Results	
	Value
Chi^2	0.0002
R^2	0.999
Rmax	0.4992
Rmax Error	± 0.009
KD (M)	2.20E-07
KD Error	± 1.1E-08

Conc. (nM)	Response	KD (M)	KD2	KD Error	KD2 Error	ka (1/Ms)	ka2	ka Error	ka2 Error	kdis (1/s)	kdis2	kdis Error	kdis2 Error	Full X^2	Full R^2	KD(%)	KD2(%)
1000	0.4081	4.88E-09	1.73E-05	1.40E-10	3.44E-06	3.84E+05	1.57E+03	1.08E+04	3.13E+02	1.87E-03	2.72E-02	9.35E-06	1.91E-04	0.3406	0.9969	4	96
333.3	0.3076	5.65E-10	5.10E-06	2.89E-11	1.09E-06	1.02E+06	4.39E+03	4.97E+04	9.39E+02	5.79E-04	2.24E-02	9.44E-06	1.85E-04	0.4525	0.9904	3	97
111.1	0.1599	1.75E-10	2.92E-06	1.80E-11	1.86E-06	1.93E+06	6.89E+03	1.66E+05	4.38E+03	3.39E-04	2.01E-02	1.91E-05	2.87E-04	0.4163	0.9658	1	99
37	0.0775	<1.0E-12	1.71E-07	2.80E-11	2.38E-08	7.38E+04	1.52E+05	2.50E+04	2.10E+04	<1.0E-07	2.59E-02	2.07E-06	4.55E-04	0.21	0.9245	8	92
12.4	0.0305	8.97E-10	6.75E-10	8.02E-11	1.65E-10	1.89E+06	1.60E+07	1.39E+05	3.59E+06	1.69E-03	1.08E-02	8.63E-05	1.06E-03	0.162	0.7682	60	40
4.12	0.0116	<1.0E-12	<1.0E-12	1.11E-10	<1.0E-12	1.46E+06	5.04E+07	1.88E+06	1.27E+07	7.85E-07	<1.0E-07	1.62E-04	2.81E-06	0.1641	0.0161	15	85
1.37	0.0036					3.04E+06	2.89E+06							0.2167	0.1115	58	42

Figure A2 (contd.).

Figure A2s. Phosphorylated MEK1 binding to BRAF in the presence of ATP and Cobimetinib.

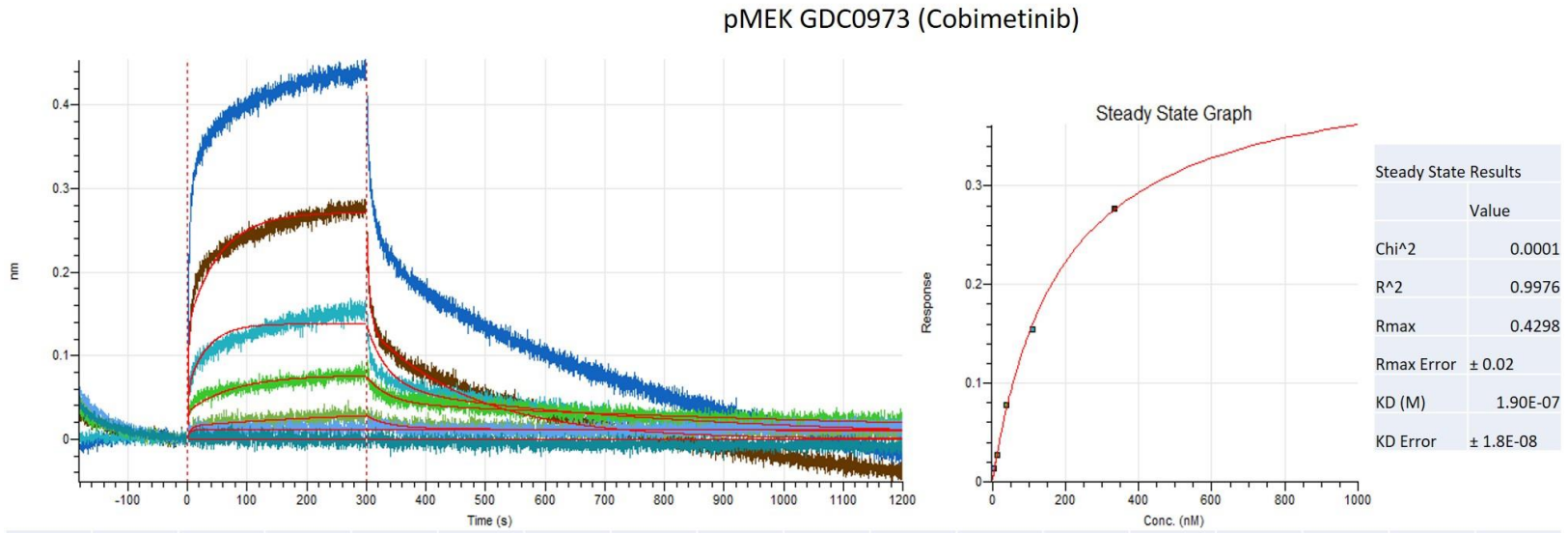

Conc. (nM)	Response	KD (M)	KD2	KD Error	KD2 Error	ka (1/Ms)	ka2	ka Error	ka2 Error	kdis (1/s)	kdis2	kdis Error	kdis2 Error	Full X^2	Full R^2	KD(%)	KD2(%)
1000	0.4398																
333.3	0.2775	1.50E-07	1.84E-07	6.13E-09	2.61E-08	3.84E+04	1.04E+06	1.50E+03	1.37E+05	5.75E-03	1.91E-01	7.01E-05	1.03E-02	1.6466	0.9764	49	51
111.1	0.1543	4.18E-10	4.05E-06	3.58E-11	5.38E-06	4.40E+06	7.10E+03	3.72E+05	9.43E+03	1.84E-03	2.87E-02	2.41E-05	6.52E-04	0.3783	0.9719	2	98
37	0.0784	2.64E-09	1.45E-09	8.94E-11	1.98E-10	3.30E+05	1.96E+07	1.01E+04	2.60E+06	8.71E-04	2.83E-02	1.29E-05	9.06E-04	0.1628	0.9203	59	41
12.4	0.0274	1.04E-09	1.72E-09	3.64E-10	3.18E-10	2.43E+05	1.50E+07	7.95E+04	2.59E+06	2.52E-04	2.57E-02	3.31E-05	1.72E-03	0.1656	0.5228	56	44
4.1	0.0134					2.57E+07	8.86E+07							0.1449	0.0034	32	68
1.4	-2.08E-03	<1.0E-12	<1.0E-12	<1.0E-12	<1.0E-12	3.57E+06	3.57E+06	0.00E+00	0.00E+00	7.99E-07	7.99E-07	<1.0E-07	<1.0E-07	0.3136			

Figure A2 (contd.).

Figure A2t. Phosphorylated MEK1 binding to BRAF in the presence of ATP and Selumetinib.

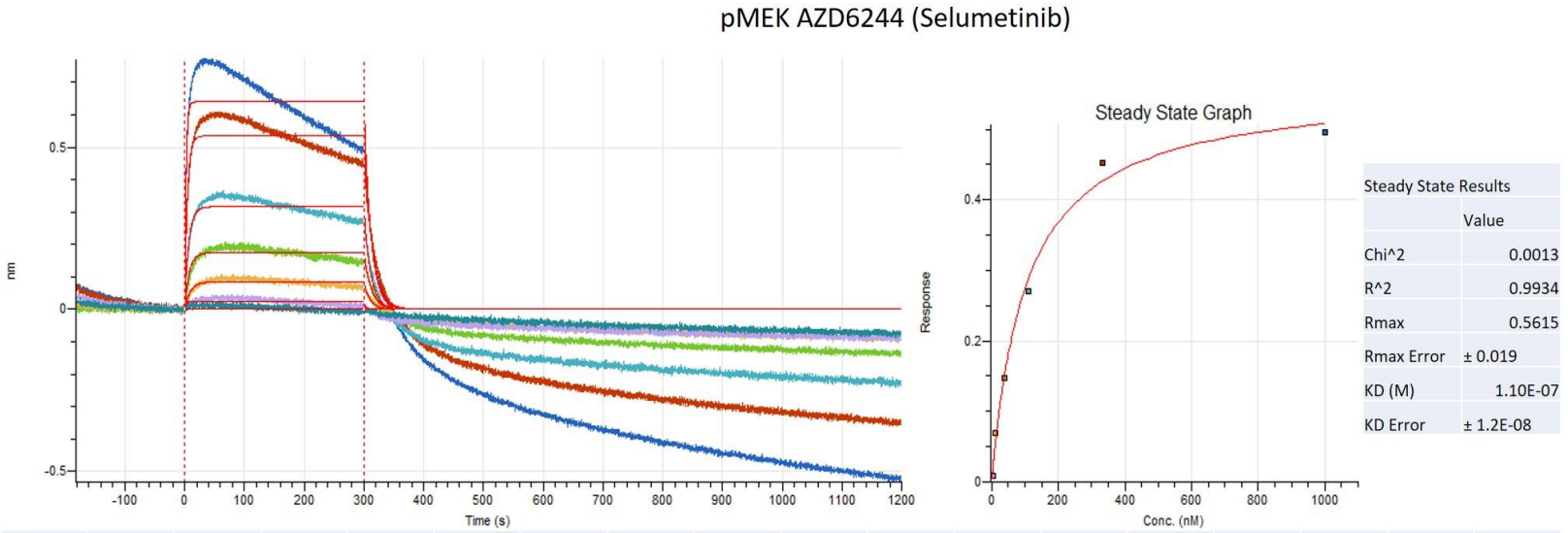

Conc. (nM)	Response	KD (M)	KD2	KD Error	KD2 Error	ka (1/Ms)	ka2	ka Error	ka2 Error	kdis (1/s)	kdis2	kdis Error	kdis2 Error	Full X^2	Full R^2	KD(%)	KD2(%)
1000	0.4953	2.60E-07	2.60E-07	7.50E-02	7.61E-02	3.36E+05	3.36E+05	9.57E+10	9.72E+10	8.74E-02	8.74E-02	3.71E+03	3.77E+03	662.5628	0.4574	50	50
333.3	0.4519	1.71E-07	1.71E-07	8.94E-04	4.55E-03	4.31E+05	4.31E+05	1.73E+09	8.81E+09	7.38E-02	7.38E-02	2.47E+02	1.26E+03	301.7977	0.5809	84	16
111.1	0.2709	1.82E-07	4.09E-01	9.72E-08		5.04E+05	8.67E+03	2.57E+05	1.79E+17	9.16E-02	3.55E+03	1.51E-02		135.8146	0.5018	91	9
37	0.1469	6.13E-08	2.52E+00	3.40E-08		1.34E+06	1.41E+03	7.11E+05		8.23E-02	3.55E+03	1.40E-02		48.7177	0.4435	92	8
12.4	0.0694	6.65E-08	7.71E-07	1.17E-07	4.11E-02	1.41E+06	3.04E+07	2.45E+06	1.62E+12	9.36E-02	2.35E+01	2.26E-02	1.40E+04	19.5077	0.2537	78	22
4.1	0.0094	1.06E-07	4.30E-08	9.86E-05	1.11E-06	8.01E+07	6.57E+06	7.43E+10	1.69E+08	8.51E+00	2.83E-01	2.28E+02	6.13E-01	20.9157		49	51
1.4	-9.42E-03	1.09E-11	1.09E-11	<1.0E-12	<1.0E-12	3.57E+06	3.57E+06	0.00E+00	0.00E+00	3.89E-05	3.89E-05	<1.0E-07	<1.0E-07	12.4771			

Figure A2 (contd.).

Figure A2u. Phosphorylated MEK1 binding to BRAF in the presence of ATP and Pimasertib.

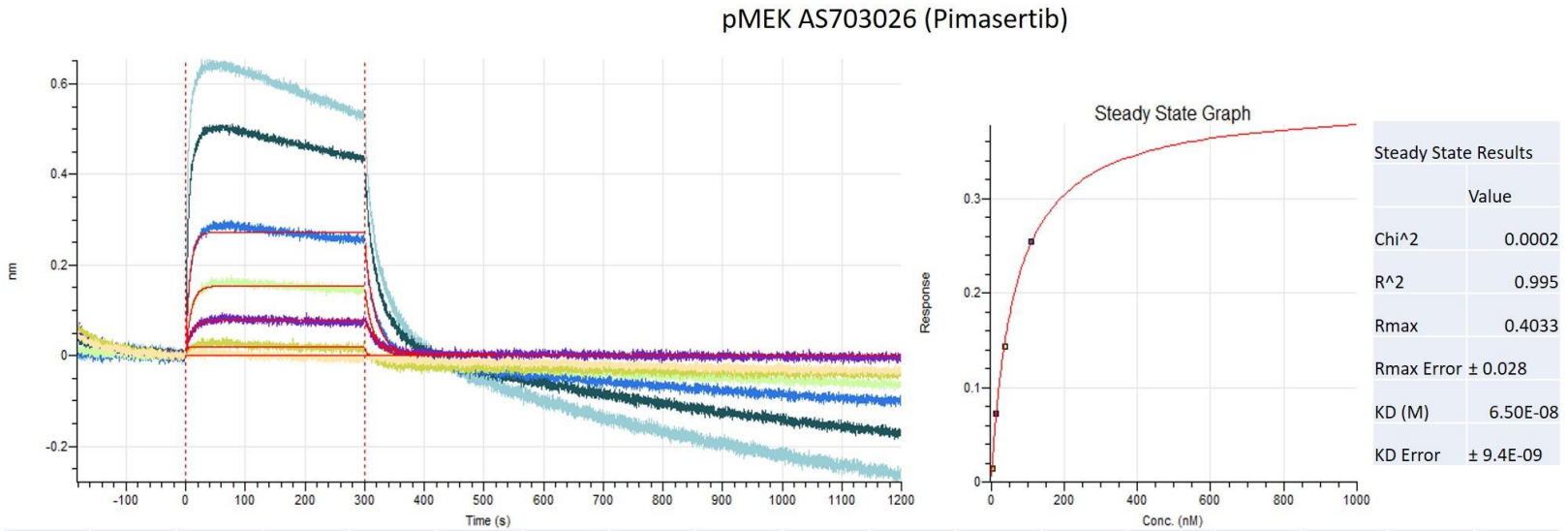

Conc. (nM)	Response	KD (M)	KD2	KD Error	KD2 Error	ka (1/Ms)	ka2	ka Error	ka2 Error	kdis (1/s)	kdis2	kdis Error	kdis2 Error	Full X^2	Full R^2	KD(%)	KD2(%)
1000	0.5311																
333.3	0.4371																
111.1	0.2546	7.88E-08	1.81E-06	1.52E-08	7.00E-05	6.86E+05	2.73E+05	1.13E+05	1.05E+07	5.41E-02	4.94E-01	5.43E-03	1.10E+00	19.3944	0.8453	49	51
37	0.1437	7.33E-08	7.62E-08	1.17E-03	7.64E-04	9.80E+05	9.44E+05	1.56E+10	9.46E+09	7.19E-02	7.19E-02	3.04E+01	1.89E+01	8.457	0.8012	37	63
12.4	0.0721	<1.0E-12	1.23E-08		8.55E-10	1.18E+10	3.93E+06		2.56E+05	6.78E-03	4.84E-02	6.54E-04	1.19E-03	0.1647	0.9753	6	94
4.1	0.0139	5.51E-08	5.14E-08	3.22E-03	2.17E-03	5.74E+06	6.27E+06	3.28E+11	2.59E+11	3.16E-01	3.22E-01	3.55E+03	2.73E+03	5.126		45	55
1.4	-7.14E-03	4.49E-12	4.49E-12	<1.0E-12	<1.0E-12	3.57E+06	3.57E+06	0.00E+00	0.00E+00	1.60E-05	1.60E-05	<1.0E-07	<1.0E-07	2.5035			

Figure A2 (contd.).

Figure A2v. MEK1 L314E does not bind BRAF in the presence of ATP.

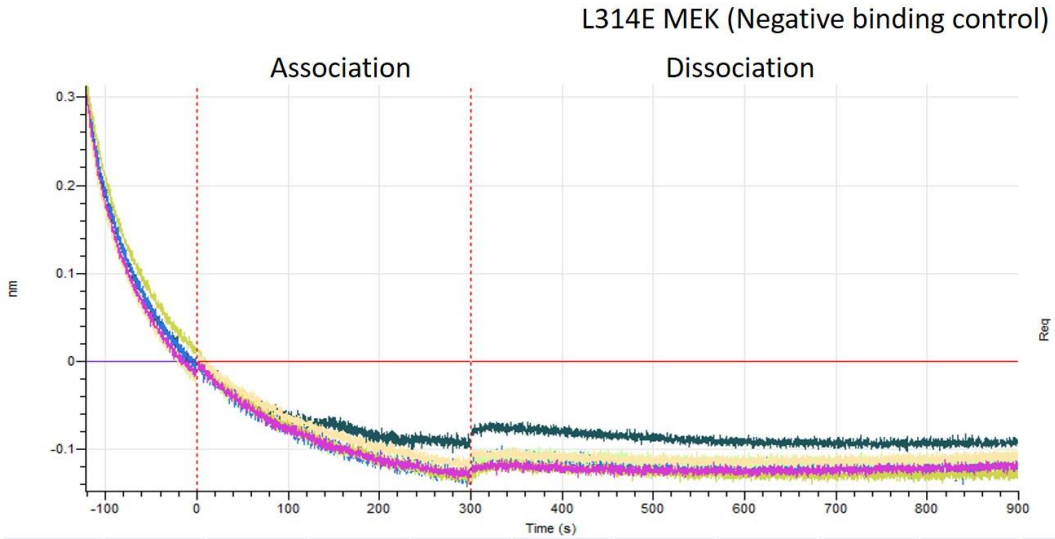

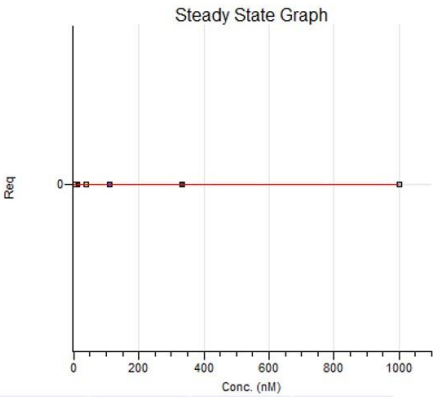

Conc. (nM)	Response	KD (M)	KD Error	ka (1/Ms)	ka Error	kdis (1/s)	kdis Error	Rmax	Rmax Error	Req	Req/Rmax(%)	Full X^2	Full R^2
1000	0.00E+00	1.00E-07	<1.0E-12	1.00E+04	0.00E+00	1.00E-03	<1.0E-07	0		0			
333.3	-9.21E-02	1.00E-07	<1.0E-12	1.00E+04	0.00E+00	1.00E-03	<1.0E-07	0		0		31.0537	
111.1	-1.27E-01	1.00E-07	<1.0E-12	1.00E+04	0.00E+00	1.00E-03	<1.0E-07	0		0		54.85	
37	-1.28E-01	1.00E-07	<1.0E-12	1.00E+04	0.00E+00	1.00E-03	<1.0E-07	0		0		51.0393	
12.4	0.00E+00	1.00E-07	<1.0E-12	1.00E+04	0.00E+00	1.00E-03	<1.0E-07	0		0			
4.12	-1.31E-01	1.00E-07	<1.0E-12	1.00E+04	0.00E+00	1.00E-03	<1.0E-07	0		0		61.237	
1.37	-1.16E-01	1.00E-07	<1.0E-12	1.00E+04	0.00E+00	1.00E-03	<1.0E-07	0		0		46.9477	
0	-1.26E-01												

Steady State Results	
	Value
Chi^2	0
R^2	0
Rmax	0
Rmax Error	± 0
KD (M)	0.00E+00
KD Error	± 0.0E00